JOURNAL OF PETROLOGY | VOLUME 47 | NUMBER 10 | PAGES 1873–1914 | 2006 | doi:10.1093/petrology/egl030

Petrogenesis of Mafic Garnet Granulite in the Lower Crust of the Kohistan Paleo-arc Complex (Northern Pakistan): Implications for Intra-crustal Differentiation of Island Arcs and Generation of Continental Crust

CARLOS J. GARRIDO[1]*, JEAN-LOUIS BODINIER[2], JEAN-PIERRE BURG[3], GEROLD ZEILINGER[4], S. SHAHID HUSSAIN[5], HAMID DAWOOD[5], M. NAWAZ CHAUDHRY[6] AND FERNANDO GERVILLA[1]

[1]DEPARTAMENTO DE MINERALOGÍA Y PETROLOGÍA, UNIVERSIDAD DE GRANADA, FACULTAD DE CIENCIAS, 18002 GRANADA, SPAIN

[2]ISTEEM, LABORATOIRE DE TECTONOPHYSIQUE, CNRS & UNIVERSITÉ DE MONTPELLIER II, 34095 MONTPELLIER, FRANCE

[3]GEOLOGISCHES INSTITUT, ETH-ZENTRUM, SONNEGGSTRASSE 5, 8092 ZÜRICH, SWITZERLAND

[4]UNIVERSITY OF BERN, INSTITUTE OF GEOLOGICAL SCIENCES, BERN, SWITZERLAND

[5]PAKISTAN MUSEUM OF NATURAL HISTORY, GARDEN AVENUE, SHAKARPARIAN, 44000 ISLAMABAD, PAKISTAN

[6]INSTITUTE OF GEOLOGY, UNIVERSITY OF THE PUNJAB, QUAID-I-AZAM CAMPUS, 54590, LAHORE, PAKISTAN

RECEIVED FEBRUARY 7, 2005; ACCEPTED APRIL 27, 2006; ADVANCE ACCESS PUBLICATION JUNE 7, 2006

We report the results of a geochemical study of the Jijal and Sarangar complexes, which constitute the lower crust of the Mesozoic Kohistan paleo-island arc (Northern Pakistan). The Jijal complex is composed of basal peridotites topped by a gabbroic section made up of mafic garnet granulite with minor lenses of garnet hornblendite and granite, grading up-section to hornblende gabbronorite. The Sarangar complex is composed of metagabbro. The Sarangar gabbro and Jijal hornblende gabbronorite have melt-like, light rare earth element (LREE)-enriched REE patterns similar to those of island arc basalts. Together with the Jijal garnet granulite, they define negative covariations of La_N, Yb_N and $(La/Sm)_N$ with Eu [Eu* = $2 \times Eu_N/(Sm_N + Gd_N)$, where N indicates chondrite normalized], and positive covariations of $(Yb/Gd)_N$ with Eu*. REE modeling indicates that these covariations cannot be accounted for by high-pressure crystal fractionation of hydrous primitive or derivative andesites. They are consistent with formation of the garnet granulites as plagioclase–garnet assemblages with variable trapped melt fractions via either high-pressure crystallization of primitive island arc basalts or dehydration-melting of hornblende gabbronorite, provided that the amount of segregated or restitic garnet was low (<5 wt %). Field, petrographic, geochemical and experimental evidence is more consistent with formation of the Jijal garnet granulite by dehydration-melting of Jijal hornblende gabbronorite. Similarly, the Jijal garnet-bearing hornblendite lenses were probably generated by coeval dehydration-melting of hornblendites. Melting models and geochronological data point to intrusive leucogranites in the overlying metaplutonic complex as the melts generated by dehydration-melting of the plutonic protoliths of the Jijal garnet-bearing restites. Consistent with the metamorphic evolution of the Kohistan lower arc crust, dehydration-melting occurred at the mature*

*Corresponding author. Fax: (+34) 958 243384. E-mail: carlosg@ugr.es

stage of this island arc when shallower hornblende-bearing plutonic rocks were buried to depths exceeding 25–30 km and heated to temperatures above c. *900°C. Available experimental data on dehydration-melting of amphibolitic sources imply that thickening of oceanic arcs to depths >30 km (equivalent to c. 1·0 GPa), together with the hot geotherms now postulated for lower island arc crust, should cause dehydration-melting of amphibole-bearing plutonic rocks generating dense garnet granulitic roots in island arcs. Dehydration-melting of hornblende-bearing plutonic rocks may, hence, be a common intracrustal chemical and physical differentiation process in island arcs and a natural consequence of their maturation, leading to the addition of granitic partial melts to the middle–upper arc crust and formation of dense, unstable garnet granulite roots in the lower arc crust. Addition of LREE-enriched granitic melts produced by this process to the middle–upper island arc crust may drive its basaltic composition toward that of andesite, affording a plausible solution to the 'arc paradox' of formation of andesitic continental-like crust in island arc settings.*

KEY WORDS: *island arc crust; Kohistan complex; Jijal complex; amphibole dehydration-melting; garnet granulite; continental crustal growth*

INTRODUCTION

Collision and accretion of oceanic terranes at convergent margins is the main mechanism of post-Archaean continental crustal growth (Taylor & McLennan, 1985; Rudnick, 1995; Condie, 1997). The contribution of island arcs (1·6 km^3/yr) to the net growth rate of young continental crust (<200 Ma) surpasses the combined volumes of submarine plateaux (0·8 km^3/yr), oceanic hotspot volcanism (0·2 km^3/yr) and continental underplating (0·2 km^3/yr) (Reymer & Schubert, 1984; Condie, 1997; Dimalanta *et al.*, 2002). The inference that continental crust is mainly derived from island arcs is consistent with the similarity of trace element patterns in arc magmas and continental crust (Taylor & McLennan, 1985; Rudnick, 1995). This hypothesis, referred to as the 'andesite model' (Taylor & McLennan, 1985), was generally well regarded by supporters of uniformitarism as it provides an observable link between continental crust genesis and plate tectonics. The andesite model for Phanerozoic crustal growth faces, however, the so-called 'arc paradox': the continental crust has an andesitic major element composition similar to that of granodioritic plutonic rocks, whereas available estimates of the composition of exposed island arc terranes and magmatic fluxes to the upper arc crust are basaltic and similar to plutonic gabbroic rocks in composition (e.g. Arculus & Johnson, 1981; Grove & Kinzler, 1986; Ellam & Hawkesworth, 1988; Pearcy *et al.*, 1990; DeBari & Sleep, 1991; Kelemen *et al.*, 2003*a*; Greene *et al.*, 2006).

How oceanic arcs become changed during, or soon after, their accretion to continents to attain the andesite bulk composition of the continental crust is poorly understood. Possible solutions to the 'arc paradox' are inherently related to some of the most controversial issues of island arc petrogenesis: namely, the composition of primary arc magmas, the composition of the mantle flux to the arc crust and the nature of intracrustal differentiation processes. Kelemen *et al.* (2003*a*) reviewed three potential differentiation mechanisms for the generation of evolved [Mg-number = MgO/(MgO + FeO) molar ratio ≈ 0·5], andesitic continental crust from primitive (Mg-number ≈ 0·7) arc magma compositions: (1) fractional crystallization from, or partial melting of, primitive (high Mg-number) arc andesite; (2) fractional crystallization from, or partial melting of, primitive arc basalt at high fO_2 and high fH_2O, forming andesite melt and leaving behind low-SiO_2 cumulates or residues; (3) mixing, or juxtaposition, of primitive arc basalts with highly evolved, granitic melts produced by intracrustal differentiation. In all of the three models, mafic or ultramafic cumulates or melting residues must be disposed of into the upper mantle to generate the andesitic composition of the continental crust. If dominated by ultramafic compositions, these rocks could be present below the seismic Moho where they would form a thick (≈10 km), ultramafic layer. Alternatively, they could become delaminated and recycled into the upper mantle. Delamination of mafic and ultramafic lower crust has been generally suggested for overthickened continental crust where high pressures and a cold thermal regime lead to formation of a dense eclogitic lower crust (Arndt & Goldstein, 1989; Kay & Kay, 1991). Jull & Kelemen (2001) demonstrated that, for feasible geological timescales, delamination of the lower crust is also a workable hypothesis for the 'hotter' geotherms of island arcs (800–1000°C at the Moho). Under these conditions, lower arc crust cumulates or residues would be denser than the underlying FeO-depleted sub-arc mantle, triggering convective instabilities and delamination of the lower crust.

Exhumed arc terranes provide a unique opportunity to evaluate the nature of the shallow sub-arc mantle and lower arc crust, to constrain the mechanisms of intracrustal differentiation and to assess the delamination hypothesis (e.g. DeBari, 1997). Recent studies of the exposed section of lower arc crust in Talkeetna (Alaska) reported the absence of a thick sub-arc cumulate–restite sequence and gave geobarometric arguments for a pressure gap in the lower crustal section (Kelemen *et al.*, 2003*a*, 2003*c*; Greene *et al.*, 2006). This was considered as indirect evidence for lower crust delamination. However, mass balance calculations of the Talkeetna paleo-arc yield a basaltic composition, suggesting that the arc underwent only a limited degree of intracrustal differentiation.

The Kohistan complex (Northern Pakistan) shows a complete, highly differentiated arc section from mantle

peridotites to upper volcanic rocks through pyroxenites, lower crustal granulites and granitic intrusions. Here we present a detailed whole-rock trace element study of lower crustal garnet granulites and associated rocks in Kohistan. We present petrological and geochemical evidence for dehydration-melting of lower arc, amphibole-bearing plutonic rocks that generated granitic melts and left restites of mafic garnet granulite, garnet hornblendite and garnet pyroxenite. Melting of the Kohistan lower crust was possibly triggered by overloading of the arc crust and heating at the Moho as a result of mantle upwelling and igneous underplating. We show that thickening of oceanic arcs at pressures greater than about 1·0 GPa, together with the hot geotherms postulated for the lower arc crust (Rose *et al.*, 2001; Grove *et al.*, 2002; Kelemen *et al.*, 2003*b*, 2003*c*), should cause dehydration-melting of amphibole-bearing plutonic rocks. Consequently, we argue that dehydration-melting of hornblende-bearing plutonic rocks must be a common process in island arcs—and a natural consequence of their maturation—leading to the addition of granitic partial melts to the middle–upper arc crust and the formation of dense, unstable garnet granulite roots in the lower arc crust.

GEOLOGICAL SETTING

The Kohistan arc complex (Western Himalaya, Northern Pakistan; Fig. 1) is an exhumed section of a Cretaceous island arc that formed during northward subduction of the Neo-Tethys Ocean beneath the Karakoram plate (Tahirkheli *et al.*, 1979; Bard, 1983*a*, 1983*b*; Burg *et al.*, 1998). It is sandwiched between the collided Indian and Karakoram plates, and separated from these blocks by two major sutures: the 'Northern Suture', or 'Main Karakorum Thrust' (MKT) to the north, and the 'Indus Suture', or 'Main Mantle Thrust' (MMT) to the south (Fig. 1). From north to south, the Kohistan complex is composed of the following units: (1) the meta-sedimentary and meta-volcanic units of the 'Jaglot' and 'Yasin–Chalt Groups', emplaced in the Aptian–Albian (104 Ma) in one or more arc-related basins (Khan *et al.*, 1996, 1998) and hosting much of the Kohistan batholith (Petterson & Windley, 1985, 1991; Petterson *et al.*, 1991); (2) the 'Kohistan batholith', composed of multiple plutons of dioritic to granitic composition (Petterson & Windley, 1985); (3) the 'Chilas complex', composed of major gabbronoritic intrusion and numerous, subordinate occurences of ultramafic rocks (Bard, 1983*b*; Khan *et al.*, 1989; Mikoshiba *et al.*, 1999); (4) the 'Kamila amphibolite belt' (Bard, 1983*a*, 1983*b*; Jan, 1988)—the section of which exposed along the Indus River will be referred to here as the 'Patan–Dasu metaplutonic complex' (Zeilinger, 2002)—comprising an upper unit of ortho-amphibolites, metapelites, metavolcanic rocks and carbonates, intruded by granitic sheets ('Kamila Amphibolites' *sensu stricto*), a middle unit of interlayered metagabbro and metadiorite sills ('Kiru Amphibolites'), also intruded by granites, and a lower unit of strongly deformed metadiorites and sheared metagabbros, including the 'Sarangar gabbro' sub-unit at its base ('Patan sheared gabbros and diorites'; Zeilinger, 2002) (Fig. 1); (5) the 'Jijal complex', located in the hanging wall of the Indus Suture and composed of granulite-facies gabbroic rocks underlain by layered ultramafic rocks (Jan & Howie, 1981; Jan & Windley, 1990; Miller *et al.*, 1991; Yamamoto & Yoshino, 1998). The Jijal section is the structurally lowest unit and the deepest outcropping level of the Kohistan island arc complex (Fig. 1).

The initiation of the Kohistan arc occurred in the Middle Cretaceous (*c.* 110 Ma) following the subduction of the Neo-Tethys Ocean, induced by fast northward drift of the Indian plate (Rolland, 2002; Rolland *et al.*, 2002). The island arc-building stage (110–90 Ma) was characterized by thickening of the arc crust via magmatic underplating, intrusion of plutonic bodies and extrusion of lavas and pyroclastics. The Jijal complex, the metaplutonic complex, and the earliest granitic intrusions are related to this stage. Around 85 Ma, the Kohistan island arc was sutured northward to the Karakorum plate, and then evolved as an Andean-type convergent margin. Suturing was followed by a stage of intra-arc rifting responsible for gabbronoritic magmatism and mantle diapirism in the Chilas complex (Khan *et al.*, 1996; Burg *et al.*, 1998), and by a second stage of granitic plutonism (Petterson & Windley, 1985; Petterson *et al.*, 1993). The final stage of the arc was characterized by renewed compression and continued intrusion of granitic plutons in the Kohistan batholith, which progressively waned until the final collision of the Indian plate. Between 65 and 55 Ma, at the onset of India–Asia continental collision, the Kohistan arc was obducted onto the Indian margin along the MMT, which resulted in the exposure of a complete section of the island arc crust (e.g. Tahirkheli *et al.*, 1979; Searle *et al.*, 1987; Treloar *et al.*, 1996; Khan *et al.*, 1998).

FIELD RELATIONS

Our study is focused on the lower to mid-crustal levels of the Kohistan arc, as exposed along the Indus valley (Figs 1 and 2). These comprise the granulitic upper section of the Jijal complex and the gabbroic lower section of the Patan–Dasu metaplutonic complex (Sarangar gabbro; Figs 1 and 2). The study also includes the leucogranitic intrusions in the Patan–Dasu

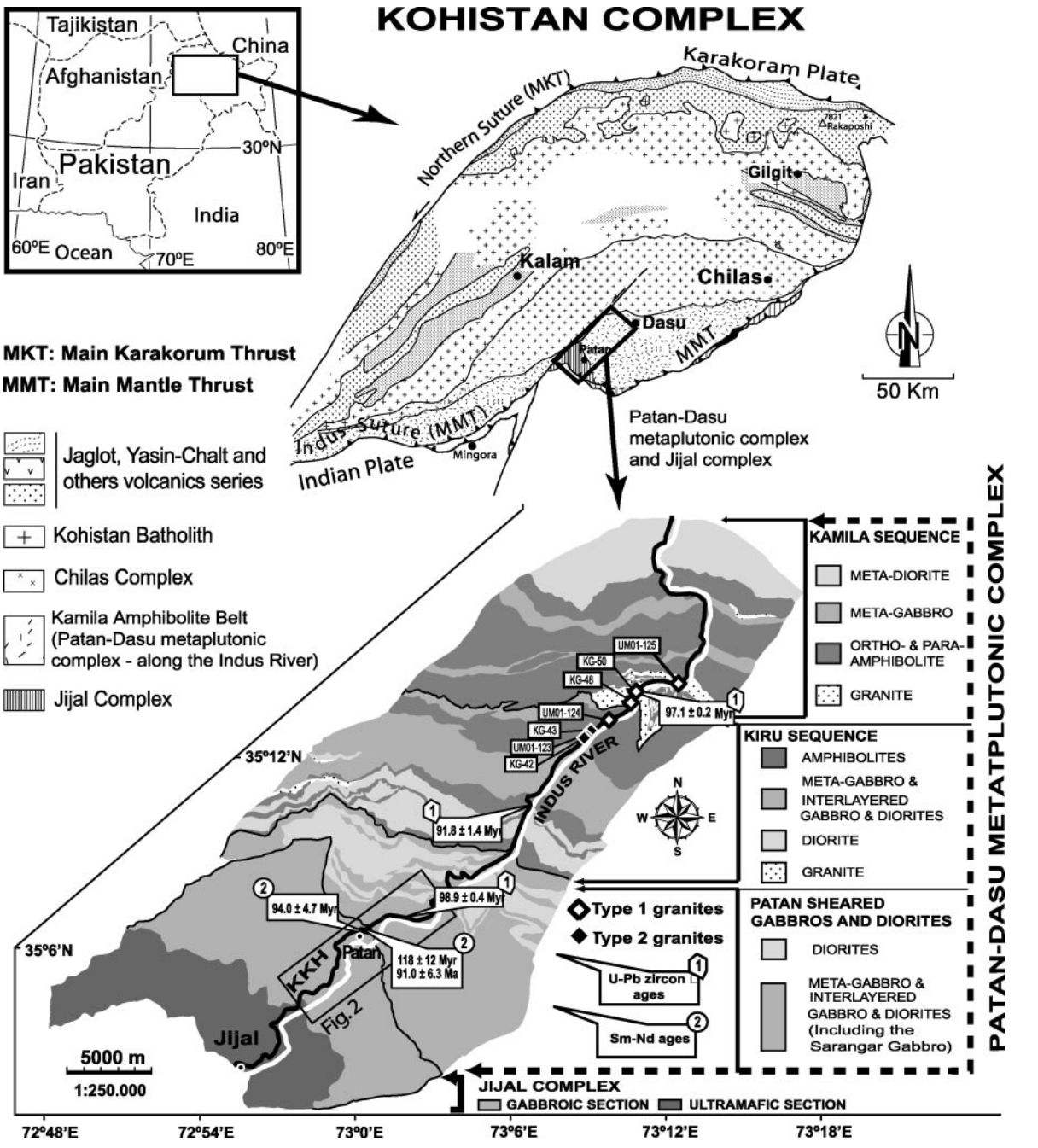

Fig. 1. Upper left: simplified geological map of the Kohistan island arc complex (Northern Pakistan) showing the location of the Jijal and the Patan–Dasu metaplutonic complexes (rectangle) (modified after Burg *et al.*, 1998). Lower right: simplified geological map of the Jijal–Dasu transect of the Kohistan arc along the Indus Valley (KKH, Karakoram highway) showing the main units and lithologies of the Jijal and metaplutonic complexes (modified after Zeilinger, 2002). Also shown is the location of the intrusive granite samples selected for our study. U–Pb zircon ages in the metaplutonic complex are multicollector delk ICP-MS data for zircons (Schaltegger *et al.*, 2002). Sm–Nd ages are isochron ages from whole-rock and mineral analyses (Yamamoto & Nakamura, 1996, 2000).

metaplutonic complex (Kiru and Kamila sequences; Fig. 1). Altogether these rocks provide a unique record of arc magmatism, high-pressure granulite metamorphism and coeval granitic magmatism during the evolution of an oceanic island arc (Bard, 1983*a*, 1983*b*; Burg *et al.*, 1998; Yamamoto & Yoshino, 1998; Yamamoto & Nakamura, 2000; Schaltegger *et al.*, 2002; Zeilinger, 2002; Yoshino & Okudaira, 2004).

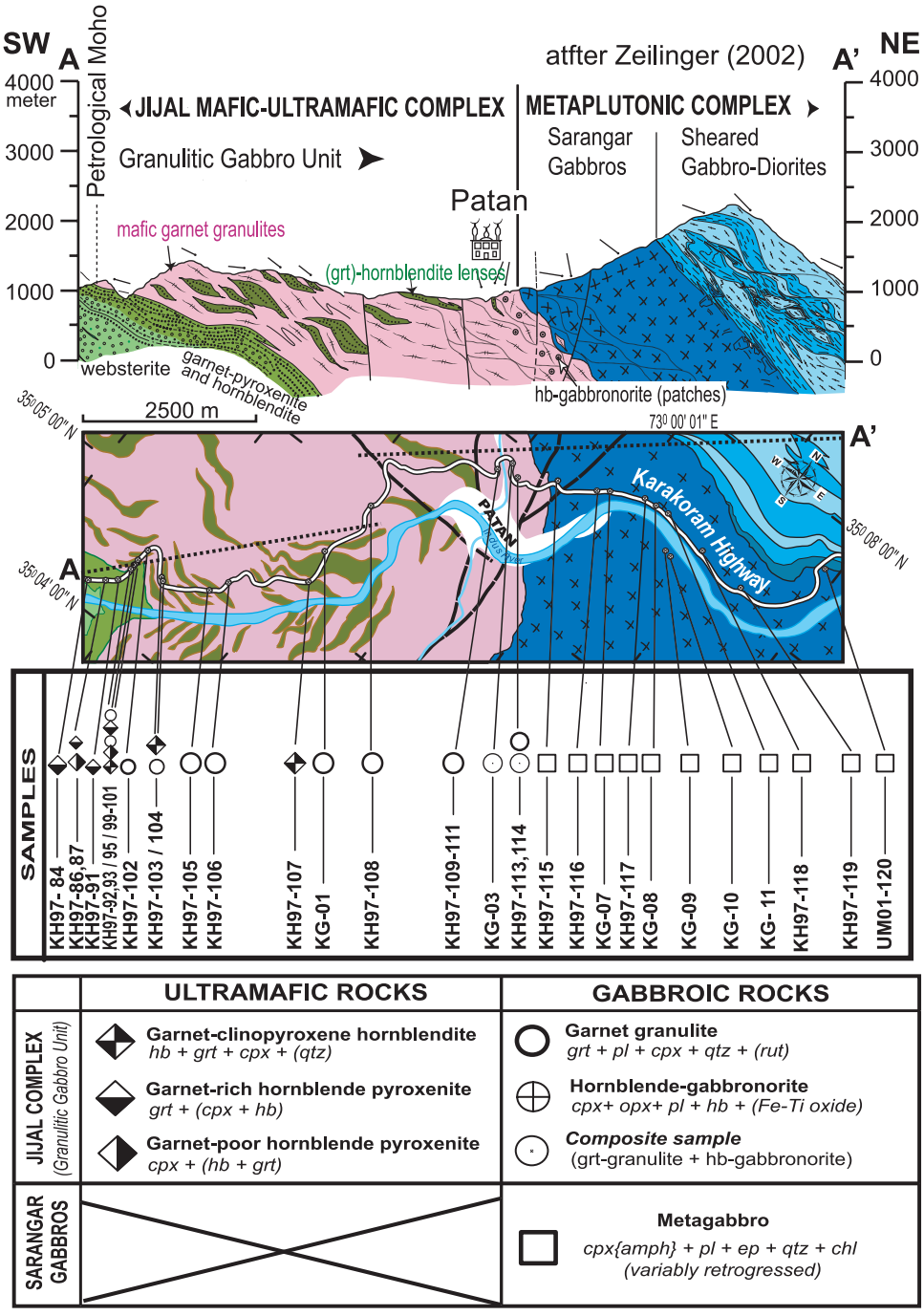

Fig. 2. Above: geological section (transect A–A′ below) along the Indus valley from the lower granulitic gabbro zone of the Jijal complex through the Sarangar gabbros of the Patan–Dasu metaplutonic complex (modified after Bard, 1983*a*, 1983*b*; Zeilinger, 2002) (see Fig. 1 for location). Below: geological map of the same section (after Zeilinger, 2002) showing the location of the samples selected for our study, their lithological classification and their primary mineral assemblages.

The Jijal granulitic complex

The Jijal complex consists of an upper zone dominated by granulite-facies gabbroic rocks overlying a thick section of peridotites and pyroxenites (Fig. 2). The intrusive contact of the granulitic gabbros with the upper part of the ultramafic section is interpreted as the petrological Moho of the Kohistan paleo-arc (Bard, 1983*a*, 1983*b*; Burg *et al.*, 1998). Several investigators

have provided comprehensive field and petrographic descriptions of the granulite section (Jan & Howie, 1981; Bard, 1983*a*; Miller *et al.*, 1991; Yamamoto, 1993; Burg *et al.*, 1998; Yamamoto & Yoshino, 1998; Zeilinger, 2002). The granulite unit is dominated by garnet-bearing meta-gabbroic rocks (mafic garnet granulite) containing tens to hundreds of meters thick, ultramafic lenses of hornblendite, garnet–clinopyroxene hornblendite and garnet–hornblende pyroxenite and rare peridotite (Fig. 2). The ultramafic lenses have sharp contacts with the enclosing garnet granulites and are subparallel to the paleo-Moho. They are more abundant towards the base of the granulite section, where the pyroxenite facies tends to predominate over hornblendites.

The upper part of the granulitic section (near the village of Patan; Fig. 2) is composed of minor hornblende gabbronorites that grade into garnet granulites through a sharp front that cross-cuts former igneous layering and is extremely convoluted in shape (Fig. 3a). In hand-specimen, the front is somewhat diffuse and appears as a few centimeters-thick transition zone where patches of garnet–hornblende gabbronorite are preserved in the anhydrous garnet granulite assemblage (Fig. 3b). Several workers have presented compelling field and petrological evidence for recrystallization of precursor hornblende gabbronorite into Jijal garnet granulite (Bard, 1983*a*; Yamamoto & Yoshino, 1998, fig. 4, p. 224; Yamamoto & Nakamura, 2000, fig. 3, p. 315). Yamamoto & Yoshino (1998) provided a detailed description of this transition, including modal variations showing hornblende breakdown and recrystallization of igneous minerals into the anhydrous garnet granulite assemblage. This transformation has been ascribed to dehydration during granulite-facies metamorphism related to compression and reheating of the sub-arc crust as a result of magmatic underplating (Yamamoto & Yoshino, 1998; Yoshino *et al.*, 1998; Yoshino & Okudaira, 2004). However, the Jijal hornblende gabbronorite to garnet granulite transition bears a strong resemblance to the gabbro–granulite transition observed in the lower arc crust of the Fiordland arc complex (New Zealand), which is related to dehydration-melting of hornblende gabbro along igneous dykes (Blattner, 1976; Clarke *et al.*, 2000; Daczko *et al.*, 2001).

Leucocratic veins of plagioclase, quartz and garnet are widespread in the Jijal garnet granulite (Fig. 3a and c) and are especially abundant in the vicinity of hornblendite lenses. The thicker hornblendite lenses show characteristic mineralogical zoning from hornblendite and garnet hornblendite cores to garnetite rims (Fig. 3d; see also Yamamoto & Yoshino, 1998). The garnetite and garnet-rich hornblendite are systematically associated with irregular patches and dense networks of felsic plagioclase-rich leucosomes (Fig. 3d and e). These features are less apparent in thinner lenses where hornblendite rimmed by garnet grades along strike into garnetite lenses, as well as into very coarse (several centimeters), poikiloblastic garnet crystals, which are spatially associated with small felsic aggregates dispersed in the garnet granulite host (Fig. 3c).

Discordant felsic veins are not conspicuous in the Jijal granulites but in places they are abundant (Fig. 3c) and may exhibit selvages of strongly hydrated and retrogressed garnet granulite (Fig. 3a) possibly the result of back-reactions typical of granulite terranes (e.g. Kriegsman, 2001). Many Jijal granulites underwent a late retrogression stage responsible for the presence of secondary, metamorphic amphibole and epidote (Yamamoto, 1993; Yamamoto & Yoshino, 1998; Yoshino *et al.*, 1998).

The Sarangar gabbro complex

The Jijal granulitic gabbros are overlain northward by the Sarangar gabbro (Fig. 2). This gabbroic intrusive body is the lowest sub-unit of the 'Patan Sheared Gabbros and Diorites' unit, which is itself the lowest of the three units distinguished by Zeilinger (2002) in the Patan–Dasu metaplutonic complex (Fig. 1). Along the Indus valley, the contact between the Sarangar gabbro and the Jijal granulitic gabbro is obscured by a set of anastamosing shear zones and late faulting (Arbaret & Burg, 2003; Zeilinger, 2002; Fig. 2). To the NW of Patan the contact crops out as a dense 1–2 m thick network of gabbroic veins enclosing xenoliths of the Jijal granulitic gabbro (Zeilinger, 2002). The Sarangar gabbro is mainly composed of strongly retrogressed, coarse-grained metagabbros, locally showing a layered structure as a result of variations of mafic and felsic mineral proportions. The dominant mineralogy is hornblende, clinopyroxene and plagioclase, with rutile, epidote and garnet as accessory minerals.

Intrusive granites in the metaplutonic complex

Metre-sized bodies of intrusive granite, forming sheets and small laccoliths, mingled in places with the gabbro–diorite rocks of this complex (Zeilinger, 2002), are exposed along the Indus Valley section of the Patan–Dasu metaplutonic complex. Leucogranites composed of quartz, plagioclase, muscovite, and minor garnet, epidote, chlorite, sulfides and apatite predominate. Although locally deformed, the granites clearly intrude the more mafic rocks of the metaplutonic complex. They belong to the 'stage 1' of Petterson & Windley's (1985) classification of Kohistan granites.

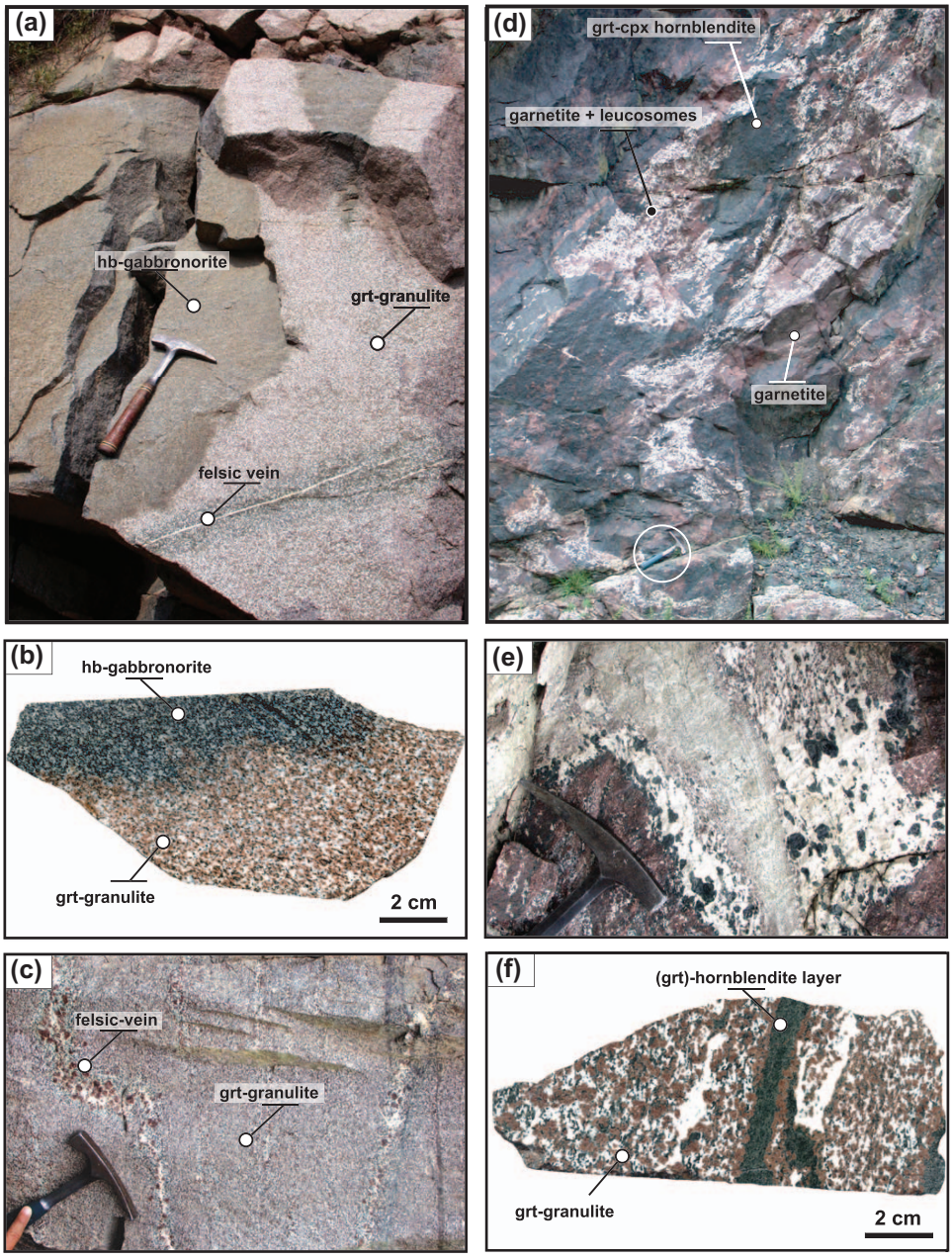

Fig. 3. (a) Transition of garnet granulite to hornblende gabbronorite in the upper part of the Jijal complex, near the village of Patan (Fig. 2), illustrating the secondary nature of the garnet granulites. (b) Hand-specimen of a Jijal composite sample illustrating the transformation of hornblende gabbronorite to garnet granulite. (c) Cross-cutting garnet-bearing felsic veins in the Jijal garnet granulite. (d) Characteristic zoning of a thick hornblendite lens in the Jijal complex. The innermost part of the lens is composed of coarse-grained hornblendite grading outward to garnet-bearing hornblendite and garnetite rims closely associated with plagioclase-rich, garnet-bearing leucosomes. (e) Close-up of the leucosome network in the outermost part of the hornblendite lens shown in (d). (f) Hand-specimen of a Jijal garnet granulite sample showing a centimeter-size hornblendite lens mantled by garnetite and hosted by garnet granulite.

GEOCHRONOLOGICAL CONSTRAINTS

In the study area, precise emplacement ages were obtained for the Patan–Dasu metaplutonic complex by high-precision U–Pb dating of zircon (Schaltegger *et al.*, 2002). The oldest ages were given by a quartz gabbro from the lower Sarangar sub-unit (98·9 ± 0·4 Ma) and by a leucogranite in the upper Kamila sequence (97·1 ± 0·2 Ma) (Fig. 1). A metadiorite from the middle Kiru

sequence was found to be slightly younger (91·8 ± 1·4 Ma) (Fig. 1). The parental magmas of these rocks were all derived from a single normal mid-ocean ridge basalt (N-MORB) mantle source based on the initial Hf isotopic signatures of zircons (Schaltegger *et al.*, 2002).

The age of granulitic metamorphism in Jijal is constrained by Sm–Nd mineral isochrons yielding cooling ages of 95·9 ± 2·6, 95·7 ± 2·7, 94·6 ± 5·3, 94·0 ± 4·7 and 91·6 ± 6·3 Ma (Yamamoto & Nakamura, 1996, 2000; Anczkiewicz & Vance, 2000; Anczkiewicz *et al.*, 2002; Fig. 1). A Lu–Hf isochron age of 94 ± 1·2 Ma was obtained for a garnet granulite, consistent with a Sm–Nd age of 95·9 ± 2·6 Ma for the same sample (Anczkiewicz *et al.*, 2002). A detailed Sm–Nd geochronological study of the gabbronorite to garnet granulite transition yielded a cooling age of 118 ± 12 Ma for the hornblende gabbronorite protolith, compared with 94·0 ± 4·7 Ma for the garnet granulite (Yamamoto & Nakamura, 2000).

The similarity of igneous ages for the Kamila sequence (99–92 Ma) and cooling ages for the Jijal granulites (96–92 Ma) suggests that the emplacement of the Kamila metaplutonic complex and the granulitic metamorphism in Jijal were roughly coeval. In this scheme, the igneous protoliths of the Jijal sequence might be somewhat older, as possibly indicated by the Sm–Nd isochron age of 118 ± 12 Ma yielded by the hornblende gabbronorite sample studied by Yamamoto & Nakamura (2000). In any case, published radiometric ages are consistent with the formation of the whole Jijal–Kamila lower-to mid-crustal sequence within the first 25 Myr of Kohistan arc evolution; i.e. during the building stage of the oceanic arc.

SAMPLING AND ROCK TYPES

All samples for this study were collected in the Indus valley, mostly along the Karakoram highway (KKH; Figs 1 and 2). The location of the ultramafic and mafic rocks sampled along the KKH, as well as the nomenclature and typical mineral assemblages for the main rock types are shown in Fig. 2 and GPS coordinates are provided in Table 1. Sampling of the Jijal section includes (1) garnet-bearing ultramafic rocks collected atop the lower ultramafic sequence (≤1 km below the paleo-Moho) and within the granulite-hosted ultramafic lenses, and (2) gabbroic rocks from the granulitic gabbro unit (Fig. 2). Ultramafic samples comprise seven garnet–hornblende pyroxenites and three garnet–pyroxene hornblendites. We further subdivided the garnet hornblende pyroxenites into garnet-poor (<15 vol. % garnet) and garnet-rich varieties depending on garnet abundance at the hand-specimen scale. Gabbroic samples from Jijal comprise 13 modally homogeneous garnet granulites and three composite samples (Fig. 3b) showing a sharp transition from the precursor hornblende gabbronorite assemblage to the garnet granulite assemblage and/or residual patches of hornblende gabbronorite in granulite. Sample KG-03 was cut and split into a garnet-free, hornblende gabbronorite sub-sample (KG-03A) and a garnet granulite sub-sample (KG-03B). Samples KG-04 and KH97-113 were too heterogeneous to be split and were, therefore, analyzed as a bulk sample. Sampling of the Sarangar gabbro comprises 11 garnet-free metagabbros, simply referred to as gabbros in the following discussion.

Figure 1 shows the location of the seven granite samples collected from the metaplutonic complex. All samples are from relatively thick (>1 m) bodies and lack traces of host rocks and/or mafic xenoliths. Samples KG-42, KG-43 and UM01-123 are fine-grained leucogranites occurring as intrusive sheets in the upper part of the Kiru sequence [the 'Madraza Amphibolite' of Zeilinger (2002)]. Sample UM01-124 is coarse-grained granite from an intrusive sheet in the upper Madraza amphibolite, close to the Kamila sequence. Elongated amphibole-rich xenoliths are noticeable in the outcrop. Samples KG-48, KG-50 and UM01-125 are coarse-grained leuco- to melanocratic granites from a thick laccolitic intrusion in the Kamila amphibolite. These granites are deformed and locally show a crenulation foliation. Sample KG-50 yielded a U–Pb zircon age of 97·1 ± 0·2 Ma (Schaltegger *et al.*, 2002).

ANALYTICAL PROCEDURES

Major and trace element analyses of the Jijal gabbroic and ultramafic rocks, Sarangar gabbros and Patan Dasu metaplutonic complex intrusive granites are given in Tables 1, 2 and 3, respectively. About 5 kg of each sample were crushed and powders were made in an agate mill. Whole-rock major elements and Zr were analyzed by X-ray fluorescence (XRF) using a Philips PW1404/10 instrument at the CIC (University of Granada, Granada, Spain). In addition, all samples were analyzed for rare earth elements (REE), U, Th, Sr, Nb, Ta, Zr, Hf, Rb and Ba on a quadrupole VG-PG2® ICP-MS at ISTEEM (Université de Montpellier 2, Montpellier, France). REE, U, Th, Sr, Zr, Hf, Rb and Ba concentrations were determined by external calibration, whereas Nb and Ta concentrations were determined using Zr and Hf, respectively, as internal standards in an analytical procedure similar to that proposed by Jochum *et al.* (1990) but adapted for inductively coupled plasma mass spectrometry (ICP-MS) analysis (see Godard *et al.*, 2000). Dissolution procedures and instrumental conditions of ICP-MS analysis at ISTEEM have been reported elsewhere (Garrido *et al.*, 2000; Godard *et al.*, 2000). The analytical

Table 1: Compositions of ultramafic and gabbroic rocks from the Jijal complex

	Garnet–clinopyroxene hornblendite			Garnet-rich hornblende pyroxenite			
Sample:	KH97-092	KH97-104	KH97-107	KH97-087	KH97-091	KH97-099	KH97-106
Lat. (°N):	35°04′25·50″	35°04′32·30″	35°05′11·89″	35°04′18·15″	35°04′21·67″	35°04′32·37″	35°04′50·33″
Long. (°E):	72°57′47·14″	72°58′07·40″	72°59′10·06″	72°57′41·28″	72°57′46·30″	72°57′47·89″	72°58′34·82″
Unit:	JPC-GHZ	JPC-GGZ	JPC-GGZ	JPC-GHZ	JPC-GHZ	JPC-GGZ	JPC-GGZ
wt %							
SiO_2	41·21	40·69	42·81	42·36	42·07	41·14	43·52
TiO_2	1·71	1·59	1·59	0·36	0·43	0·61	0·88
Al_2O_3	14·20	14·57	14·06	17·13	17·59	16·56	18·96
Fe_2O_3	14·06	15·28	12·80	17·59	17·25	17·19	15·00
MnO	0·13	0·14	0·09	0·47	0·37	0·35	0·29
MgO	12·30	11·61	12·60	11·20	11·19	9·40	6·70
CaO	12·30	11·08	12·14	12·22	11·69	12·88	11·40
Na_2O	1·89	2·35	1·82	0·23	0·08	0·42	1·41
K_2O	0·16	0·30	0·17	b.d.	b.d.	b.d.	b.d.
P_2O_5	0·02	0·02	0·02	0·01	0·03	0·02	0·03
LOI	0·63	1·85	1·41	—	—	—	—
Total	98·61	99·48	99·51	101·58	100·70	98·57	98·19
Mg-no.	63·4	60·1	66·1	55·8	56·3	52·0	47·0
ppm							
Ti		9866			2763	4067	6454
Sc*	52·0	61·0	55·0	106·0			
Sc	61·1			82·9	77·1	50·9	
V*	715	512	687	411			
V		566			398	436	416
Cr*	201	109	205	111			
Cr		60			51	27	22
Ni*	90	49	61	27			
Ni		62			38	31	24
Rb	0·531	0·993	0·527	0·051	0·030	0·050	0·055
Sr	175·3	123·9	179·0	11·1	12·6	26·8	196·8
Y	7·56	11·52	5·55	29·70	28·62	23·17	28·30
Zr	6·7	20·4	7·0	3·17	4·98	4·04	13·62
Zr*	7·5	20·0	9·0	11·22	9·2	9·7	14
Zr†							
Nb	0·31	0·45	0·28	0·03	0·07	0·03	0·21
Cs	0·07	0·02	0·02	0·03	0·01	0·03	0·02
Ba	27·34	35·66	29·57	1·38	1·20	1·15	8·08
La	0·53	0·54	0·65	0·34	0·13	0·21	0·48
Ce	2·14	2·66	2·38	1·04	0·67	0·93	1·47
Pr	0·55	0·62	0·61	0·22	0·17	0·22	0·32
Nd	3·81	4·51	4·15	1·37	1·42	1·71	2·50
Sm	1·556	1·836	1·583	0·824	1·004	1·033	1·506
Eu	0·707	0·799	0·665	0·587	0·681	0·684	0·825
Gd	2·04	2·53	1·84	2·27	2·49	2·25	3·21
Tb	0·31	0·39	0·25	0·55	0·53	0·46	0·63
Dy	1·95	2·53	1·52	5·14	4·45	3·65	4·81
Ho	0·373	0·489	0·275	1·377	1·015	0·826	1·061
Er	0·948	1·216	0·670	4·699	2·881	2·497	3·007
Tm	0·124	0·161	0·086	0·8	0·431	0·377	0·455
Yb	0·71	0·94	0·49	5·74	2·88	2·45	3·03
Lu	0·107	0·138	0·071	1·053	0·474	0·407	0·504
Hf	0·376	0·566	0·401	0·134	0·163	0·157	0·279
Hf†							
Ta	0·014	0·016	0·011	0·001	0·003	0·002	0·007
Pb	0·174	0·210	0·282	0·034	0·115	0·058	0·488
Th	0·004	0·005	0·005	0·005	0·002	0·002	0·001
U	0·004	0·003	0·003	0·007	0·002	0·004	0·004

Table 1: continued

	Garnet-poor hornblende pyroxenite			Gabbroic composite samples			
Sample:	KH97-084	KH97-086	KH97-093	KG-03-A	KG-03-B	KH97-113	KG-04
Lat. (°N):	35°04′16·02″	35°04′18·15″	35°04′25·50″	35°06′51·30″	35°06′51·30″	35°06′46·25″	35°07′41·84″
Long. (°E):	72°57′31·66″	72°57′41·28″	72°57′47·14″	72°59′59·21″	72°59′59·21″	73°00′05·81″	72°59′09·06″
Unit:	JPC-GHZ	JPC-GHZ	JPC-GHZ	JPC-GGZ	JPC-GGZ	JPC-GGZ	JPC-GGZ
wt %							
SiO_2	49·17	42·49	44·63	51·32	52·06	51·35	53·35
TiO_2	0·44	1·19	0·93	0·70	0·81	0·73	0·92
Al_2O_3	6·89	13·24	12·88	17·46	17·51	17·60	16·34
Fe_2O_3	9·35	11·62	11·36	10·51	9·91	10·59	10·09
MnO	0·13	0·09	0·12	0·19	0·17	0·19	0·17
MgO	14·04	13·40	13·40	6·08	5·22	5·34	4·56
CaO	20·65	13·26	14·97	10·03	9·64	9·83	9·84
Na_2O	0·32	1·63	1·06	1·85	2·57	2·71	2·05
K_2O	b.d.	0·05	0·02	0·22	0·38	0·27	0·49
P_2O_5		0·00	0·01	0·05	0·07	0·08	0·16
LOI	0·17	1·48	0·16	0·58	0	0·13	0·64
Total	101·16	98·45	99·55	98·99	98·34	98·80	98·61
Mg-no.	74·9	69·6	70·0	53·4	51·1	50·0	47·3
ppm							
Ti				2878	4216		5387
Sc*	70·0	46·0	54·0			27·0	
Sc				34·3	33·6		34·8
V*	589	737	695			271	
V				230	262		276
Cr*	767	867	747			65	
Cr				244	82		170
Ni*	94	211	172			21	
Ni				37	21		27
Rb	0·040	0·528	0·139	0·626	1·004	1·415	2·879
Sr	17·8	86·7	57·9	265·0	286·9	255·2	202·9
Y	4·26	6·40	7·49	12·30	15·12	15·62	22·05
Zr	2·35	2·21	2·25	16·6	29·3	19·7	31·5
Zr*	b.d.	b.d.	b.d.	25·9	36·3	22·0	44·8
Zr†				21·8	34·0		
Nb	0·03	0·14	0·09	0·43	1·03	0·86	1·54
Cs	0·02	0·17	0·01	0·04	0·03	0·02	0·15
Ba	0·78	51·6	8·53	91·7	155	105	129
La	0·21	0·34	0·28	3·16	5·05	3·32	6·03
Ce	0·64	1·02	0·87	7·22	11·50	7·42	16·39
Pr	0·18	0·28	0·23	1·01	1·56	0·99	2·44
Nd	1·28	1·96	1·62	5·20	7·69	5·14	12·65
Sm	0·667	1·029	0·850	1·596	2·241	1·521	3·675
Eu	0·349	0·571	0·487	0·692	0·843	0·737	1·143
Gd	1·06	1·67	1·42	2·14	2·88	2·01	4·43
Tb	0·18	0·27	0·25	0·37	0·50	0·35	0·72
Dy	1·17	1·66	1·71	2·68	3·54	2·54	4·92
Ho	0·218	0·306	0·354	0·576	0·746	0·543	1·022
Er	0·533	0·741	0·949	1·704	2·252	1·645	2·975
Tm	0·0713	0·096	0·1362	0·255	0·332	0·251	0·432
Yb	0·40	0·55	0·87	1·74	2·26	1·65	2·89
Lu	0·057	0·082	0·135	0·284	0·363	0·280	0·470
Hf	0·175	0·162	0·161	0·619	1·098	0·691	1·213
Hf†				0·772	1·193		
Ta	0·001	0·011	0·003	0·031	0·079	0·043	0·081
Pb	0·015	0·217	0·109	1·545	5·155	1·564	2·131
Th	0·001	0·022	0·002	0·056	0·098	0·115	0·156
U	0·001	0·006	0·002	0·023	0·040	0·044	0·050

	Garnet granulite (type 2)		Garnet granulite (type 1)				
Sample:	KH97-108	KG-01	KH97-095	KH97-100	KH97-101	KH97-102	KH97-103
Lat. (°N):	35°05′57·69″	35°06′43·78″	35°04′28·16″	35°04′32·37″	35°04′32·37″	35°04′37·72″	35°04′33·81″
Long. (°E):	72°59′12·18″	72°89′55·90″	72°57′47·07″	72°57′47·89″	72°57′47·89″	72°57′48·23″	72°58′05·04″
Unit:	JPC-GGZ	JPC-GGZ	JPC-GGZ	JPC-GGZ	JPC-GGZ	JPC-GGZ	JPC-GGZ
wt %							
SiO_2	50·72	53·80	46·48		53·08	44·17	41·15
TiO_2	0·77	0·81	0·76		0·78	0·93	0·84
Al_2O_3	17·81	17·57	19·32		17·68	19·43	20·37
Fe_2O_3	11·69	10·51	13·37		11·76	14·30	15·53
MnO	0·19	0·19	0·22		0·22	0·24	0·32
MgO	5·75	4·32	6·15		4·76	6·59	6·43
CaO	10·51	8·88	11·49		9·38	12·41	13·31
Na_2O	1·96	2·41	1·20		2·10	1·02	1·04
K_2O	0·23	0·12	0·04		0·08	0·05	0·02
P_2O_5	0·08	0·14	0·05		0·12	0·11	0·04
LOI	0·02	0·45	0·46		0·04	0·59	0·37
Total	99·73	99·20	99·53	—	100·00	99·83	99·42
Mg-no.	49·4	44·9	47·7		44·5	47·8	45·1
ppm							
Ti		3155		6988			
Sc*	32·0		42·0		32·0	43·0	46·0
Sc		32·7		47·6			
V*	357		406		283	438	270
V		226		354			
Cr*	103		59		38	75	77
Cr		160		14			
Ni*	27		18		10	18	11
Ni		17		16			
Rb	0·286	0·167	0·596	0·333	0·328	0·224	
Sr	217·8	266·3	242·5	377·7	225·9	295·7	
Y	18·96	13·97	9·02	16·68	12·76	15·64	
Zr	18·4	11·4	7·1	17·39	7·8	9·8	
Zr*	16·5	24·5	8·4		9·3	9·3	12
Zr†							
Nb	1·02	0·61	0·29	0·66	0·54	0·65	
Cs	0·08	0·02	0·09	0·05	0·04	0·06	
Ba	89·9	101·1	32·14	50·4	68·8	25·32	
La	3·30	4·47	1·54	2·63	2·62	2·17	
Ce	8·01	10·80	3·62	6·44	5·73	5·50	
Pr	1·11	1·53	0·59	0·95	0·90	0·83	
Nd	5·83	7·86	3·02	5·23	4·52	4·73	
Sm	1·795	2·252	1·033	1·682	1·486	1·526	
Eu	0·677	0·925	0·593	0·995	0·835	0·869	
Gd	2·47	2·96	1·49	2·45	2·22	2·11	
Tb	0·44	0·49	0·26	0·42	0·38	0·37	
Dy	3·13	3·41	1·87	3·08	2·69	2·62	
Ho	0·660	0·711	0·410	0·651	0·571	0·558	
Er	1·967	2·086	1·210	1·794	1·678	1·665	
Tm	0·292	0·304	0·184	0·268	0·2462	0·247	
Yb	1·89	1·98	1·24	1·78	1·62	1·61	
Lu	0·311	0·327	0·209	0·295	0·274	0·271	
Hf	0·720	0·489	0·288	0·430	0·316	0·404	
Hf†							
Ta	0·052	0·044	0·017	0·032	0·026	0·035	
Pb	1·666	1·938	0·595	11·350	1·002	0·702	
Th	0·019	0·025	0·004	0·011	0·028	0·005	
U	0·023	0·011	0·015	0·011	0·013	0·006	

Table 1: continued

	Garnet granulite (type 1)				
Sample:	KH97-105	KH97-109	KH97-110	KH97-111	KH97-114
Lat. (°N):	35°04′42·61″	35°06′44·15″	35°06′45·31″	35°06′45·31″	35°06′46·25″
Long. (°E):	72°58′29·44″	72°59′54·72″	72°59′55·62″	72°59′55·62″	73°00′05·81″
Unit:	JPC-GGZ	JPC-GGZ	JPC-GGZ	JPC-GGZ	JPC-GGZ
wt %					
SiO_2	51·40	50·75	47·87	48·95	52·40
TiO_2	0·78	0·71	0·65	0·72	0·82
Al_2O_3	18·21	17·87	19·09	18·73	17·87
Fe_2O_3	12·65	10·90	11·26	11·35	11·01
MnO	0·23	0·20	0·20	0·20	0·20
MgO	5·14	5·44	6·59	5·99	5·76
CaO	9·56	10·11	11·28	11·04	9·80
Na_2O	1·87	2·26	1·91	2·08	1·62
K_2O	0·10	0·28	0·08	0·04	0·16
P_2O_5	0·11	0·06	0·02	0·03	0·10
LOI	—	0·82	0·71	—	2·63
Total	100·07	99·40	99·66	99·13	102·37
Mg-no.	44·6	49·7	53·7	51·1	50·9
ppm					
Ti		4317	4395	4799	
Sc*	34·0		41·0	30·0	33·0
Sc		33·5	43·8	41·2	
V*	321		300	247	289
V		263	396	419	
Cr*	48		84	87	81
Cr		29	55	54	
Ni*	13		28	19	23
Ni		25	37	29	
Rb	0·175	0·813	0·225	0·064	0·617
Sr	225·9	241·1	298·5	320·2	261·1
Y	15·89	13·00	8·81	10·25	16·10
Zr	11·9	15·0	6·4	7·4	22·83
Zr*	16·9	22·3	14·0	14·0	25·93
Zr†			7·4	9·1	
Nb	1·25	0·54	0·18	0·28	1·09
Cs	0·02	0·04	0·01	0·01	0·02
Ba	75·7	100	39·2	40·57	97·2
La	3·41	2·40	1·06	1·06	3·61
Ce	7·56	5·45	2·39	2·51	8·21
Pr	1·17	0·76	0·35	0·39	1·11
Nd	5·73	3·93	2·01	2·30	5·73
Sm	1·858	1·220	0·718	0·831	1·680
Eu	0·884	0·749	0·515	0·626	0·836
Gd	2·69	1·78	1·08	1·25	2·24
Tb	0·46	0·32	0·19	0·23	0·39
Dy	3·30	2·34	1·43	1·67	2·81
Ho	0·706	0·502	0·312	0·365	0·589
Er	2·049	1·425	0·931	1·092	1·791
Tm	0·3024	0·222	0·143	0·168	0·268
Yb	2·01	1·47	0·94	1·12	1·76
Lu	0·340	0·249	0·160	0·190	0·295
Hf	0·448	0·420	0·258	0·302	0·859
Hf†			0·270	0·315	
Ta	0·060	0·030	0·010	0·015	0·061
Pb	1·400	1·383	0·526	0·550	1·493
Th	0·017	0·070	0·006	0·002	0·062
U	0·011	0·028	0·004	0·002	0·026

LOI, loss on ignition. JPC-GHZ, garnet hornblendite and garnet pyroxenite zone of the Jijal complex; JPC-GGZ, garnet granulite zone of the Jijal complex (see Fig. 2). b.d., below detection limit.
*XRF measurements on sample powder pressed pellets.
†Solution ICP-MS analyses of combined $Li_2B_4O_7$ melting and $HF–HNO_3$ dissolution attacks.

Table 2: Compositions of Sarangar gabbros

Sample:	KH97-115	KH97-116	KH97-117	KH97-118	KH97-119	UM01-120	KG-07	KG-08	KG-09	KG-10	KG-11
Lat. (°N):	35°06′56·12″	35°07′04·46″	35°07′15·64″	35°07′10·55″	35°07′07·96″	35°07′36·0″	35°07′07·28″	35°07′14·23″	35°06′59·54″	35°07′12·54″	35°06′58·90″
Long. (°E):	73°00′26·02″	73°00′46·26″	73°01′16·20″	73°01′54·89″	73°02′22·84″	73°02′53·1″	73°00′52·38″	73°01′22·73″	73°01′38·78″	73°01′35·58″	73°01′45·16″
Unit:	PAT-GBS	PAT-GBS	PAT-GBS	PAT-GBS	PAT-GBS	PAT-GBS	PAT-GBS	PAT-GBS	PAT-GBS	PAT-GBS	PAT-GBS
wt %											
SiO_2	48·18	51·62	53·66	53·15	51·99	51·17	52·14	49·80	53·91	52·49	53·49
TiO_2	0·71	0·89	0·79	1·05	0·69	1·48	0·82	0·81	0·95	0·80	0·84
Al_2O_3	18·22	16·60	17·08	16·70	18·19	17·10	17·49	17·65	19·28	17·57	16·62
Fe_2O_3	11·41	10·39	9·97	9·95	10·18	12·01	10·07	11·46	10·55	9·65	10·15
MnO	0·18	0·18	0·19	0·16	0·18	0·20	0·17	0·19	0·16	0·16	0·17
MgO	6·18	5·15	4·92	4·81	5·57	4·35	5·52	5·90	4·68	5·03	4·93
CaO	10·95	9·46	9·32	9·45	10·46	9·26	9·78	10·47	10·17	9·62	9·10
Na_2O	2·14	3·76	2·43	2·41	1·96	2·56	2·09	1·73	2·26	2·27	2·32
K_2O	0·29	0·69	0·38	0·45	0·31	0·30	0·49	0·44	0·24	0·41	0·34
P_2O_5	0·03	0·18	0·14	0·17	0·08	0·36	0·11	0·06	0·13	0·21	0·09
LOI	1·12	1·27	0·63	1·12	0·04	1·20	0·90	0·61	0·63	0·87	1·08
Total	99·41	100·18	99·50	99·42	99·65	99·99	99·58	99·12	102·96	99·08	99·13
Mg-no.	51·8	49·6	49·5	48·9	52·0	41·8	52·1	50·5	46·8	50·8	49·1
ppm											
Ti				6150		8443	4993	4856	4486	3674	4081
Sc*	38·0	37·0	34·0	33·0	25·0	32·0					
Sc				32·7		35·7	32·4	34·8	26·9	34·0	32·7
V*	245	262	253	221	250	272					
V				246		300	249	270	266	235	301
Cr*	80	79	73	61	94	57					
Cr				42		29	176	88	121	105	94
Ni*	20	23	19	16	19	13					
Ni				16		15	30	24	18	22	20
Rb	1·507	3·710	1·605	2·511	2·85	1·10	2·77	3·20	0·967	3·36	1·02
Sr	253·4	234·9	242·5	237·7	232·0	358·3	292·8	291·0	265·6	271·8	256·1
Y	12·27	20·77	20·71	18·62	15·74	32·52	15·04	15·55	15·46	16·16	14·38
Zr	18·9	8·9	6·9	8·0	24·4	7·1	19·3	21·0	7·6	5·8	8·2

Sample:	KH97-115	KH97-116	KH97-117	KH97-118	KH97-119	UM01-120	KG-07	KG-08	KG-09	KG-10	KG-11
Lat. (°N):	35°06′56·12″	35°07′04·46″	35°07′15·64″	35°07′10·55″	35°07′07·96″	35°07′36·0″	35°07′07·28″	35°07′14·23″	35°06′59·54″	35°07′12·54″	35°06′58·90″
Long. (°E):	73°00′26·02″	73°00′46·26″	73°01′16·20″	73°01′54·89″	73°02′22·84″	73°02′53·1″	73°00′52·38″	73°01′22·73″	73°01′38·78″	73°01′35·58″	73°01′45·16″
Unit:	PAT-GBS	PAT-GBS	PAT-GBS	PAT-GBS	PAT-GBS	PAT-GBS	PAT-GBS	PAT-GBS	PAT-GBS	PAT-GBS	PAT-GBS
Zr*	25·0	48·2	38·9	43·0	31·8	66·0	44·1	49·0	43·3	42·7	35·8
Zr†	24·9	47·8		48·8		66·5					
Nb	0·87	2·04	2·16	1·78	1·22	3·05	1·24	0·97	1·11	0·76	0·60
Cs	0·02	0·24	0·06	0·11	0·09	0·08	0·16	0·12	0·06	0·08	0·09
Ba	108	233	156	139	120	143	138	185	80·5	115	71·7
La	3·68	7·65	8·32	6·65	4·43	12·07	5·59	5·24	5·49	6·41	4·18
Ce	7·64	16·45	17·94	15·48	10·22	29·06	13·06	11·87	12·65	15·31	9·77
Pr	1·12	2·39	2·55	2·10	1·34	3·99	1·73	1·58	1·70	2·06	1·36
Nd	5·21	10·91	11·36	10·27	6·70	19·73	8·34	7·71	8·40	10·12	6·75
Sm	1·539	2·995	2·991	2·804	1·844	5·342	2·248	2·180	2·376	2·733	1·985
Eu	0·768	1·083	1·062	1·089	0·731	1·558	0·812	0·863	0·929	1·063	0·793
Gd	2·09	3·76	3·69	3·66	2·34	6·51	2·86	2·81	3·06	3·38	2·60
Tb	0·36	0·62	0·61	0·61	0·39	1·04	0·48	0·48	0·50	0·55	0·45
Dy	2·55	4·32	4·26	4·16	2·79	7·10	3·33	3·35	3·49	3·80	3·14
Ho	0·547	0·920	0·905	0·865	0·581	1·459	0·693	0·707	0·728	0·779	0·659
Er	1·620	2·618	2·580	2·510	1·714	4·223	2·039	2·134	2·135	2·268	1·914
Tm	0·2472	0·3939	0·3946	0·366	0·255	0·596	0·297	0·31	0·307	0·32	0·275
Yb	1·62	2·53	2·59	2·41	1·65	3·95	1·99	2·14	1·99	2·16	1·85
Lu	0·276	0·417	0·425	0·387	0·273	0·634	0·325	0·343	0·325	0·346	0·295
Hf	0·675	0·519	0·441	0·495	0·929	0·454	0·831	0·838	0·481	0·393	0·452
Hf†	0·771	1·409		1·370		1·932					
Ta	0·047	0·112	0·118	0·122	0·071	0·190	0·094	0·071	0·083	0·057	0·041
Pb	1·470	6·566	3·266	2·876	1·952	2·846	3·063	2·510	2·304	2·753	1·703
Th	0·116	0·264	0·132	0·415	0·290	0·398	0·208	0·118	0·290	0·669	0·170
U	0·045	0·083	0·047	0·133	0·078	0·133	0·063	0·047	0·086	0·185	0·092

LOI, loss on ignition. PAT-GAB, Sarangar gabbros of the Patan Sheared gabbro unit (see Fig. 2).
*XRF measurements on sample powder pressed pellets.
†Solution ICP-MS analyses of combined $Li_2B_4O_7$ melting and HF–HNO_3 dissolution attacks.

Table 3: Compositions of intrusive leucogranites in the Patan Dasu metaplutonic complex

	Type 1 granites				Type 2 granites		
Sample:	UM01-124	UM01-125	KG-48	KG-50	KG-43	UM01-123	KG-42
Lat. (°N):		35°14′38·60″	35°14′15·47″	35°14′30·62″	35°13′07·28″	35°13′03·80″	35°02′46·90″
Long. (°E):		73°12′12·4″	73°10′36·08″	73°10′42·49″	73°09′01·48″	73°09′05·7″	72°56′48·80″
Unit:	KIR-AMMA	KAM-GR	KAM-GR	KAM-GR	KIR-AMKI	KIR-AMMA	KIR-AMMA
wt %							
SiO_2	64·72	71·20	74·03	67·88	74·80	74·09	74·35
TiO_2	0·38	0·22	0·11	0·21	0·05	0·03	0·05
Al_2O_3	17·40	15·37	14·88	16·56	14·66	14·87	14·95
Fe_2O_3	3·85	2·61	1·44	2·61	1·00	0·91	1·21
MnO	0·10	0·07	0·03	0·06	0·22	0·15	0·18
MgO	1·32	0·73	0·54	0·86	0·25	0·26	0·27
CaO	5·84	3·38	2·81	4·52	2·13	1·80	2·20
Na_2O	3·48	3·77	4·35	3·88	3·13	2·90	3·56
K_2O	0·90	1·28	0·75	1·15	1·86	2·28	1·57
P_2O_5	0·13	0·05	0·03	0·09	0·05	0·04	0·07
LOI	1·60	1·18	0·89	1·54	0·99	1·22	0·97
Total	99·72	99·86	99·86	99·36	99·14	98·55	99·38
Mg-no.	40·5	35·7	42·7	39·5	33·1	36·2	30·6
ppm							
Ti	1500	872	562	1415	222	236	257
Sc*	7·0	3·0				3·0	
Sc	3·1	0·6	0·7	2·2	1·6	1·5	1·4
V*	41	25				21	
V	35	11	12	30	9·3	6·2	4·8
Cr*	27	27				24	
Cr	5	1	47	39	105	1	209
Ni*	2					2	
Ni	3	1	3	3	6	1	9
Rb	33·5	48·7	22·3	44·0	53·206	63·6	50·4
Sr	386·2	364·2	289·4	331·9	147·8	153·9	206·2
Y	5·75	2·84	1·02	2·59	13·33	8·02	9·79
Zr	3·0	3·7	5·5	14·4	6·0	2·6	2·9
Zr*	78·0	70·0	89·7	73·7	47·5	38·0	42·0
Zr†	92·4					38·1	
Nb	2·50	5·55	1·03	1·82	6·88	7·12	5·89
Cs	0·43	0·48	0·31	0·51	0·98	1·13	1·12
Ba	431	889	343	516	773	841	853
La	10·53	50·86	2·81	10·97	6·95	6·38	8·35
Ce	21·05	93·72	5·15	20·32	14·58	13·30	17·25
Pr	2·35	8·29	0·55	2·02	1·67	1·53	1·94
Nd	9·64	28·80	2·17	7·44	6·56	6·17	7·61
Sm	1·943	3·429	0·376	1·109	1·687	1·459	1·624
Eu	0·768	0·815	0·257	0·582	0·275	0·294	0·354
Gd	1·80	2·02	0·32	0·90	1·98	1·67	1·70
Tb	0·23	0·19	0·04	0·10	0·35	0·25	0·26
Dy	1·36	0·78	0·23	0·54	2·41	1·54	1·79
Ho	0·252	0·113	0·042	0·095	0·448	0·270	0·346
Er	0·693	0·253	0·124	0·259	1·280	0·743	1·009
Tm	0·099	0·032	0·02	0·036	0·195	0·112	0·16
Yb	0·68	0·22	0·13	0·24	1·37	0·83	1·11
Lu	0·113	0·039	0·024	0·041	0·219	0·137	0·193
Hf	0·144	0·132	0·202	0·243	0·372	0·183	0·137
Hf†	2·363					1·728	
Ta	0·170	0·210	0·061	0·091	0·750	0·747	0·650
Pb	3·248	5·080	2·813	2·595	8·222	11·901	15·647
Th	2·208	13·956	0·418	2·082	1·600	1·610	2·051
U	0·450	0·774	0·043	0·315	0·535	0·359	0·559

LOI, loss on ignition. KIR-AMMA, Madraza amphibolite unit from the Kiru sequence; KAM-GR, granite unit from the Kamila sequence; KIR-AMKI, Kiru amphibolites from the Kiru sequence (see Fig. 1).
*XRF measurements on sample powder pressed pellets.
†Solution ICP-MS analyses of combined $Li_2B_4O_7$ melting and $HF–HNO_3$ dissolution attacks.

reproducibility of the international standard UB-(n) is in the range 13–20% for Nb, Ta and U and <10% for the rest of the trace elements (Garrido *et al.*, 2000). For the international standard PCC-1 (Godard *et al.*, 2000), it is in the range of 2–15% for all elements but Ta (19%).

For the Jijal gabbroic and ultramafic rocks (Table 1), Zr contents determined by ICP-MS by following the ISTEEM dissolution procedure (combining HF–$HClO_4$–HNO_3) are in good agreement with XRF values obtained on fused beads of sample powders. For the Sarangar gabbro and intrusive granite, ICP-MS values for Zr are systematically lower than the XRF values (Table 1), suggesting that the ISTEEM procedure failed to dissolve accessory minerals. To further assess the accuracy of our ICP-MS Zr and Hf data, powders of selected samples were mixed with $Li_2B_4O_7$ flux, placed into a carbon crucible and fused in a muffle furnace. The fusion beads were ground and analyzed by ICP-MS using the conventional ISTEEM dissolution procedure (Garrido *et al.*, 2000; Godard *et al.*, 2000). Zr data obtained by the combined melting–dissolution procedure agree well with the XRF data (Table 1). In the light of these results, but only for the Sarangar gabbro and granite samples, we use the Zr data obtained by XRF and/or, when available, Zr and Hf data obtained by ICP-MS analysis of fused beads in the following sections.

COMPOSITIONAL VARIATIONS OF THE JIJAL AND SARANGAR ROCKS

Jijal and Sarangar gabbroic rocks

Major elements

Figure 4 shows the variation of whole-rock major elements relative to Mg-number [$100 \times MgO/(MgO + FeO_{Total})$ on a molar basis] for the Jijal and Sarangar gabbroic rocks, in conjunction with published data for the Jijal hornblende gabbronorite and garnet granulite (Yamamoto & Yoshino, 1998). We have also plotted on this figure the compositions of gabbroic rocks from fast- and slow-spreading mid-ocean ridges (MORs), island arc (IA) complexes, and ultramafic (garnet pyroxenite and garnet hornblendite) and granulite xenoliths from the Sierra Nevada Batholith, USA (CA; continental arc).

The SiO_2 contents of the Jijal and Sarangar gabbroic rocks (Fig. 4) show that the lowermost Kohistan arc-crust has, on average, a basaltic to basaltic–andesitic composition (Miller & Christensen, 1994). Considering this mafic bulk composition, a striking feature of the Jijal and Sarangar gabbroic rocks is their rather low Mg-number (42–55; mean = 49 ± 2). Their Mg-number and SiO_2 range are similar to those of evolved island arc basalts and MORB (see Kelemen *et al.*, 2003*a*, fig. 1, p. 597). In arc settings, where most basalts have low FeO contents, such low Mg-numbers are comparable only with that of Fe–Ti-oxide–hornblende gabbros from the Tanzawa complex (Honshu arc) and other oceanic arc plutonic complexes (e.g. Whalen, 1985; Muir *et al.*, 1995), and with that of the more evolved gabbros in the Tonsina–Talkeetna complex (DeBari & Coleman, 1989; Greene *et al.*, 2006) (Fig. 4). Low Mg-numbers are also characteristic of mafic granulite xenoliths in Cordilleran batholiths (Fig. 4). In MOR settings, a comparably low Mg-number is mostly found in slow-spreading MOR gabbros (Fig. 4). There, oxide-bearing gabbros crop out in a dissimilar manner to the Kohistan gabbros, as they occur as intrusions within serpentinized peridotite tectonites (e.g. Cannat, 1993; Cannat *et al.*, 1997; Dick *et al.*, 2000). In addition, slow-spreading MOR oxide gabbros exhibit statistically higher Mg-numbers than the Kohistan gabbros for the same range of SiO_2 content (Fig. 4). The unusually low Mg-number of the Kohistan lower crust gabbroic rocks indicates that their parental basaltic melts were not primitive (Mg-number >60), implying that they had fractionated large amounts of ultramafic minerals either in the lower arc crust (e.g. Kay & Kay, 1985; Jull & Kelemen, 2001; Müntener *et al.*, 2001, and references therein; Kelemen *et al.*, 2003*a*; Greene *et al.*, 2006) or in the lithospheric mantle.

The Jijal and Sarangar gabbroic have high Al_2O_3 contents (16·3–20·4 wt %; Fig. 4). At least for the Sarangar gabbros, which have trace element compositions similar to island arc basalts (IAB), these high Al_2O_3 contents are not due to plagioclase accumulation but are a primary characteristics of the parental melts. Jijal and Sarangar gabbros display similar Al_2O_3 contents to Tanzawa and Talkeetna IA gabbros and greater contents than MOR gabbros and CA granulite xenoliths (Fig. 4). High Al_2O_3 contents are an attribute of evolved arc magmas (*c.* 15–20 Al_2O_3 wt % for Mg-number range 40–50; e.g. Beard, 1986; Beard & Day, 1986), as their rather high H_2O contents (*c.* >2 wt %) inhibit plagioclase crystallization (e.g. Baker & Eggler, 1983; Sisson & Grove, 1993*a*; Müntener *et al.*, 2001). Evolved MORB contain substantially lower Al_2O_3 contents for the same Mg-number range (see Kelemen *et al.*, 2003*a*, fig. 1 and p. 600).

The FeO_T contents of the Jijal and Sarangar gabbros are high (8·2–12·9 wt %; Fig. 4) and slightly higher than in evolved island arc volcanic rocks (FeO_T <10 wt % for the same Mg-number range; Kelemen *et al.*, 2003*a*). For the same Mg-number range, Jijal–Sarangar FeO_T contents are similar to those of gabbros in IA complexes and granulite xenoliths in CA batholiths (Fig. 4). High FeO_T for similarly low Mg-number are also distinctive of slow-spreading MOR gabbros (Fig. 4). The Jijal–Sarangar gabbros exhibit a restricted range of

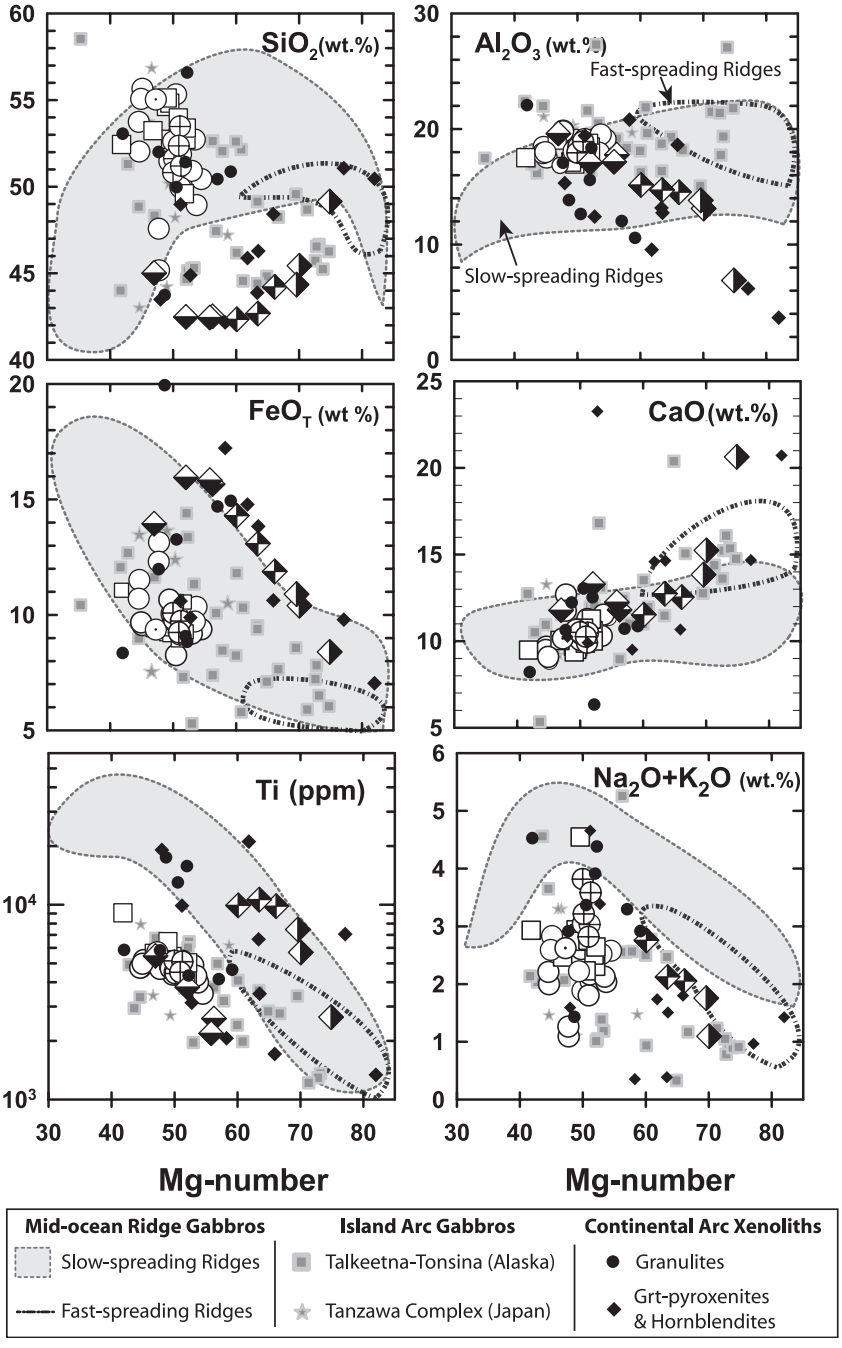

Fig. 4. Major element variations vs Mg-number [= 100 × MgO/(MgO + FeO_T) on a molar basis] for the gabbroic and ultramafic rocks of the Jijal and Sarangar complexes. Symbols for Kohistan samples (not provided in the legend) are as in Fig. 2. Kohistan data include Jijal gabbroic samples reported by Yamamoto & Yoshino (1998). Also shown are oceanic gabbroic rocks of island arc and mid-ocean ridge settings, and granulitic and ultramafic xenoliths from the Sierra Nevada batholith. Data sources are as follows. Slow-spreading mid-ocean ridges: gabbroic rocks (olivine gabbro, gabbro, oxide gabbro and oxide gabbronorite; $n = 155$) and troctolite ($n = 11$) from the South-West Indian Ridge drilled at ODP Leg 176 site 735B (Dick *et al.*, 1999) and strip-sampling data from the same site (Hart *et al.*, 1999). Gabbros from the Mid-Atlantic Ridge drilled in ODP Leg 153 (Cannat *et al.*, 1995) (mainly oxide gabbro; $n = 19$). Fast-spreading mid-ocean ridges: gabbroic rocks from the Kafhifah massif [see Garrido *et al.* (2001) for modes and sample location] of the Oman ophiolite (P. B. Kelemen & C. J. Garrido, unpublished data, 1998) (mainly olivine gabbro; $n = 43$). Island arc plutonic rocks: hornblende gabbronorite from the Tanzawa plutonic complex (Central Japan) (Kawate & Arima, 1998) (only the gabbroic suite; $n = 8$). Gabbroic rocks from the Talkeetna paleo-arc section (south–central Alaska, USA) (gabbro, $n = 2$; gabbronorite, $n = 24$; hornblende gabbronorite, $n = 1$; garnet gabbro, $n = 3$) (Greene *et al.*, 2006). Continental arc xenoliths: granulitic xenoliths and ultramafic xenoliths (eclogite, garnet websterite and amphibolite) from the Sierra Nevada Batholith (California, USA) (Ducea & Saleeby, 1996, 1998*a*, 1998*b*; Ducea, 2002). All data are plotted on an anhydrous basis.

variation in CaO (8·7–13·3 wt %; Fig. 4), which is similar to the range in evolved IAB, and fast-spreading and slow-spreading MOR gabbros (Fig. 4).

Ti and $Na_2O + K_2O$ contents clearly discriminate Kohistan gabbros from MOR gabbros. As with other IA gabbros with similar Mg-number (Fig. 4), the Jijal–Sarangar gabbros have very low Ti contents (0·6–1·5 wt %; mean = 0·8 wt %). The Ti content of IAB is highly variable, exhibiting a maximum (*c.* 3 wt %) at an Mg-number of *c.* 50 and decreasing at lower Mg-number (see Kelemen *et al.*, 2003*a*, fig. 1, p. 597). The Ti content of the Jijal–Sarangar gabbros is in the same range as evolved IAB with Mg-number of 50, but substantially lower than evolved MORB (*c.* 1·5–3 wt %; see Kelemen *et al.*, 2003*a*, fig. 1, p. 600) and MOR gabbros with similar Mg-number (Fig. 4).

There are no statistically significant differences between the Jijal and Sarangar gabbroic rocks for most major and transition elements. The only significant difference is the higher K_2O content of the Sarangar gabbros, which is double that of the Jijal gabbroic rocks (0·40 ± 0·1 wt % for Sarangar, $n = 11$; 0·20 ± 0·1 wt % for Jijal, $n = 26$). The Sarangar gabbro and Jijal hornblende gabbronorite have $Na_2O + K_2O$ contents similar to other IA plutonic rocks and lower than MOR gabbros (Fig. 4). Low K_2O and Na_2O discriminate Jijal garnet granulites (K_2O wt % = 0·12 ± 0·09; Na_2O wt % = 1·8 ± 0·5; $n = 12$) from the Jijal hornblende gabbronorites (K_2O wt % = 0·30 ± 0·05; Na_2O wt % = 2·9 ± 0·4; $n = 12$), which have comparable contents of these elements to the Sarangar gabbro. Jan & Howie (1981) interpreted this difference in terms of crystal fractionation control on the composition of the igneous protolith of the Jijal garnet granulites. Yamamoto & Yoshino (1998) have argued that the differing alkali contents of the Jijal hornblende gabbronorites and the garnet granulites was caused by dehydration reactions. Alkali depletion is a common characteristic of garnet granulites from continental terranes and crustal xenoliths (Heier, 1973; Taylor & McLennan, 1985, and references therein; Rudnick & Presper, 1990; Rudnick, 1992).

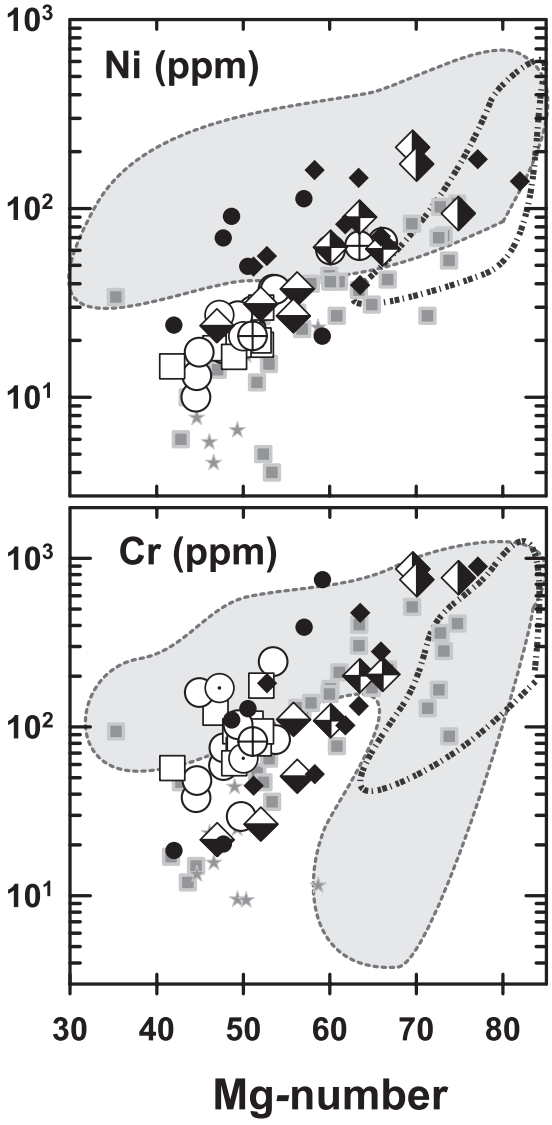

Fig. 5. Ni and Cr variations vs Mg-number for the gabbroic and ultramafic rocks of the Jijal and Sarangar complexes. Also shown are oceanic gabbros from island arcs and mid-ocean ridge settings, and granulitic and ultramafic xenoliths from the Sierra Nevada batholith (see Fig. 4 for symbols and data sources). Ni data for Kohistan samples are solution ICP-MS analyses or, where not available, XRF analyses, whereas Cr data correspond to XRF analyses or, where not available, to solution ICP-MS analyses.

Transition elements

The Jijal and Sarangar gabbroic rocks exhibit very similar transition element contents (Tables 1 and 2). Their Ni contents are very low (18·6 ppm on average), in the range of evolved IA basalts and gabbros (Fig. 5), but lower than those of MOR gabbros. Ni is positively correlated with Mg-number, probably as a result of olivine fractionation (Fig. 5). The Cr content of the Jijal–Sarangar gabbros is in the same range as that of other evolved IA gabbros and is positively correlated with Mg-number (Fig. 5). Relative to MOR gabbros, the higher Cr content for a given Mg-number of the Jijal–Sarangar gabbros probably indicates accumulation of Fe–Ti-oxides. Many MOR gabbros show a similar correlation but follow a trend with a different slope, with oxide gabbros mostly plotting off the trend.

The Jijal–Sarangar gabbros have high V (Fig. 6) and Sc (Table 1) contents for a given Ti content. Jijal garnet granulites exhibit higher V contents than the Jijal hornblende gabbronorite and Sarangar gabbros (Fig. 6).

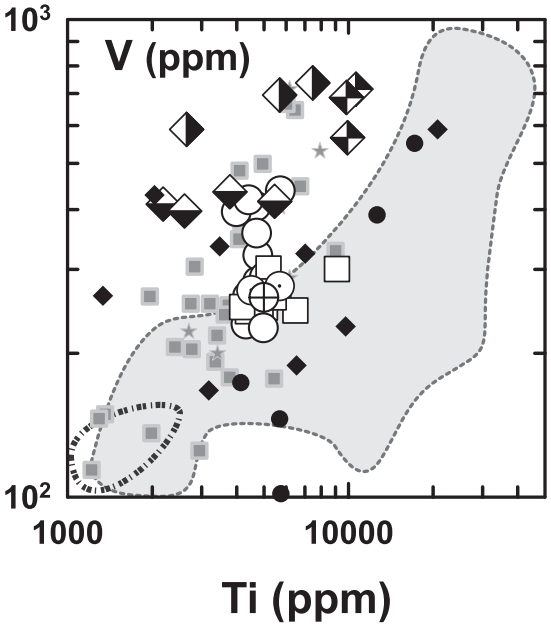

Fig. 6. Ti vs V for gabbroic and ultramafic rocks of the Jijal and Sarangar complexes. Sample symbols are as in Fig. 2. Also shown are oceanic gabbros from island arcs and mid-ocean settings (active settings and on-land exposures), and granulitic and ultramafic xenoliths from the Sierra Nevada batholith (see Fig. 4 for symbols and data sources). Ti and V data for Kohistan samples are solution ICP-MS analyses or, where not available, XRF analyses.

As the garnet granulites have similar Ti and Cr contents to the garnet-free gabbros (Figs 5 and 6), higher V contents for the garnet granulites cannot be due to oxide accumulation and may indicate the presence of accumulated or restitic igneous garnet in these rocks.

Rare earth elements (REE)

The chondrite-normalized REE patterns of the Sarangar gabbros are enriched in LREE with variable REE abundances ($6{\cdot}6 \leq Yb_N \leq 16{\cdot}0$; $8{\cdot}3 \leq La_N \leq 27{\cdot}1$; where N indicates chondrite normalized) (Fig. 7). Sarangar gabbro patterns are characterized by relatively flat middle REE (MREE) to heavy REE (HREE) ($0{\cdot}97 \leq Gd_N/Yb_N \leq 1{\cdot}24$), and LREE enrichment relative to the MREE ($1{\cdot}2 \leq La_N/Sm_N \leq 1{\cdot}6$). For similar REE abundances, the Sarangar REE patterns are similar to those of Jijal hornblende gabbronorite KG-03-B and garnet granulite KG-01 (Fig. 7). Sarangar gabbros with the lowest REE and silica abundances display subtle positive Eu anomalies [$Eu^* = 1{\cdot}28$; $Eu^* = 2 \times Eu_N/(Sm_N + Gd_N)$] indicative of plagioclase accumulation (Fig. 7), but most Sarangar samples display slight positive ($0{\cdot}96 \leq Eu^* \leq 1{\cdot}6$) or negative Eu anomalies (e.g. sample UM01-120; $Eu^* = 1{\cdot}28$).

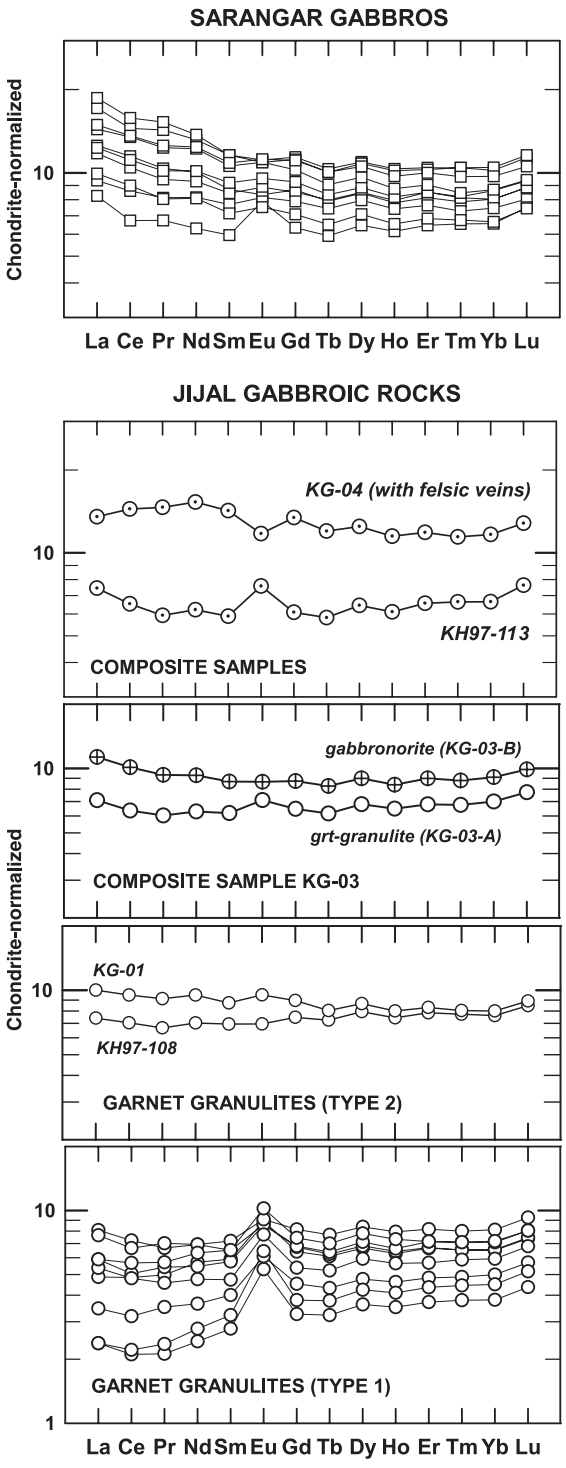

Fig. 7. Chondrite-normalized REE patterns for the Sarangar and Jijal gabbroic rocks. Jijal gabbroic rock patterns include the bulk analyses of garnet granulite and composite samples of hornblende gabbronorite and garnet granulite (KG-04 and KH97-113). Patterns for Jijal composite sample KG-03 correspond to analyses of the garnet granulite and the hornblende gabbronorite parts of this composite sample. Symbols as in Fig. 2. Normalization values are from Anders & Grevesse (1989).

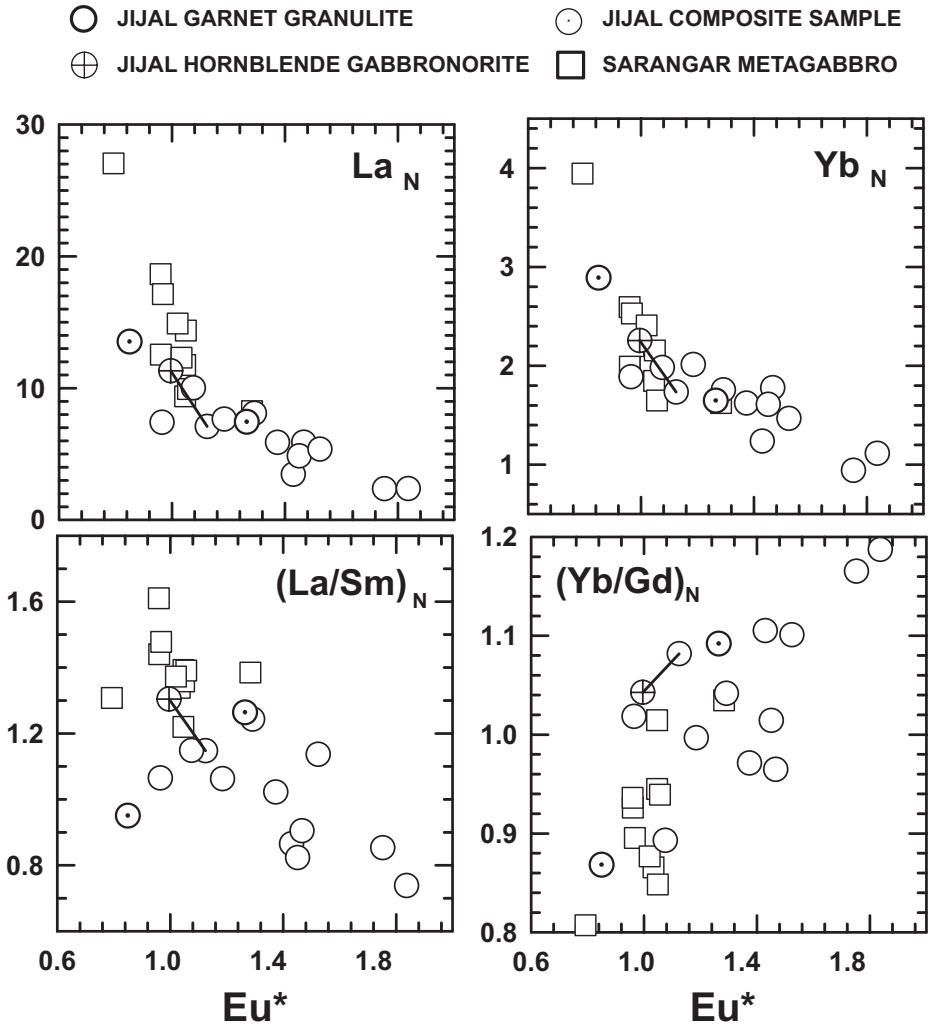

Fig. 8. Variation of La_N, Yb_N, $(La/Sm)_N$ and $(Yb/Gd)_N$ vs Eu* [$Eu^* = 2 \times Eu_N/(Sm_N + Gd_N)$; N indicates chondrite-normalized; normalization values are from Anders & Grevesse (1989)]. The tie-line links the composition of the hornblende gabbronorite (KG-03-B, crossed circle) and the garnet granulite (KG-03-A, open circle) parts of Jijal composite sample KG-03. Symbols are as in Fig. 2.

We distinguish two types of REE pattern in the Jijal garnet granulite samples (Fig. 7): Type 1 patterns are widespread and characterized by parallel patterns with variable LREE ($2{\cdot}4 \leq La_N \leq 8{\cdot}1$) and HREE ($1{\cdot}6 \leq Yb_N \leq 3{\cdot}5$) abundances, marked positive Eu anomalies ($1{\cdot}12 \leq Eu^* \leq 1{\cdot}84$) and slightly depleted REE patterns ($0{\cdot}5 \leq Ce_N/Yb_N \leq 1{\cdot}0$) (Fig. 7). The least fractionated type 1 patterns ($0{\cdot}8 \leq Ce_N/Yb_N \leq 1{\cdot}0$) have the highest LREE abundances ($La_N > 5$). Type 2 patterns are flat and lack Eu anomalies. This pattern is observed in only two samples (KG-01 and KH97-108).

The REE pattern of the garnet granulite (KG-03-A) and the hornblende gabbronorite sub-sample (KG-03-B) of composite sample KG-03 are broadly similar (Fig. 7). The hornblende gabbronorite is characterized by a LREE-enriched pattern and high REE abundances (Fig. 7), whereas the REE pattern of the garnet granulite, which is similar to the more REE-enriched type 1 garnet granulites, is flat and has a slight positive Eu anomaly (Fig. 7). REE variations in this composite sample point to open-system behavior of REE during the transformation of hornblende gabbronorite to garnet granulite. Composite sample KG-04 shows the highest REE abundances among the Jijal samples and is characterized by a concave-upward REE pattern with a negative Eu anomaly and a flat HREE segment (Fig. 7). These features may be due to the presence of granitic veins in the sample.

The Jijal garnet granulite, Jijal hornblende gabbronorite and Sarangar gabbros define a continuum of REE variations between two end-members (Figs 7 and 8): (1) type 1 Jijal granulites; (2) the most enriched Sarangar

gabbro that lacks a positive Eu anomaly and shows a melt-type REE pattern characterized by high REE abundances, selective LREE enrichment (LREE/MREE > chondrites) and a flat HREE segment (Figs 7 and 8). These REE variations result in continuous trends of decreasing La_N and Yb_N abundances and $(La/Sm)_N$ ratios, and increasing $(Yb/Gd)_N$ as a function of Eu* (Fig. 8). These correlations not only provide evidence for plagioclase–melt segregation but also for the presence of igneous (i.e. cumulus or restitic) garnet, as suggested by the positive correlation between $(Yb/Gd)_N$ and Eu* (Fig. 8). These trends follow the REE variations observed between the garnet-free and garnet-bearing part of composite sample KG-03 (tie-line in Fig. 8), suggesting that they may be produced by the same processes that generated the Jijal composite samples. To some extent, these REE fractionations are reminiscent of those observed between the middle and the lower continental crust (e.g. Taylor & McLennan, 1985, and references therein; Taylor *et al.*, 1986; Rudnick, 1992, 1995).

Other trace elements

Figure 9 compares the N-MORB-normalized trace element patterns of the Sarangar gabbros to those of oceanic arc basalts and basaltic andesites from the Marianas (Peate & Pearce, 1998) and Lesser Antilles (Zellmer *et al.*, 2003). The broad similarity of the Sarangar gabbro patterns with those of IAB confirms that the former are not cumulative plutonic rocks but mostly 'melt-frozen' plutonic rocks. Like IAB, the trace element patterns of the Sarangar gabbros show enrichments in highly incompatible elements, and relative depletions of Nb, Ta and Zr that are typical of subduction-related basalts. There are, however, noteworthy differences between the Sarangar gabbros and some IAB for the highly incompatible elements, particularly Rb, Th, U, and, to a lesser extent, Cs and Ba, which are more depleted in the Sarangar gabbros; this may be due to a primary characteristic of the magmas or due to trace element mobility during metamorphism (Fig. 9). The abundances of highly incompatible elements and LREE in the Lesser Antilles basaltic volcanic rocks (Zellmer *et al.*, 2003) have greater similarities to those of the Sarangar gabbros, than to other Lesser Antilles and Marianas IAB (Fig. 9). These differences may be due to variable slab components in the parental magmas, or to mobilization of the most incompatible elements during metamorphism of the Sarangar gabbro. On the other hand, the Sr, Zr, Y, MREE and HREE abundances of the Sarangar gabbros are comparable with those of IAB. Sarangar gabbros also show positive Sr anomalies that may reflect plagioclase accumulation in some samples or/and

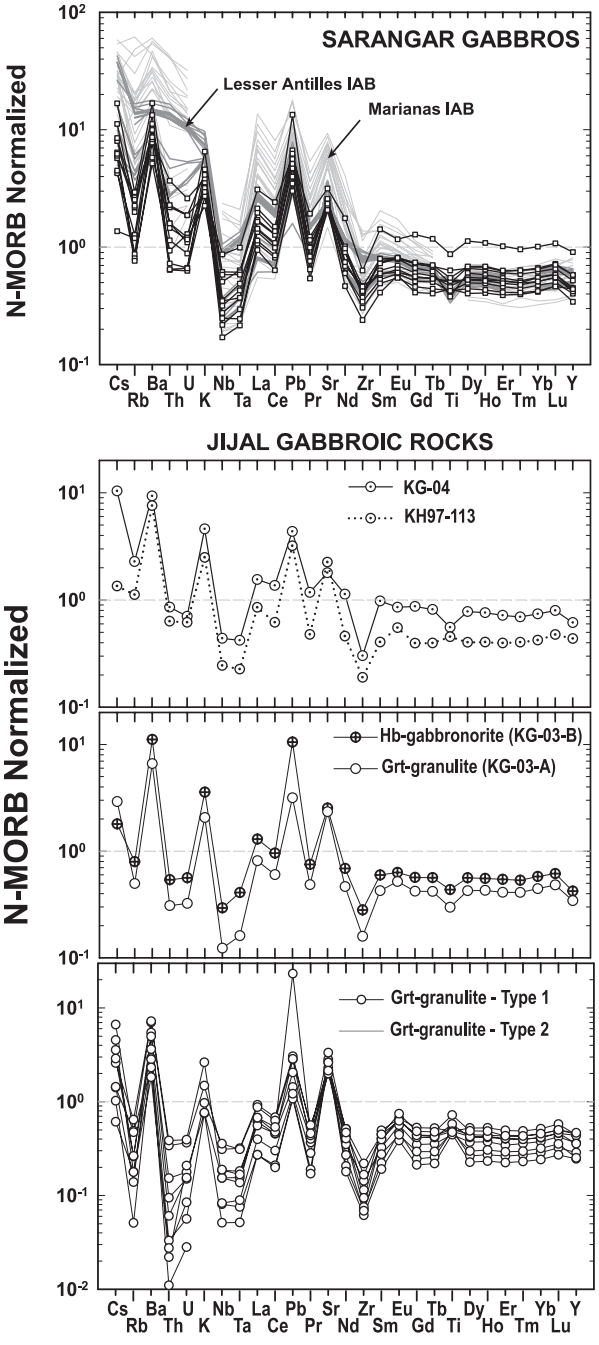

Fig. 9. Extended trace element diagrams for Sarangar and Jijal gabbroic rocks. Jijal gabbroic rock patterns include bulk analyses of garnet granulite and composite samples of hornblende gabbronorite and garnet granulite (KG-04 and KH97-113). Patterns for Jijal composite sample KG-03 correspond to analyses of the garnet granulite (KG-03-A). Concentrations are normalized to N-MORB (Hofmann, 1988) and arranged in terms of increasing incompatibility (to the left) in a peridotite–basaltic melt system. Also shown along with the Sarangar gabbro patterns are the patterns of island arc basalts from the Marianas (grey dashed lines; Peate & Pearce, 1998) and the Lesser Antilles (grey continuous lines; Soufrière Hills Volcano, Montserrat; Zellmer *et al.*, 2003).

they may represent the arc-type signature of the parental melts.

Jijal hornblende gabbronorite and composite samples exhibit MORB-normalized trace element patterns that are similar to those of the Sarangar gabbros (Fig. 9). In addition to REE variations, the Jijal garnet granulites differ from the Jijal hornblende gabbronorite and Sarangar gabbros by their lower abundances of large ion lithophile elements (LILE; notably Rb), Th and U (Fig. 9). Likewise, depletion of alkalis and LREE, LILE and Th–U is a characteristic of granulites in many high-grade continental crust terranes and crustal xenoliths. The origin of LILE depletion in continental granulites is debated but usually attributed to preferential mobility of these elements in fluids or melts released by dehydration or dehydration-melting of hydroxyl-bearing minerals, such as amphibole and mica, at peak metamorphic/melting conditions (e.g. Heier, 1973; Taylor & McLennan, 1985, and references therein; Rudnick & Presper, 1990; Rudnick, 1992).

Jijal garnet hornblendite and garnet pyroxenite

Major and transition elements

The Jijal garnet hornblendites and hornblende pyroxenites have highly variable Mg-numbers (45–75). The highest and lowest Mg-numbers are shown by the garnet-rich and garnet-poor hornblende pyroxenites, respectively (Fig. 4). Garnet hornblendites have intermediate Mg-numbers (Fig. 4). They are all characterized by low SiO_2 contents, very low $Na_2O + K_2O$ abundances and high FeO contents, especially in the samples with the highest modal garnet abundances (Fig. 4). They have Ni and Cr abundances in the same range as other IA plutonic rocks with similar Mg-number (Fig. 5), and high V abundances, probably as a result of garnet accumulation (Fig. 6). Overall, the major and transition element compositions of the Jijal garnet hornblendites and garnet pyroxenites are comparable with those of garnet–hornblende–pyroxene xenoliths found in some Californian arc batholiths and interpreted as residues of partial melting of basaltic protoliths (e.g. Ducea, 2001, 2002).

REE and other trace elements

As shown in Fig. 10, the garnet-rich hornblende pyroxenites have highly fractionated REE patterns characterized by a strong depletion of LREE ($0{\cdot}03 \leq La_N/Yb_N \leq 0{\cdot}09$) and high HREE abundances ($9{\cdot}9 \leq Yb_N \leq 23{\cdot}2$). All samples show subtle positive Eu anomalies ($1{\cdot}1 \leq Eu^* \leq 1{\cdot}3$), highly depleted LREE segments ($0{\cdot}08 \leq La_N/Sm_N \leq 0{\cdot}24$) and, in all but sample KH97-087, relatively flat HREE segments

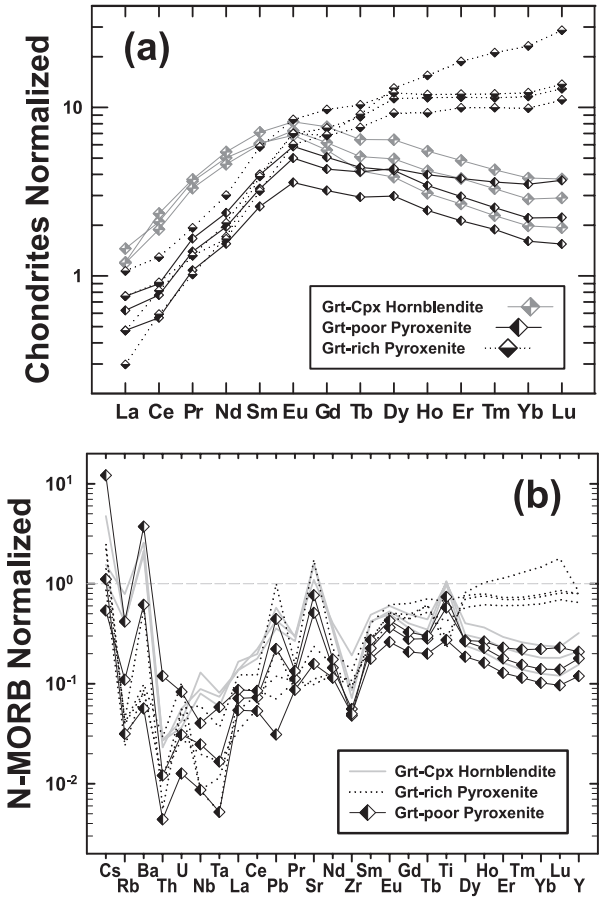

Fig. 10. (a) Chondrite-normalized REE patterns for Jijal ultramafic samples. Normalization values are from Anders & Grevesse (1989). (b) Extended trace element diagrams for Jijal complex ultramafic samples. Concentrations are normalized to N-MORB (Hofmann, 1988). Symbols and sample classification as in Fig. 2.

($0{\cdot}6 \leq Gd_N/Yb_N \leq 0{\cdot}8$). Garnet-poor hornblende pyroxenites display LREE depleted patterns comparable with the garnet-rich hornblende pyroxenites and positive Eu anomalies ($1{\cdot}24 \leq Eu^* \leq 1{\cdot}32$) (Fig. 10a). Their REE patterns differ significantly from the latter by having lower HREE abundances ($1{\cdot}6 \leq Yb_N \leq 3{\cdot}5$) and a depletion of HREE relative to MREE ($1{\cdot}2 \leq Gd_N/Yb_N \leq 2{\cdot}3$). Garnet hornblendites (samples KH97-104, KH97-092 and KH97-107) have convex-upward REE patterns with higher LREE abundaces ($1{\cdot}19 \leq La_N \leq 1{\cdot}45$) than the garnet–hornblende pyroxenites, and HREE abundances ($1{\cdot}98 \leq Yb_N \leq 3{\cdot}80$) and HREE/MREE fractionations ($2{\cdot}0 \leq Gd/Yb_N \leq 2{\cdot}8$) similar to the more HREE-depleted garnet-poor hornblende pyroxenites (Fig. 10a). The N-MORB-normalized trace element patterns of the Jijal garnet hornblendites and pyroxenites show depletion of Zr relative to other trace elements of similar compatibility (Fig. 10b). They are strongly

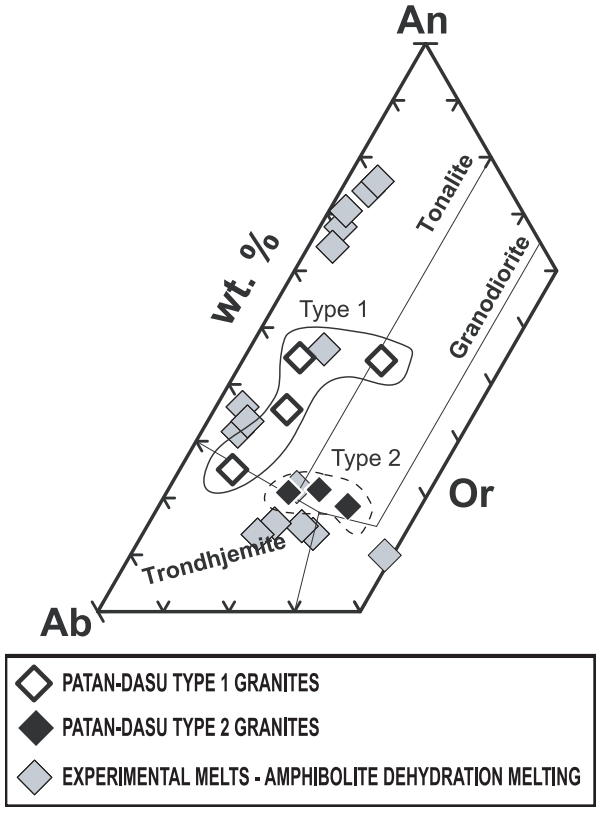

Fig. 11. Ternary diagram of normative An–Ab–Or (wt %) showing the composition of leucogranites in the Patan–Dasu metaplutonic complex. Fields are from Barker (1979) modified after O'Connor (1965). Grey diamonds are selected experimental melts compiled by Johannes & Holtz (1996, table 9.14) produced by dehydration-melting of amphibolite of variable composition leaving garnet-bearing restites.

depleted in LILE, especially Rb, as well as Th, U, Nb and Ta (Fig. 10b). This depletion demonstrates the highly residual character of these Jijal ultramafic rocks, consistent with them being partial melting residues or igneous cumulates. The REE and N-MORB-normalized trace element patterns of the Jijal hornblende pyroxenites are similar to those of garnet pyroxenite layers in orogenic peridotite massifs (Garrido & Bodinier, 1999; Bodinier & Godard, 2003, and references therein) and garnet pyroxenite–hornblendite xenoliths in the Sierra Nevada batholith (Ducea, 2001, 2002).

COMPOSITION OF THE GRANITES

In terms of their normative An–Ab–Or (wt %) composition, and following the classification of Barker (1979) (modified after O'Connor, 1965), the intrusive granites in the Patan–Dasu metaplutonic complex are tonalitic to granodioritic (Fig. 11). In terms of the Al-saturation index [A/CNK= mol % $Al_2O_3/(CaO + Na_2O + K_2O)$], they show a progressive trend from intermediate ($1 < A/CNK < 1{\cdot}1$) to peraluminous ($A/CNK > 1{\cdot}1$) compositions, with generally low Al_2O_3 contents (Fig. 12a). They have variable SiO_2 contents ranging from andesitic to rhyolitic, and low Mg-numbers in the range 30–44 (Fig. 12b). The normative composition, Al-saturation index and Mg-number of the granites are within the compositional field of melts produced by dehydration-melting of amphibolite at intermediate to high pressures (>1·0 GPa) (see compilation of experimental data in Figs 11 and 12).

On the basis of their REE patterns and field occurrence we classify the discordant granites in the Patan–Dasu metaplutonic complex into two main types (Figs 13 and 14), as follows.

Type 1 granites have strongly fractionated REE patterns that are LREE enriched ($12 \leq La/Yb_C \leq 130$) with rather variable LREE abundances ($6 \leq La_N \leq 110$). They have low HREE abundances ($0{\cdot}52 \leq Yb_N \leq 0{\cdot}96$) (Fig. 14). Samples with the lowest REE abundances have positive Eu anomalies indicating plagioclase accumulation. The most LREE enriched sample (UM01-125) has a slightly negative Eu anomaly ($Eu^* = 0{\cdot}86$) and a REE pattern very similar to those of Archean trondhjemite–tonalite–granodiorite (TTG), adakites and Na-rich granitoids. Type 1 granites have high Ab/Or ratios (Fig. 11), and they are slightly peraluminous to intermediate in composition (Fig. 12a). All type 1 granites, with the exception of sample UM01-124, occur as granite sheets intruding the upper part of the metaplutonic complex (Kamila amphibolite) (Fig. 1).

Type 2 granites have weakly fractionated REE patterns characterized by rather low REE abundances. All patterns are LREE enriched ($2{\cdot}8 \leq La_N/Yb_N \leq 8{\cdot}6$), variably depleted in HREE ($2{\cdot}8 \leq Yb_N \leq 5{\cdot}5$) (Fig. 14), and display negative Eu anomalies ($0{\cdot}45 \leq Eu^* \leq 0{\cdot}64$). They tend to show higher Ab/Or and Ab/An ratios (Fig. 11), and are peraluminous and silica rich (Fig. 12a and b). They occur as intrusive dykes in the Kiru and Madraza amphibolites, which form the lowermost units of the Patan–Dasu metaplutonic complex (Fig. 1).

Both granite types are characterized by N-MORB-normalized trace element patterns enriched in highly incompatible elements and depleted in MREE and HREE (Fig. 15) compared with the Sarangar gabbros. The MREE–HREE depletion precludes the possibility that the granites could be melts produced by crystal fractionation of the same parental basaltic melts that formed the Sarangar gabbros or other Kohistan lower crust gabbros. The N-MORB trace element normalized patterns of both types of granites are characterized by positive Pb and Sr spikes and Nb–Ta depletions relative to K and LREE (Fig. 15). The pattern of type 2 granites

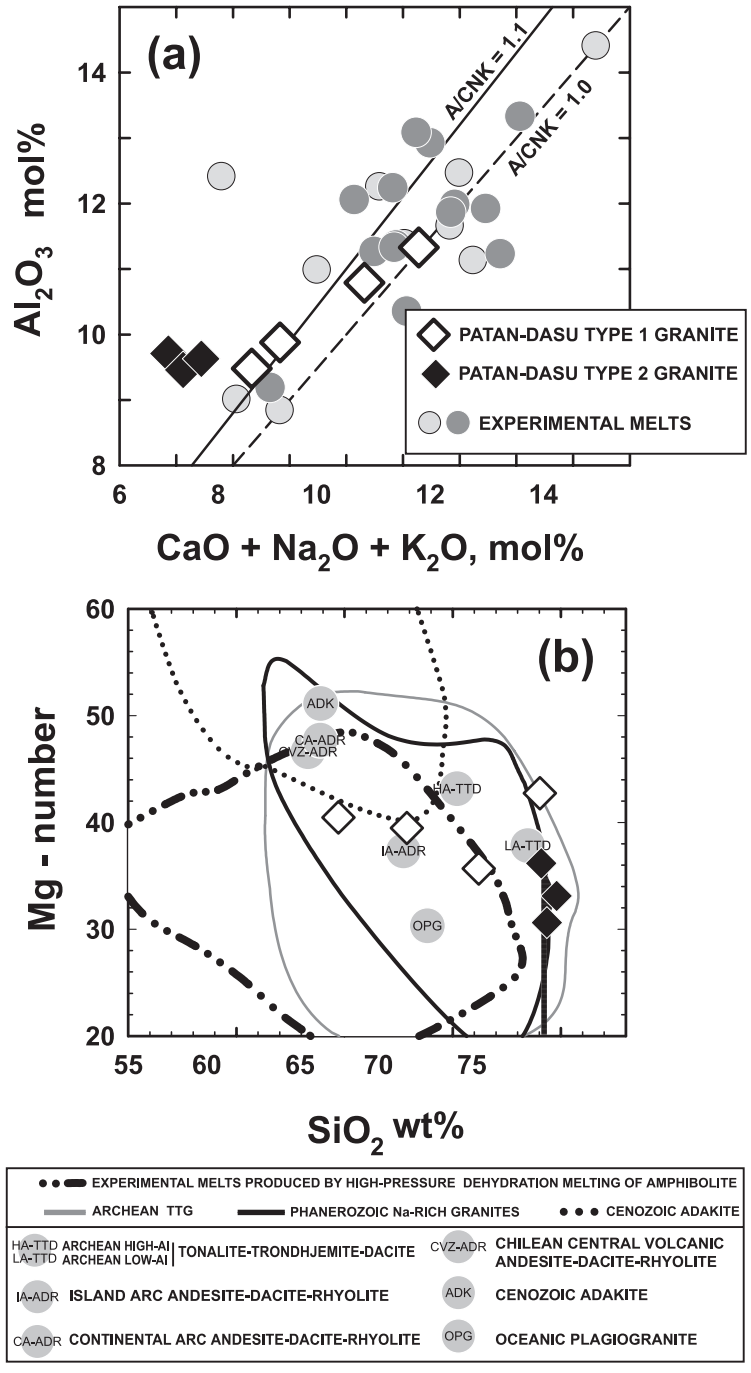

Fig. 12. (a) Al_2O_3 mol % (= A) vs CaO + Na_2O + K_2O (= CNK) plot for type 1 (◇) and type 2 (♦) granites of the metaplutonic complex, showing the peraluminous (A/CNK >1·1) and metaluminous (A/CNK <1·0) fields. Circles are granitic melts produced by dehydration-melting of amphibolite bulk compositions leaving garnet-bearing restites (dark grey circles, in the main at $P > 0{\cdot}9$ GPa) and garnet-free restites (light grey circles, in the main at $P < 0{\cdot}9$ GPa). Experimental data are well-equilibrated experimental runs compiled by Johannes & Holtz (1996). (b) Mg-number vs SiO_2 wt % comparing the composition of Patan–Dasu granites with the field of Cenozoic adakites (dotted line), Archaean TTGs (>3 Ga) (grey line), and Phanerozoic Na-rich granitoids (bold black line) [compositional fields after Smithies (2000, fig. 5, p. 121)]. Also shown is the field of experimental melts produced by melting of hydrous basaltic sources (bold double-dot–dashed line) at pressures ranging from 1 to 3·2 GPa (Sen & Dunn, 1994; Rapp & Watson, 1995; Rapp *et al.*, 1999) and leaving garnet-bearing (grt + cpx ± amph) residues (Rapp *et al.*, 1999, fig. 1, p. 336, and references therein). Large grey circles are the average composition [averages compiled by Drummond *et al.* (1996, table 1, p. 307)] of Archaean high-Al (HA-TTD), low-Al tonalites–trondhjemites–dacites (LA-TTD), island arc (IA-ADR) and continental arc (CA-ADR) andesite–dacite–rhyolite suites [similar to post-Archaean granites of Martin (1986)], andesites–dacites–rhyolites from the Chilean Central volcanic zone [CVZ-ADR; ca., Na-rich granites of Smithies (2000)], Cenozoic adakites (ADK), and oceanic plagiogranites (OPG).

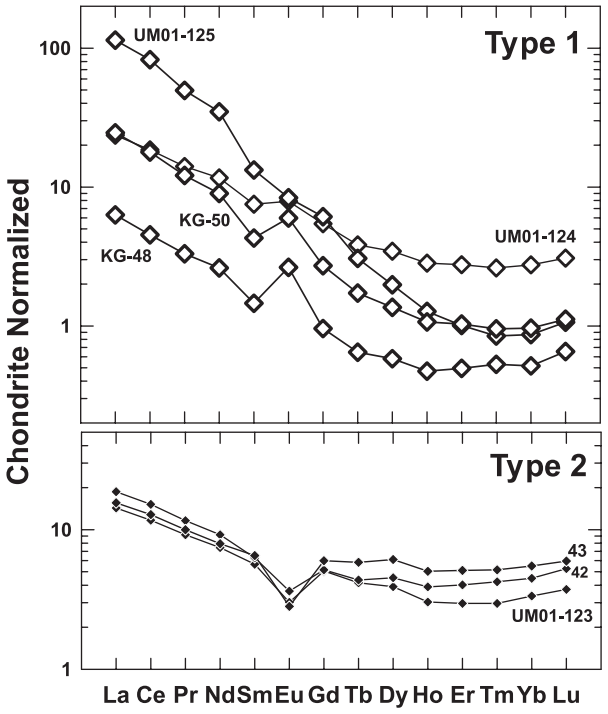

Fig. 13. Chondrite-normalized REE patterns for type 1 and type 2 granites from the Patan–Dasu metaplutonic complex. Symbols are as in Fig. 1.

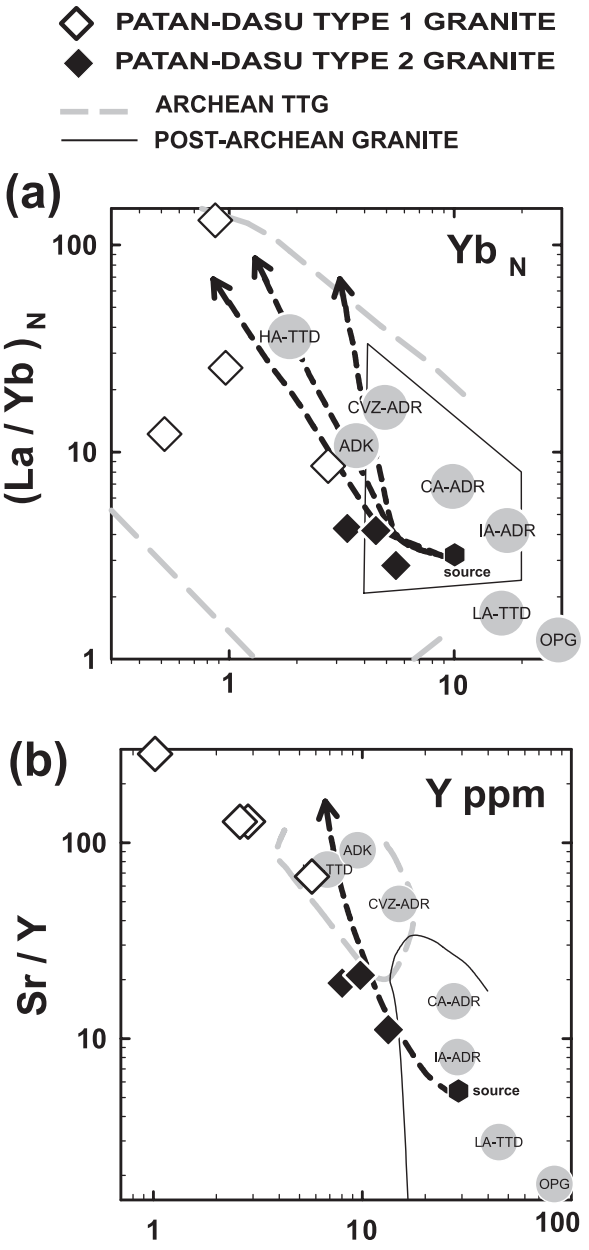

Fig. 14. (a) $(La/Yb)_N$ vs Yb_N [N indicates chondrite normalized; normalization values are from Anders & Grevesse (1989)]; (b) Sr/Y vs Y ppm for type 1 (◇) and type 2 (♦) granites in the Patan–Dasu metaplutonic complex. Also shown in (a) and (b) are the trends (bold dashed lines) of melts generated by batch-partial melting of basaltic sources leaving garnet hornblendite and garnet pyroxenite restites (Petford & Atherton, 1996, fig. 115, p. 1511, Source C1). Grey dashed and fine black lines in (a) and (b) are respectively the field of Archean TTG and the post-Archean granite field (Martin, 1986). Large grey circles as in Fig. 12b.

is also characterized by a negative Ti anomaly (Fig. 15) that may be indicative of the involvement of Fe–Ti oxides in their petrogenesis.

Comparison with silica-rich rocks in arc settings

Type 1 and 2 granites have Mg-numbers lower than those of adakites but similar to those of high-alumina TTG suites (Fig. 12b). Some debate exists as to which of these silica-rich rocks represent partial melts of subducting oceanic crust (i.e. subcrustal sources) or of basaltic amphibolite at the base of the thickened arc crust (i.e. crustal sources) (Martin, 1986, 1999; Drummond *et al.*, 1996; Rapp *et al.*, 1999; Smithies, 2000; Foley *et al.*, 2002). The Mg-number of primary melts produced by melting of basaltic sources (Mg-number 30–50) (Rapp, 1995; Rapp & Watson, 1995; Rapp *et al.*, 1999) is thought to increase by interaction with mantle olivine giving rise to hybridized, high Mg-number melts (Mg-number 50–70) (Rapp *et al.*, 1999; Smithies, 2000). Consequently, high Mg-number has been proposed to be characteristic of melts generated by melting of basaltic sources within the mantle (Rapp *et al.*, 1999; Smithies, 2000). The low Mg-number of the Kohistan granites, which are in the range of experimental melts produced by dehydration-melting of amphibolites (Rapp *et al.*, 1999), is consistent with them being melts produced by melting of a basaltic crustal source (Fig. 12b).

Many trace element characteristics of type 1 granites match those of melts produced by melting of

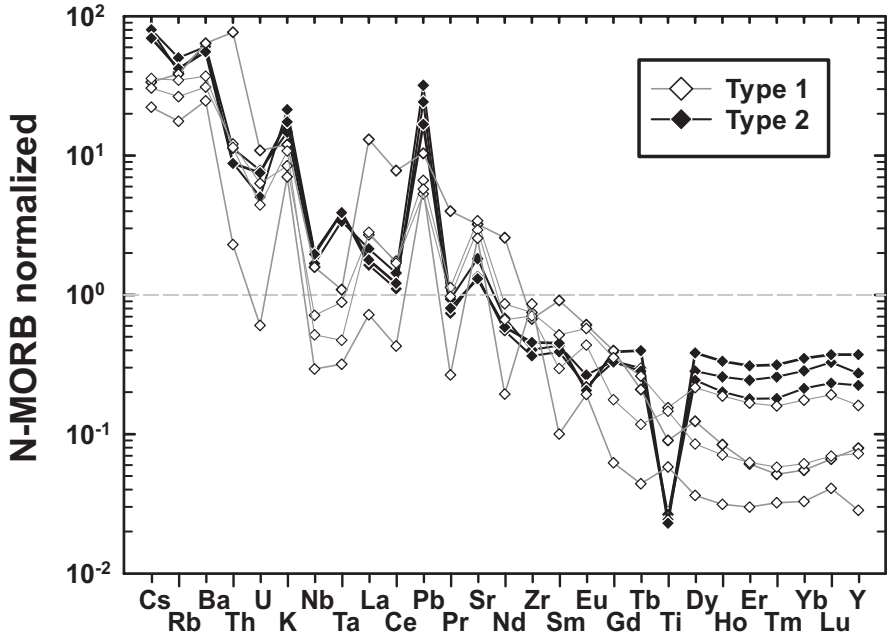

Fig. 15. Extended trace element diagrams for type 1 and type 2 granites of the Patan–Dasu metaplutonic complex. Concentrations are normalized to N-MORB (Hofmann, 1988) and arranged in terms of increasing incompatibility order (to the left) in a peridotite–basaltic melt system.

garnet-bearing basaltic sources (garnet amphibolite and/or eclogitic protholiths) such as adakite, Archaean high-Al trondhjemites, and Cenozoic high-Na granitoids or andesite–dacite–rhyolite suites in arcs (Figs 13 and 14) (e.g. Martin, 1986; Drummond *et al.*, 1996; Petford & Atherton, 1996; Smithies, 2000; and references therein). These similarities include low HREE (average Yb 0·32 ppm) and Y (<6 ppm, averaging 3 ppm) abundances, high LREE/HREE ratios (average $La_N/Yb_N = 44$) (Figs 13 and 14a), high Sr abundances (>300 ppm; averaging 343 ppm) and high Sr/Y ratios (average 152 ppm) (Fig. 14b). The low Yb and high La/Yb ratios, and the lack of negative Eu anomalies in the REE patterns of type 1 granites, indicate that they were in equilibrium with plagioclase-free, garnet-rich restites (Fig. 13). As high-pressure (>1·0 GPa) dehydration-melting of amphibolite generates garnet amphibolite and garnet residues (e.g. Wolf & Wyllie, 1993; Rapp, 1995), one possible hypothesis is that type 1 granites formed from melts produced by melting of amphibolite leaving as restites Jijal garnet hornblendites and pyroxenites. On the other hand, because of their low La/Yb and Sr/Y ratios, type 2 granites share some similarities with the most evolved members of andesite–dacite–rhyolite suites (Figs 12 and 14). Their La/Yb and Sr/Y ratios are higher than those of Archaean high-Al trondhjemites and oceanic plagiogranites (Fig. 14), and lower than those of adakites and Na-rich granitoids. Type 2 granites differ, however, from the latter and from other island arc andesite–dacite suites by their lower Yb and Y contents, and La/Yb and Sr/Y ratios (Fig. 14a and b).

DISCUSSION

Origin of the Jijal garnet granulites

Garnet granulites in island arcs may be formed by metamorphism of former oceanic crust (e.g. Kay & Kay, 1985) or via processes occurring in island arcs. Three main hypotheses may account for the formation of garnet granulite via arc magmatism: (1) closed-system metamorphism of shallow arc rocks; (2) high-pressure igneous crystallization of garnet granulite assemblages from mantle-derived melts; and (3) open-system dehydration or dehydration-melting of amphibole-bearing arc plutonic rocks. In hypotheses (1) and (3), garnet granulite is derived from shallow arc plutonic rocks formed during the juvenile stages of the Kohistan arc. Garnet granulite then forms subsequently at the mature stage of arc evolution owing to progressive burial and heating of these shallow intrusions. In the dehydration-melting scenario, garnet granulite is restitic and produced by partial melting of amphibole-bearing plutonic rocks, leading to small volumes of granitic melts. Hypothesis (2) implies direct formation of igneous garnet granulite by high-pressure crystallization at the mature stages of the Kohistan arc when the thickness of the crust exceeded *c.* 30 km.

Are garnet granulites remnants of former oceanic crust?

A possible origin for the Jijal garnet granulites is that they are remnants of gabbroic cumulates that formed part of the Tethyan oceanic crust upon which the Kohistan arc was built, metamorphosed under granulite-facies conditions (Jan, 1979; Jan & Howie, 1981; Treloar *et al.*, 1996, and references therein). The REE patterns of type 1 garnet granulites (Fig. 7) are broadly similar to those of gabbros in the lower part of ophiolites and oceanic crust drilled in active fast- and slow-spreading MORs, which are interpreted as low-pressure cumulates of N-MORB. However, in addition to the subduction signatures shown in their trace element patterns, several compositional features make it improbable that the Jijal garnet granulites are remnants of oceanic crust. Jijal granulites have low Mg-numbers that are not observed in lower crust cumulates formed at fast-spreading MORs (Fig. 4). Such a low Mg-number is observed only in oxide-bearing gabbros from slow-spreading MORs; however, these have substantially higher Ti, and lower Al_2O_3 and Cr abundances than the Jijal granulites (Fig. 4). In terms of their major and transition element compositions, the Jijal granulites are clearly akin to gabbroic rocks exposed in oceanic arc plutonic complexes such as the Tanzawa complex in Japan (Kawate & Arima, 1998) and to the more evolved gabbroic rocks from the Tonsina–Talkeetna complex in Alaska (Figs 4–6) (DeBari & Sleep, 1991; Greene *et al.*, 2006). These features indicate that the Jijal garnet granulites are plutonic rocks generated in an oceanic arc via arc magmatism. This conclusion is consistent with the existence in the Jijal complex of gabbroic rocks (hornblende gabbronorites; Figs 7 and 8) with REE patterns comparable with Sarangar gabbros that are unequivocally akin to IAB (Fig. 9).

Formation of Jijal garnet granulites by high-pressure crystal fractionation of arc magmas

Primitive arc magmas are generally H_2O rich compared with anhydrous mantle melts at arc Moho depths (e.g. Kelemen *et al.*, 2003*a*, and references therein). Under hydrous conditions, available experimental work shows that primitive arc basalts are not saturated in garnet at the pressures attained in the lower crust of island arcs (0·8–1·2 GPa) (Müntener *et al.*, 2001). Although the current belief is that the mantle flux to the arc crust is basaltic (posing the 'arc paradox'), some workers consider that high Mg-number andesites may contribute significantly to the growth of the arc crust (Kelemen *et al.*, 2003*a*, and references therein). In this alternative view, one may envisage crystallization of magmatic garnet granulites by high-pressure crystallization of hydrous andesitic melts (Müntener *et al.*, 2001; Alonso-Perez *et al.*, 2004). Different types of garnet-bearing assemblages have been obtained experimentally by crystal fractionation of water undersaturated high Mg-number andesites (Müntener *et al.*, 2001) and/or derivative andesites formed by fractional crystallization of pricritic basalts (Alonso-Perez *et al.*, 2004). At 1·2 GPa, fractional crystallization of hydrous andesite produces garnet-bearing ultramafic assemblages ranging from garnet pyroxenite (grt + cpx + amph) to garnet amphibolite (amph + grt) with increasing water contents (Alonso-Perez *et al.*, 2004). At *c.* 0·8 GPa, garnet and plagioclase assemblages with no or little clinopyroxene form at high water contents (H_2O >8 wt %), resulting in plagioclase amphibolites (Alonso-Perez *et al.*, 2004).

The primary mineralogy of the Jijal garnet granulites is anhydrous and dominated by garnet (*c.* 30–35 vol. %), plagioclase (*c.* 30–35 vol. %) and clinopyroxene (30–40 vol. %) with minor quartz (Jan, 1979; Miller *et al.*, 1991; Yamamoto, 1993; Miller & Christensen, 1994; Yamamoto & Yoshino, 1998). These mineral assemblages and modes have not been yet reproduced by high-pressure crystal fractionation of either hydrous arc basalt or andesite. In particular, high-pressure crystallization of hydrous andesite generates hornblende-rich cumulates lacking clinopyroxene, unlike the Jijal garnet granulite assemblages (Jan, 1979; Miller *et al.*, 1991; Yamamoto, 1993; Miller & Christensen, 1994; Yamamoto & Yoshino, 1998). Metamorphic amphibole and epidote are pervasive in some Jijal garnet granulites but clearly related to late retrogression of peak anhydrous assemblages (Jan, 1979; Yamamoto, 1993; Yamamoto & Yoshino, 1998; Yoshino *et al.*, 1998). Therefore, although it is a viable mechanism for the origin of igneous garnet in thickened island arcs, crystal fractionation of hydrous arc magmas is an improbable scenario for the origin of the Jijal garnet granulites.

Origin of garnet granulites by dehydration or dehydration-melting of amphibole-bearing arc plutonic rocks

Field and petrographic evidence. As discussed above, there is compelling field evidence for the formation of the Jijal garnet granulites by replacement of hornblende gabbronorites (Fig. 3a and b) (Bard, 1983*b*; Yamamoto & Yoshino, 1998; Yamamoto & Nakamura, 2000). This demonstrates that the Jijal garnet granulites were derived from shallower amphibole-bearing arc gabbros similar in composition to the Sarangar gabbros (Figs 7 and 8). Such an origin is well supported by composite samples showing transformation of hornblende gabbronorite to anhydrous garnet granulite (Fig. 3b). This transformation has been interpreted as due to formation of anhydrous garnet granulite by metamorphic dehydration reactions (Yamamoto & Yoshino, 1998).

Dehydration vs dehydration-melting. An important issue is whether transformation of hornblende gabbronorite to

garnet granulite was due to dehydration or to dehydration-melting. Both processes lead to amphibole breakdown but dehydration produces H_2O-rich fluids whereas dehydration-melting generates H_2O-undersaturated granitic melts (Johannes & Holtz, 1996, and references therein). At high pressure both processes result in anhydrous garnet-bearing granulitic assemblages comparable with the Jijal garnet granulite (e.g. Pattison, 2003, and references therein). The existence of intrusive leucocratic veins associated with coarse garnets—conspicuous in some Jijal garnet granulites (Fig. 3a and c)—may be interpreted as field evidence for dehydration-melting. However, in high-pressure mafic granulites that often show diffuse leucosomes intimately associated with restitic assemblages, field and/or textural criteria cannot unambiguously discriminate between these scenarios (e.g. Hartel & Pattison, 1996; Pattison, 2003).

Trace element variations may discriminate between dehydration-melting and dehydration, however. Depletion of LILE, U and, to a lesser extent, Th is commonplace in some granulitic terranes. The origin of these depletions by dehydration, dehydration-melting or crystal fractionation, as well as their bearing on the intracrustal differentiation of the lower continental crust, was a major issue in the 1970s and 1980s (e.g. Heier, 1973; Rollinson & Windley, 1980; Taylor & McLennan, 1985, Chapter 4 and references therein; Rudnick, 1992). The debate as to which LILE are mobilized by H_2O-rich fluids or melts simmers on in the context of granulite-facies metamorphism and slab devolatilization processes in subducting slabs (Kelemen *et al.*, 2003*a*, p. 624, and references therein). It is widely accepted that Th is much less soluble than U in hydrous fluids, owing to the dissimilar complexing behavior of U and Th in fluids (Keppler & Wyllie, 1990; Keppler & Wyllie, 1991; Keppler, 1996). This has been demonstrated by experimental studies of eclogite–aqueous fluid and peridotite–aqueous fluid partitioning (Brenan *et al.*, 1995; Ayers, 1998; Stalder *et al.*, 1998; Johnson & Plank, 1999). On the other hand, the LREE show limited solubility in amphibolite dehydration fluids, and Nb and other HFSE are highly immobile (Kogiso *et al.*, 1997). HFSE, Th and La are strongly enriched in granitic melts formed by low degrees of melting of amphibolite, eclogite or granulite (Springer & Seck, 1997; Johnson & Plank, 1999; Rapp *et al.*, 1999, 2003; Foley *et al.*, 2002).

The transformation of the Jijal hornblende gabbronorite to garnet granulite was accompanied by concomitant loss of La, Th, U and Nb, as illustrated by the relative variations of Nb with La, and Th/U with La (Fig. 16). These trace element variations cannot be attributed to dehydration reactions as they involve depletion in incompatible trace elements insoluble in

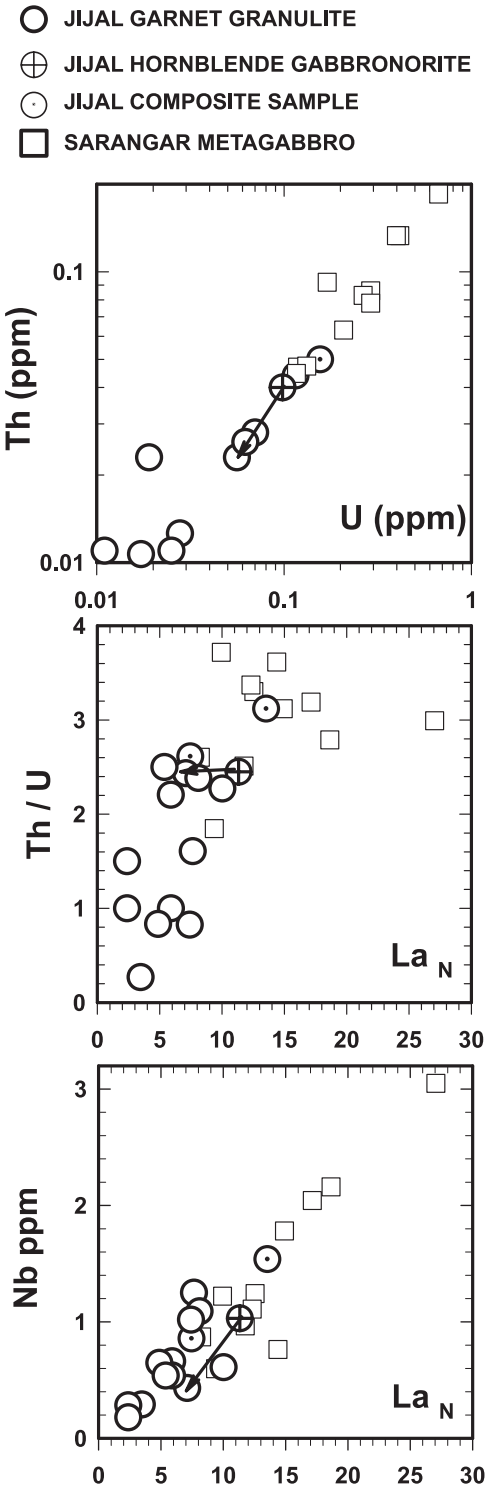

Fig. 16. Variation of Th vs U, and Th/U and Nb vs La_N [N indicates chondrite normalized; normalization values are from Anders & Grevesse (1989)] for Jijal garnet granulite and hornblende gabbronorite, and Sarangar gabbros. The arrow in each diagrams links the composition of the hornblende gabbronorite (KG-03-B, crossed circle) and the garnet granulite (KG-03-A, open circle) parts of the Jijal composite sample KG-03.

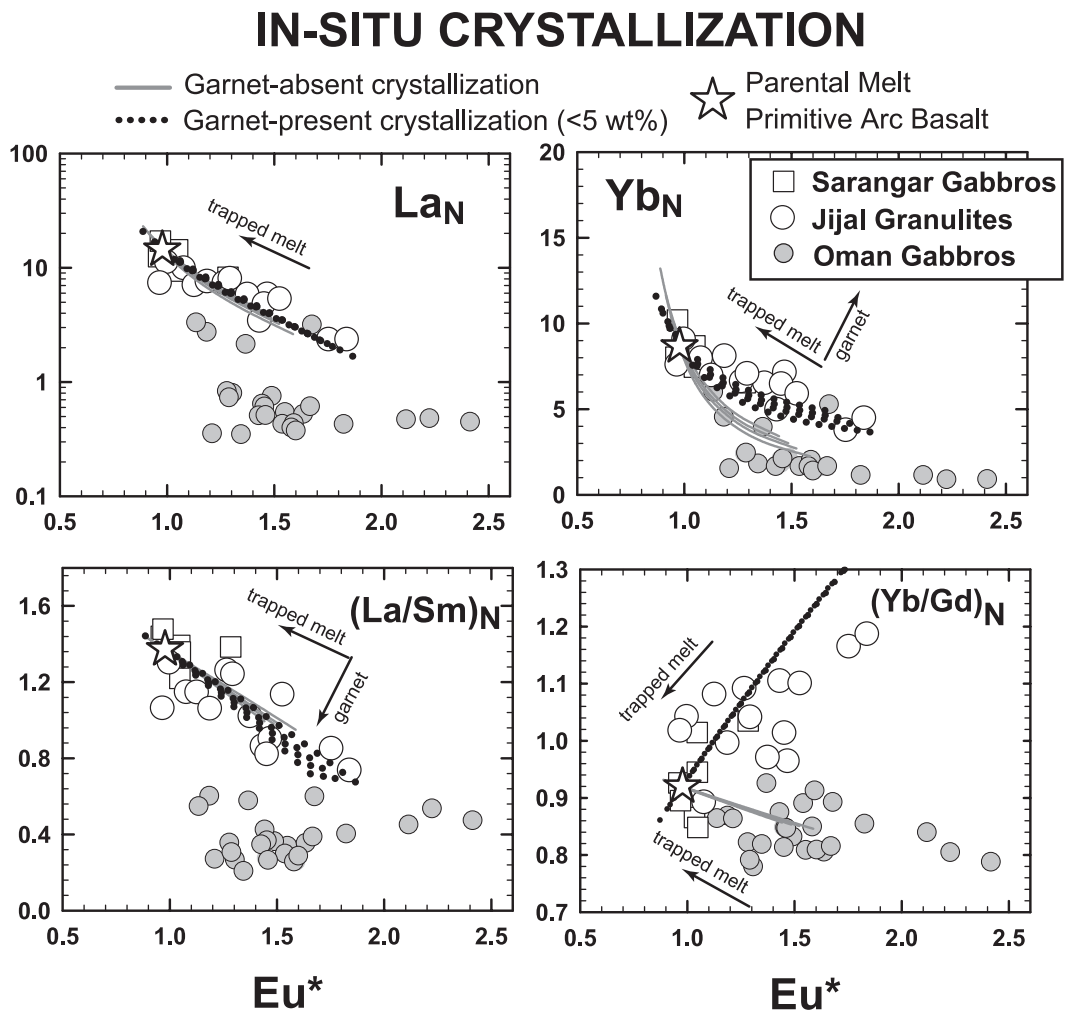

Fig. 17. Variation of La_N, Yb_N, $(La/Sm)_N$ and $(Yb/Gd)_N$ vs Eu* [Eu* = $2 \times Eu_N/(Sm_N + Gd_N)$; N indicates chondrite-normalized; normalization values are from Anders & Grevesse (1989)] displaying the results of the *in situ* crystallization (Langmuir, 1989) of average primitive arc basalt [star, average island arc basalt after Kelemen *et al.* (2003*a*)] with variable degrees of trapped melt. The effect of increasing amounts of trapped melts is indicated by the trapped melt arrow. Two crystallization scenarios are shown: 'low-pressure' crystallization of gabbronoritic assemblages (pl + opx + cpx; grey continuous lines), and 'high-pressure' crystallization of garnet granulite assemblages (pl + cpx + gt; black dotted lines). Solids are modeled as mixtures of crystallizing assemblages with variable amounts of trapped melt.

hydrous fluids. They are probably due to dehydration-melting and formation of a water-undersaturated granitic melt that mobilized these elements. It can also be argued that similar covariations observed when considering the Jijal garnet granulites and Sarangar gabbros together (Fig. 16) result from the same process. This is particularly suggested by the positive correlation of La_N with Th/U (Fig. 16), a ratio that is hardly fractionated by crystal fractionation but that can be readily fractionated by extraction of small melt fractions of hydrous granitic melts (e.g. McKenzie, 1989). As a result of this process, the Jijal granulites acquired low Th/U values akin to those of some granulite terranes and the lower continental crust (Taylor & McLennan, 1985; Rudnick & Gao, 2003).

Constraints from REE variations and fractionations

As suggested above, the REE covariations relative to Eu* observed for the ensemble of Kohistan gabbros (Figs 8, 17 and 18) may be accounted for by fractional crystallization and/or accumulation from a single parental melt, or by partial melting of a gabbro source. Figures 17 and 18 show, respectively, the results of trace element crystallization and melting models aimed at further discriminating between these scenarios. The compositions of Oman gabbros are also shown in both figures as a reference for low-pressure igneous cumulates from N-MORB crystallization. The Oman gabbros are distinguished from those from Kohistan by their lower REE abundances and selective depletion of LREE ($La_N/Sm_N < 1$) as a result of olivine accumulation and

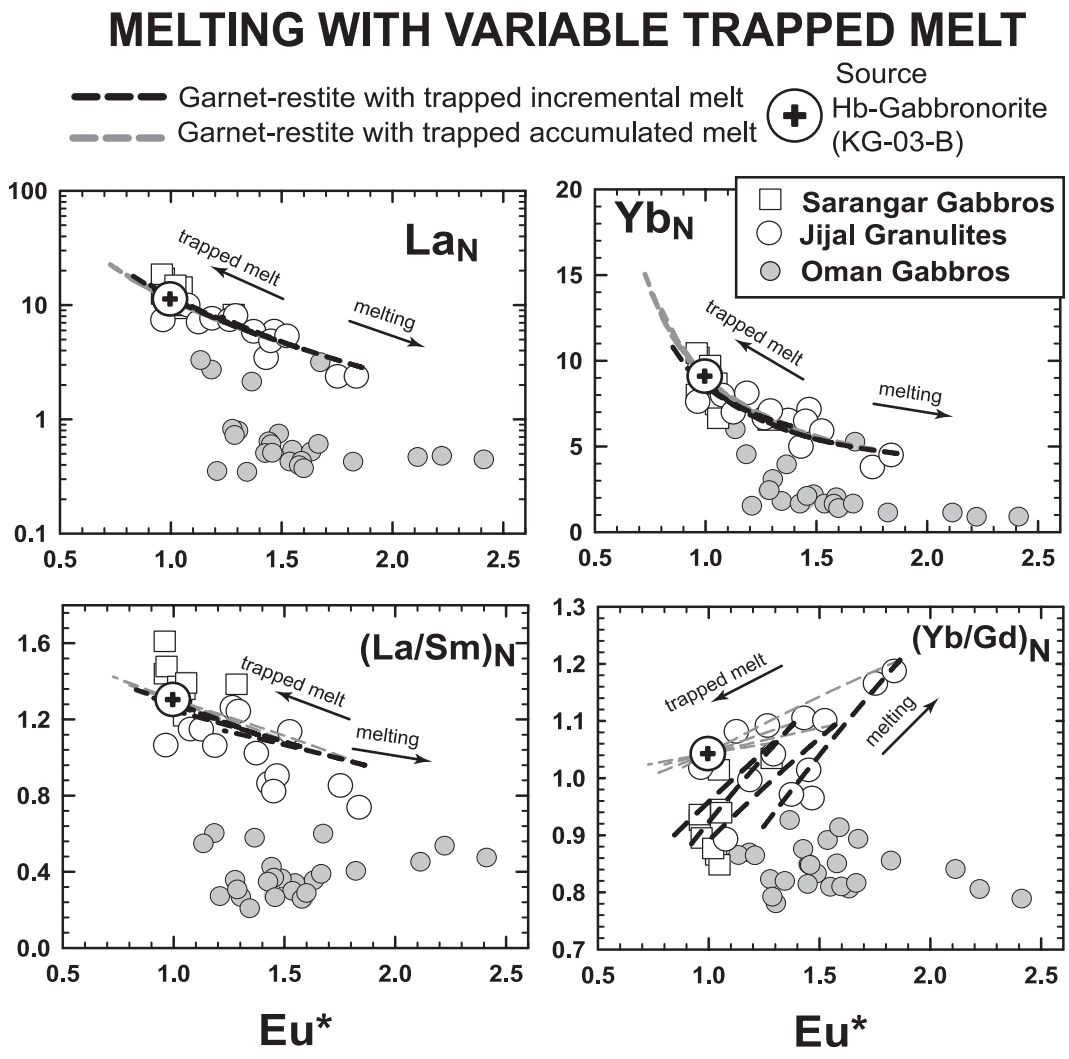

Fig. 18. Variation of La_N, Yb_N, $(La/Sm)_N$ and $(Yb/Gd)_N$ vs Eu* [Eu* = $2 \times Eu_N/(Sm_N + Gd_N)$; N indicates chondrite-normalized; normalization values are from Anders & Grevesse (1989)] displaying the results of melting a hornblende gabbronorite source (pl + opx + cpx + hb) using as a source Jijal hornblende gabbronorite sample KG-03-B (crossed circle). Restites are modeled as mixtures of 60–100% residual assemblages generated by incremental melting mixed with variable fractions (0–40%) of incremental melts (black short-dashed lines) or accumulated melts (grey dashed lines). In both figures, open symbols are Jijal ({○}) and Sarangar ({□}) gabbroic rocks, and grey circles are olivine gabbros from the Oman ophiolite (P. B. Kelemen & C. J. Garrido, unpublished data, 1998; Garrido *et al.*, 2001). Mineral melt distribution coefficients are from Martin (1987) and Kawate & Arima (1998). (See text for further model details.)

differences in the parental melts (Fig. 17 and 18). The Oman gabbros lack, however, a positive correlation between $(Yb/Gd)_N$ and Eu*, lending some support to the idea that the Kohistan gabbros record segregation of supersolidus garnet.

Crystallization model. For the crystallization model we used two parental melt compositions: (1) an average primitive high Mg-number andesite, and an average primitive arc basalt reported by Kelemen *et al.* (2003*a*; Table 1). Because the high Mg-number andesite is too HREE depleted and LREE enriched compared with the Kohistan gabbros, its crystallization is unable to reproduce the REE variations observed in the Kohistan gabbros (results not shown in Fig. 17). Primitive or derivative arc andesite is hence discarded as the parental melt for the Kohistan gabbros.

Figure 17 shows the result of an *in situ* crystallization model (Langmuir, 1989) for an average primitive arc basalt (star in Fig. 17). This model is more consistent with the Kohistan data. Two *in situ* crystallization scenarios are illustrated in this figure: 'low-pressure' crystallization of gabbronoritic assemblages (pl + opx + cpx; grey lines in Fig. 17); and 'high-pressure' crystallization of garnet granulite assemblages (pl + cpx + gt;

dotted black line in Fig 17). The crystallized solids (shown by the extent of individual lines in Fig. 17) are modelled as mixtures of cumulus assemblages and *in situ* crystallization of residual melts with mixing proportions in the range 0–100%. The calculations were performed with residual melt fraction (f) in the range 1–0·5 (see Langmuir, 1989). Because of the strong similarity of the REE content of amphibole to that of clinopyroxene [our unpublished laser ablation (LA)-ICP-MS data], amphibole was neglected in the calculations and recast as clinopyroxene for simplicity. The most critical parameters to fit turned out to be the Eu plagioclase/melt partition coefficient ($K_{Eu}^{pl/m}$) and the amount of garnet in the cumulus assemblage. The results reported in Fig. 17 were obtained with a $K_{Eu}^{pl/m}$ value of 0·45, which provides the best fit for the La_N and $(La/Sm)_N$ vs Eu* covariations.

The main result of the crystallization model is that low-pressure crystal fractionation does not account for the positive correlation of $(Yb/Gd)_N$ with Eu* observed in the Kohistan gabbros, which is better matched by the high-pressure crystallization model but with a very limited amount of cumulus garnet (3 wt % in Fig. 17, calculated with $K_{Gd}^{garnet/melt} = 1$ and $K_{Yb}^{garnet/melt} = 7$; using higher $K^{garnet/melt}$ constrains the amount of cumulitic garnet to $\leq$5 wt %). *In situ* crystallization models with higher amounts of cumulitic garnet result in much higher Yb_N abundances and $(Yb/Gd)_N$ ratios for a given Eu* than those observed in the Kohistan gabbros.

Melting model. Figure 18 shows the results of the melting models for a hornblende gabbronorite (pl + opx + cpx + hb) (Jijal hornblende gabbronorite sample KG-03-B, crossed circle in Fig. 18). The melting reaction involved total dissolution of orthopyroxene and hornblende coupled with garnet precipitation, generating a garnet granulite restite. Calculations were performed with an incremental melting model with F (melting degree) in the range 0·12–0·27. Restites were modelled as mixtures of 60–100% residual assemblages mixed with variable fractions (0–40%) of 'incremental melts' (short-dashed black lines in Fig. 18) or 'accumulated melts' (short-dashed grey lines in Fig. 18). The differences between these two types of melt mixing are significant only for the variation of $(Yb/Gd)_N$ vs Eu* (Fig. 18).

The melting model fits the REE variations of the Kohistan gabbros well and predicts the higher HREE abundances and REE fractionations observed in the Jijal garnet granulites (Fig. 18). As for the crystallization model, however, the partial melting model requires small amounts of garnet to account for the observed HREE fractionations (2·5–4·2, depending on melting degree, for $K_{Gd}^{garnet/melt}$ and $K_{Yb}^{garnet/melt} = 1$ and 7, respectively), and needs $K_{Eu}^{pl/m}$ around 0·45 to fit the steep slopes of the La_N and $(La/Sm)_N$ vs Eu* covariations (Fig. 18). This $K_{Eu}^{pl/m}$ is significantly lower than the values generally envisioned for the crystallization of arc magmas (e.g. Martin, 1987; $K_{Eu}^{pl/m} = 1·3$), which may indicate that granulite formation was associated with a drop in oxygen fugacity.

Preferred hypothesis for the origin of Jijal garnet granulite

REE modeling indicates that the Jijal garnet granulites were not formed by crystallization of primitive andesitic melts or derivative andesites, but either by high-pressure crystallization of island arc basalts or dehydration-melting of Jijal hornblende gabbronorite. In both models only a small fraction of igneous garnet is required to fully account for the REE variations of the Jijal garnet granulites. The crystallization and melting models fail to reproduce the high garnet modal proportions (33 wt %) of the Jijal granulites that must be of closed-system origin. In the melting scenario, substantial subsolidus garnet may be formed by metamorphic reactions proceeding in parallel with dehydration-melting reactions (e.g. Hartel & Pattison, 1996; Pattison, 2003).

Available experimental data, however, preclude liquidus garnet in arc basalts crystallizing at the pressures of the lower island arc crust (e.g. Müntener *et al.*, 2001). Together with field and petrographic observations, this leads us to favor a melting scenario involving arc plutonic sources, such as the Jijal hornblende gabbronorite or Sarangar gabbro (Fig. 18), in the origin of the Jijal garnet granulites. We cannot preclude, however, that the compositional variations of the Jijal granulites reflects 'primary' compositional variations of their protoliths resulting from low-pressure igneous crystallization. In particular, some parts the granulite protolith were possibly cumulative; that is, depleted in REE, with a positive Eu anomaly. In this scenario, the actual melting degree obtained in our partial melting models would be less than that estimated based on a homogeneous parental gabbroic source with a melt-like signature. An interesting result of our modelling is that dehydration-melting of gabbroic sources with melt-like compositions similar to arc basalts generates granulitic restites with positive Eu anomalies and low $(La/Sm)_N$ (Fig. 18). Positive Eu anomalies and low $(La/Sm)_N$ ratios are key trace element attributes of the lower continental crust (e.g. Rudnick, 1992; Rudnick & Gao, 2003). Our data indicate that the Kohistan island arc crust underwent a similar intracrustal differentiation to that inferred for the continental crust.

Origin of the Jijal garnet-bearing ultramafic lenses

The Jijal garnet-bearing ultramafic lenses might have been generated by: (1) amphibolite-facies metamorphism of plutonic or volcanic rocks from the island arc or

the oceanic crust (Jan & Howie, 1981; Jan, 1988; Yamamoto & Yoshino, 1998); (2) high-pressure fractional crystallization of arc magmas (e.g. Müntener *et al.*, 2001; Alonso-Perez *et al.*, 2004); and/or (3) dehydration-melting of amphibolites of igneous or metamorphic origin (e.g. Beard & Lofgren, 1991; Rapp *et al.*, 1991; Rushmer, 1993; Wolf & Wyllie, 1994; Rapp & Watson, 1995).

The major and trace element composition of the Jijal garnet amphibolites and pyroxenites indicates that they have a cumulitic or residual (i.e. mineral-like) composition dominated by variable amounts of amphibole, garnet and clinopyroxene. This, in conjunction with their ultrabasic major element composition, excludes the possibility that they were derived by closed-system metamorphism of arc volcanic or mafic plutonic rocks. High-pressure (*c.* 1·2 GPa) crystal fractionation of hydrous andesite magma reproduces the mineral assemblage of the Jijal ultramafic lenses (Müntener *et al.*, 2001; Alonso-Perez *et al.*, 2004). Alternatively, garnet-bearing hornblendite may have been generated by variable degrees of dehydration partial melting of pre-existing shallower igneous rocks or metamorphic amphibolites buried at depths equivalent to >1·0 GPa (e.g. Wolf & Wyllie, 1991, 1993; Rushmer, 1993; Wyllie & Wolf, 1993; Sen & Dunn, 1994; Rapp & Watson, 1995; Johannes & Holtz, 1996; López & Castro, 2001; Ducea, 2002). Dehydration-melting of a hornblende-rich source is consistent with the inferred metamorphic evolution of the Jijal complex, which indicates that the entire complex underwent burial and heating (Yamamoto, 1993; Yamamoto & Yoshino, 1998; Yamamoto & Nakamura, 2000; Yoshino & Okudaira, 2004). Jijal garnet hornblendite lenses probably were generated by dehydration-melting of pre-existing garnet-free hornblendite lenses interbedded within the gabbroic protolith of Jijal garnet granulite.

Genetic link between granites and the Jijal garnet-bearing lithologies

Dehydration-melting of amphibolitic protoliths at lower crustal depths is capable of generating granitic melts and garnet-bearing mafic and ultramafic restites (Johannes & Holtz, 1996, p. 282, and references therein). Many workers have emphasized the potential genetic link between granulites and granites in the continental crust (Clemens, 1990, and references therein; Vielzeuf *et al.*, 1990). In island arc settings, some silica-rich volcanism may have been generated by dehydration-melting of lower arc plutonic rocks (e.g. Smith & Leeman, 1987; Beard, 1995; Tamura & Tatsumi, 2002). The Jijal garnet granulite has been cited as a potential source of some rhyolitic paleo-volcanic rocks of the Kohistan arc complex (Shah & Shervais, 1999). Therefore, a possible scenario is that the granites in the Patan–Dasu metaplutonic complex were derived by dehydration-melting of hornblende-bearing gabbro and hornblendite, leaving as restites the Jijal garnet granulite and garnet amphibolite. The similarity of the metamorphic ages of the Jijal granulite to the igneous ages of the granites (Schaltegger *et al.*, 2002) is consistent with this scenario.

The major and trace element compositions of type 1 and type 2 granites in the Patan–Dasu metaplutonic complex are consistent with their being crustal melts leaving garnet-bearing restites. We propose that type 1 granites were produced by dehydration-melting of hornblendites leaving garnet amphibolite and pyroxenite restites similar to the Jijal garnet hornblendite lenses (Fig. 3d–f), whereas type 2 granites were generated by melting of hornblende gabbro sources leaving garnet granulite restites similar to the Jijal garnet granulites (Fig. 3a–c). Below, we quantitatively assess these hypotheses by means of conventional melting models.

Figure 19a illustrates the result of the melting model to account for the origin of type 1 granites by incremental melting of a hornblendite source. As a source, we used the composition of a hornblende cumulate from the Patan–Dasu metaplutonic complex. The highly fractionated REE patterns of type 1 granites (Fig. 13) are readily obtained by aggregated and instantaneous melts produced by partial melting of hornblendite (Fig. 19a) (see also Petford & Atherton, 1996). The REE patterns of some type 1 granites with Eu positive anomalies (Fig. 13) can be obtained by mixing of variable amounts of accumulated plagioclase and aggregate melts (Fig. 19a). The melting model generates garnet amphibolite restites (grt + amp + cpx) enriched in HREE and depleted in LREE. These features are broadly similar to the Jijal garnet-bearing ultramafic lenses, although the model restites are more LREE depleted (compare Figs 10a and 19). This may be due to smaller amounts of trapped melt in the Jijal hornblendite lenses.

Figure 19b shows the results of the melting model to account for type 2 granites by partial melting of Jijal hornblende gabbronorite leaving garnet granulite as restite. This model succeeds in reproducing the REE pattern of type 2 granites as incremental melts of such a source; however, the REE abundances of the model melts are higher than those of this type of granite (compare Figs 12 and 19b). Fractionation of amphibole is required to attain the low REE abundances (Fig. 19). On the other hand, this model reproduces well the REE pattern of the Jijal garnet granulites (compare Figs 7 and Fig 19b), as restites formed by incremental melting degrees of *c.* 20% melting. This melting degree is much higher than that predicted on the basis of water solubility in granite magmas and field evidence. Lower melting

degrees are obtained using sources with initial cumulitic REE patterns, corroborating the idea that some of the gabbroic protoliths of the Jijal garnet granulites might have been cumulates.

Overall, the REE modeling results validate our starting hypothesis, according to which the intrusive granites in the Patan–Dasu metaplutonic complex were formed by dehydration-melting of hornblende-bearing gabbroic and ultramafic sources, leaving Jijal garnet-bearing lithologies as restites.

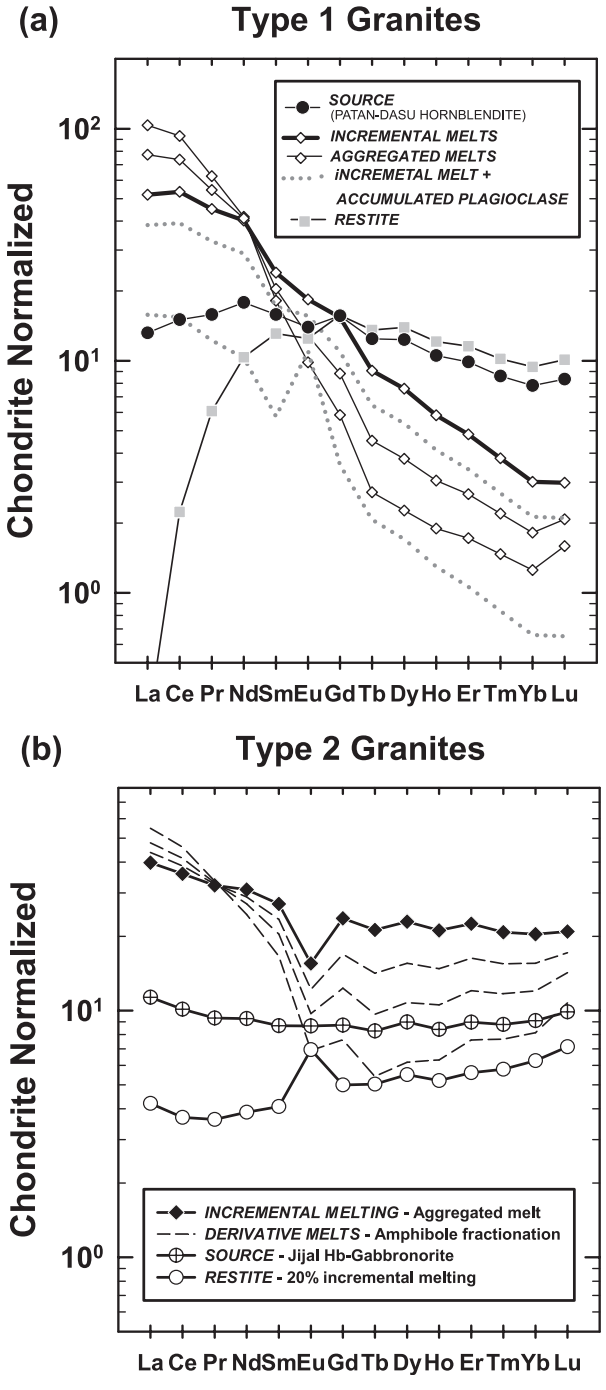

Fig. 19. (a) Forward trace element modeling of incremental melting of an amphibolite source to generate type 1 granites leaving garnet–clinopyroxene hornblendite residues. The melting source is a garnet-free hornblendite from the Patan–Dasu metaplutonic complex (our unpublished data). ◇, melts after 0·25 incremental melting. Melts and residue are compatible with experiments of partial melting of amphibolite to produce tonalitic melts (Rushmer, 1993; Sen & Dunn, 1994; Rapp & Watson, 1995; Johannes & Holtz, 1996). Also shown (dotted line) are derived melts produced by small fractions of crystal fractionation of apatite from primary incremental melts and the effect of mixing of variable amounts of accumulated plagioclase with incremental melts. Mineral–melt distribution coefficients are from Martin (1987) and Kawate & Arima (1998). Normalizing values after Anders & Grevesse (1989). (b) Forward trace element modeling of incremental melting of a hornblende gabbronorite source to generate type 2 intrusive granites producing garnet granulite restites. Melts are modeled as aggregated melts from 20% incremental melting of Jijal hornblende gabbronorite sample KG-03-B. The restites are garnet granulites with 7 wt % of garnet. Also shown are residual melts after variable crystal fractionation (30, 50 and 70%) of hornblende (0·93) and apatite (0·07). Mineral–melt distribution coefficients are taken from the compilation of Martin (1987) and Kawate and Arima (1998). Normalizing values after Anders & Grevesse (1989). Further details are provided in the text.

Granitic melt productivity of the Jijal hornblende gabbronorite and hornblendite lenses

The melt productivity of a rock undergoing dehydration-melting is controlled by the amount of water bound in hydroxyl-bearing minerals (Clemens & Vielzeuf, 1987; Thompson & Connolly, 1988; Johannes & Holtz, 1996, Chapter 9, and references therein; Clemens & Watkins, 2001; Vielzeuf & Schmidt, 2001). The Jijal hornblende gabbronorite contains 15–25 wt % of hornblende (Yamamoto & Yoshino, 1998) with *c.* 2 wt % of H_2O, limiting the whole-rock amount of H_2O bound in amphibole to 0·4–0·5 wt %. The maximum water solubility in granitic melts depends mostly on pressure and, to a lesser extent, on temperature (e.g. Johannes & Holtz, 1996, and references therein; Burnham, 1997; Holtz *et al.*, 2001). For measured maximum solubility of water in granitic melts at pressures attained in the lower crust of oceanic arcs (>12 wt % H_2O at 1–1·2 GPa) (Burnham, 1997, and references therein; Holtz *et al.*, 2001), we estimate that the Jijal hornblende gabbronorite generated only a few per cent of granitic melt (2·6–3·3 wt %). This result agrees well with Jijal field and textural evidence showing a prominent lack of leucosomes compared with migmatitic terranes. Hornblende-rich patches within the Jijal garnet granulites and the protoliths of Jijal garnet amphibolite lenses contained greater amounts of amphibole and, therefore, were more fertile, generating at least 17 wt % granitic melt. This result is in good agreement with field evidence showing abundant leucocratic veins near these ultramafic lenses and substantial amounts of leucosome within these lenses (Fig. 3e and f). These calculations also indicate that the

volume of granitic melts generated by dehydration-melting of the Jijal protoliths was rather low, in accordance with the small size and low proportion of both types of intrusive granite in the Patan–Dasu metaplutonic complex (Fig. 1).

Formation of garnet granulite roots in island arcs by dehydration-melting

Available geochronological data indicate that the Jijal garnet granulites and the Patan–Dasu metaplutonic complex granites formed during the building stage of the Kohistan island arc. Furthermore, our results point to dehydration-melting as a plausible and alternative scenario for the formation of garnet granulite roots and intracrustal differentiation in island arcs [see also Ducea (2001, 2002) for the case of continental arcs]. As delamination of garnet granulites and ultramafic rocks is at present one of the most appealing mechanisms for the transformation of basaltic island arc crust towards an andesitic continental-like crust (e.g. Jull & Kelemen, 2001), formation of garnet granulites by dehydration-melting in island arcs deserves further analysis. The relevance of this process depends mostly on (1) the stability of amphibole-bearing plutonic rocks in the middle–lower crust of island arcs and (2) the attainment of temperatures sufficiently high for the formation of garnet-bearing restites by dehydration-melting of amphibolitic sources.

Stability of igneous amphibole in Kohistan plutonic rocks

The stability of igneous amphibole in island arc plutonic rocks depends on pressure and temperature, crystallization redox conditions, and the composition and water content of the melts (e.g. Cawthorn & O'Hara, 1976; Helz, 1976; Grove & Kinzler, 1986; Moore & Carmichael, 1998; Macdonald *et al.*, 2000; Carmichael, 2002). There is little doubt that amphibole plays a significant role in the evolution of oceanic arc andesite–dacite–rhyolite suites. Amphibole phenocrysts are common in andesites and dacites in the Aleutians (Romick, 1990; Romick *et al.*, 1992) and the Lesser Antilles oceanic island arcs (Macdonald *et al.*, 2000), and quantitative models have identified it as a fractionating phase (e.g. Macdonald *et al.*, 2000, and references therein). The role of amphibole in the petrogenesis of water-undersaturated basaltic rocks is less clear, because amphibole phenocrysts are lacking in most primitive island arc basalts (e.g. Grove *et al.*, 1982; Wilson, 1989, and references therein; Macdonald *et al.*, 2000). Although the occurrence of amphibole-bearing gabbroic xenoliths in some island arc basalts attests to amphibole crystallization at depth in island arcs (e.g. Arculus & Wills, 1980; Conrad *et al.*, 1983; Fichaut *et al.*, 1989), a cogenetic relationship of these xenoliths with basalts is uncertain (Macdonald *et al.*, 2000, and references therein). In the Soufrière Hills (Montserrat) arc volcano, Zellmer *et al.* (2003) have suggested that the island arc basalts were formed by open-system fractional crystallization, whereas entrained amphibole-bearing mafic inclusions, with mineral and REE compositions analogous to the Jijal hornblende gabbronorite, formed by deep, closed-system crystallization of the same basalts.

Crystallization of amphibole in basaltic compositions such the Kohistan gabbros requires crystallization depths exceeding 3 km, where the appearance of liquidus amphibole is favored as a result of increasing water solubility in the melts (e.g. Cawthorn & O'Hara, 1976; Helz, 1976; Moore & Carmichael, 1998; Carmichael, 2002). In addition to high water contents, amphibole crystallization is favored by high Na_2O abundances and requires temperatures $<1050°C$ (Macdonald *et al.*, 2000, and references therein). Crystallization temperatures of primitive basaltic compositions are $>1180°C$ and generally too high to stabilize amphibole (Sisson & Grove, 1993*a*, 1993*b*). Because of the evolved composition, attested by their low Mg-number and high Na_2O abundances (Fig. 5), crystallization of the Sarangar and Jijal hornblende gabbronorites might have occurred at temperatures $<1050°C$, leading to the appearance of liquidus amphibole at middle arc crust conditions (>5–7 km) in the Kohistan arc. Alternatively, igneous amphibole in the Kohistan gabbros might be produced during the latest stages of deep, *in situ* crystallization (e.g. Langmuir, 1989) of relatively hydrous basaltic compositions when the water content of the residual melt rose and temperatures decreased below 1050°C (see also DeBari, 1994).

P–T conditions for the formation of island arc garnet granulite by dehydration-melting

Jull & Kelemen (2001) have shown that the formation of garnet granulite with a bulk composition similar to that of the Talkeetna arc gabbronorite is possible where crustal thickness exceeds 25–30 km for a hot geotherm with Moho temperatures in the range 800–1000°C. Those workers considered high-pressure transformation of gabbronorite to garnet granulite through subsolidus reactions involving olivine such as anorthite + forsterite = pyrope–grossular. As most Kohistan gabbros are rather evolved and lack olivine, formation of garnet granulite by subsolidus reactions involving olivine is unlikely. Dehydration-melting involves supersolidus reactions such as amphibole + plagioclase = melt + anhydrous mafic minerals. At pressure exceeding *c.* 1·0 GPa, this reaction generates garnet-bearing restites and water-undersaturated granitic melts (Johannes & Holtz, 1996, Chapter 9, and references therein).

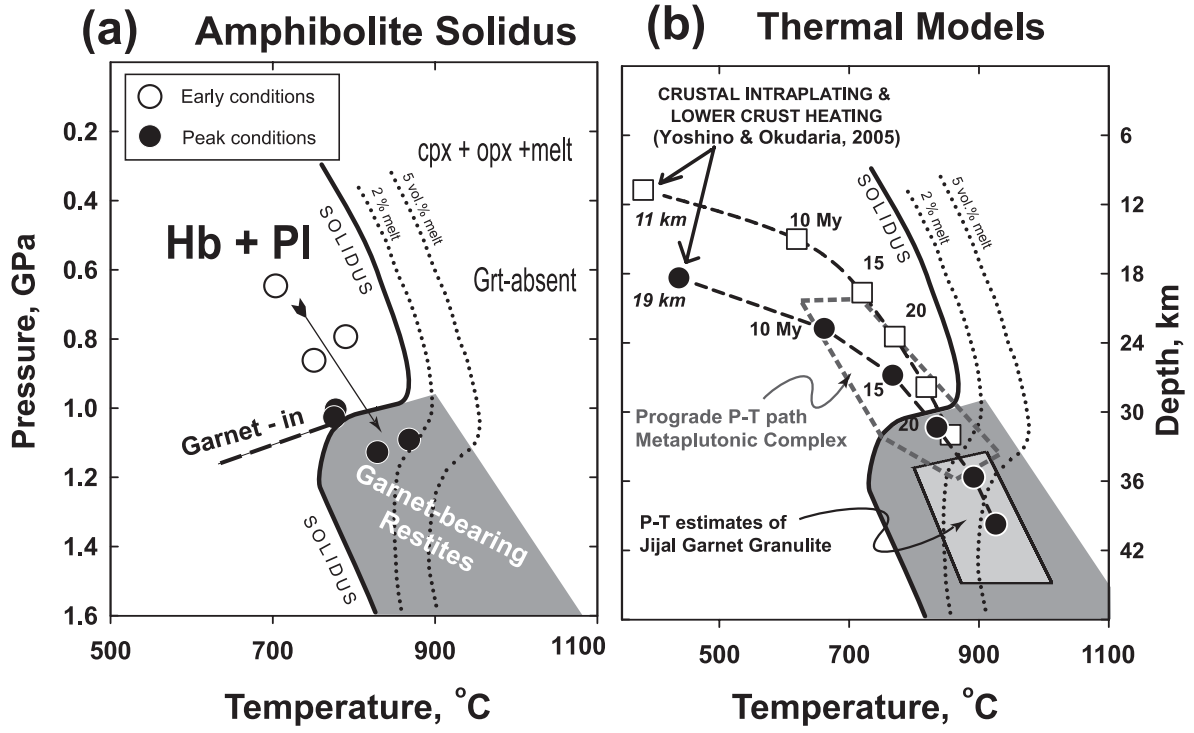

Fig. 20. (a) Pressure–temperature diagram showing the solidus for dehydration-melting of amphibolite [modified after López & Castro (2001)]. A characteristic of the amphibolite solidus is the abrupt back bend towards lower temperatures at pressures greater than 1·0 GPa. (Rapp *et al.*, 1991; Wyllie & Wolf, 1993; Wolf & Wyllie, 1994; Rapp & Watson, 1995; López & Castro, 2001). Above this pressure, amphibolite dehydration-melting occurs, forming garnet-bearing granulite, amphibolite and pyroxene amphibolite, and, at higher temperature, garnet pyroxenite restites. Also shown in the figure are the experimentally determined hypersolidus curves for 2 and 5 vol. % of N-MORB amphibolite (López & Castro, 2001), and the early (○) and peak (●) metamorphic conditions recorded by the Kohistan granulites (Yoshino & Okudaira, 2004). It should be noted that peak metamorphic conditions lie below the solidus for amphibolite dehydration-melting. (b) As (a), but also showing two *P–T–t* paths inferred by thermal modeling and proposed for the evolution of the Kohistan lower crust by Yoshino & Okudaira (2004). The thermal model shown is the double-plate model of Yoshino & Okudaira (2004) with simultaneous intrusions in the middle arc crust and at the Moho. Dashed lines show the *P–T–t* evolution in 5 Myr intervals for the case of simultaneous intrusions intruded at initial depths of 11 km (□) and 19 km (●). Also shown are the *P–T* estimates for the Patan–Dasu metaplutonic complex and the Jijal granulites (Yoshino & Okudaira, 2004, and references therein).

Unlike subsolidus reactions, dehydration-melting is a favorable kinetic environment for the formation of garnet granulite because the presence of hydrous melt drastically enhances reaction rates and garnet growth (e.g. Rushmer, 1993; Wolf & Wyllie, 1993).

The topology of the vapor-absent solidus of amphibolite determines the onset of dehydration-melting of amphibole, and has a positive dP/dT slope at pressures below *c.* 0·9 GPa (e.g. Wyllie & Wolf, 1993; López & Castro, 2001) (Fig. 20a). This topology implies that generation of granulites by dehydration-melting of amphibolite throughout most the crust needs an anomalously hot geothermal gradient (Thompson, 1999, and references therein). At pressures exceeding *c.* 1·0 GPa, however, the amphibolite solidus bends back (Fig. 20a). This abrupt change in the solidus slope coincides with the appearance of garnet in dehydration-melting residues (Wyllie & Wolf, 1993, and references therein; López & Castro, 2001). This topology is reproduced by virtually all dehydration-melting experiments on amphibolites (Loock *et al.*, 1990; Wyllie & Wolf, 1993, and references therein; Sen & Dunn, 1994; Rapp & Watson, 1995). This topology implies that when an island arc thickens to more than about 25–30 km (Fig. 20), and through a substantial temperature interval (Fig. 20a), hornblende-bearing plutonic or metavolcanic rocks would partially melt, generating granitic magma and dense garnet-bearing restites (see also Ducea, 2001, 2002). Crustal thickness greater than 25–30 km are attained only in mature oceanic arcs (e.g. Schubert & Sandwell, 1989; Boutelier *et al.*, 2003) and this mechanism for the formation of garnet granulite is, therefore, relevant only for mature island arcs. In addition, the melt fractions generated at this pressure are too low (<5 vol. %; Fig. 20a) to be considered significant for the generation of large volumes of granitic melt (Johannes & Holtz, 1996). None the less, the outcome of this reaction is highly relevant for the stability of the lower island arc crust and the intracrustal physical and chemical differentiation of mature island arcs.

The prograde metamorphic evolution of the Patan–Dasu metaplutonic complex involves *P–T* paths recording burial and heating of shallower arc plutonic rocks (Yamamoto, 1993; Jan & Karim, 1995; Yoshino *et al.*, 1998; Yoshino & Okudaira, 2004) (Fig. 20b). Peak metamorphic conditions in this complex were at pressures >1·0 GPa, where the onset of dehydration-melting of hornblende occurs (Fig. 20a and b). Higher pressure peak conditions are recorded in the Jijal complex garnet granulites that are well inside the dehydration-melting field of hornblende (Fig. 20b). Yoshino & Okudaira (2004) have shown that the *P–T–t* evolution of the Patan–Dasu metaplutonic metagabbros and the Jijal granulites requires a thermal model with simultaneous igneous underplating at crustal and sub-Moho levels (Fig. 20b). Their 'double-plate' model accounts for the metamorphic evolution of the Kohistan granulites for the case of buried plutonic bodies intruded at initial depths of 11 and 19 km (Yoshino & Okudaira, 2004) (Fig. 20b). These conditions lasted for 15–25 Myr, which is slightly longer that the 15 Myr interval inferred on the basis of geochronological data for the accretion of the Kohistan island arc (Yoshino & Okudaira, 2004) (Fig. 20b) and is a feasible timescale for mature island arcs. The double-plate scenario unavoidably leads to a *P–T* path where high-pressure dehydration-melting is attained when the arc becomes thicker than 25–30 km (Fig. 20b). Moreover, the double-plate model is consistent with growing evidence for higher temperatures in the roots of island arcs than those predicted by steady-state geothermal models: Elkins Tanton *et al.* (2001) have concluded that high-temperature mantle (1300–1450°C) was in transient contact with the lower arc crust in the Cascades. Likewise, there is thermometric and structural evidence for a hot and wet sub-arc mantle in the exposed mantle section of some paleo-island arc terranes (Kelemen *et al.*, 2003*b*; Mehl *et al.*, 2003). To account for a high temperature at the base of the Kohistan island arc crust, Yoshino & Okudaira (2004) considered underplating of primitive basalts. We think that a more suitable heating source was probably the transient intrusions of hot mantle diapirs to the base of the arc crust.

A working scenario for the Kohistan paleo-arc and island arcs and its bearing on the Andesite Model of continental crustal growth

Figure 21 summarizes our model for the formation of garnet granulite in the lower crust of the Kohistan paleo-island arc. A similar accretion scenario for island arcs was originally proposed by Kuno (1968) (see also Kelemen *et al.*, 2003*a*, fig. 26). The onset of arc growth, initiated by northward subduction of the paleo-Tethys, was marked by shallow intrusions into pre-existing oceanic crust and sediments (Fig. 21a). As in other island arc sections, however, there is little evidence for pre-existing oceanic crust in Kohistan except perhaps for some Kamila amphibolite-facies metavolcanic rocks (Jan, 1988). This stage of arc growth is preserved in the Swat River section of the Kamila amphibolite belt (Jan & Kempe, 1973; Jan, 1988; Khan & Coward, 1991; Khan *et al.*, 1993; Treloar *et al.*, 1996).

Further intrusion into the middle arc crust, and intracrustal igneous differentiation, characterized the juvenile stage of the Kohistan island arc (Fig. 21b; intrusion A). Shallower units of the metaplutonic complex formed at this stage. Fractionation of andesitic melts at various depths and deep closed-system crystallization of hydrous arc basalts generated amphibole-bearing rocks ranging from mafic (hornblende-bearing gabbros and diorites) to ultramafic (hornblende cumulates) in the middle arc crust. In addition, metamorphic amphibolites may be also produced after earlier magmatism by water ingression owing to crystallization of deeper igneous intrusions. Further shallow intrusions gradually depressed earlier intrusions into the roots of the growing arc edifice (Fig. 21b; intrusion B) and, at the mature stage, the thickness of the Kohistan crust was greater than 25–30 km (Fig. 21c; intrusion C). Deep crustal hornblende-bearing plutonic rocks (Fig. 21c; intrusion A) underwent dehydration-melting leading to formation of mafic and ultramafic garnet-bearing restites and small volumes of highly incompatible trace element and LREE-enriched granitic melts (Figs 20 and 21c). Dehydration-melting was probably coeval with episodic intrusions of hot mantle diapirs near the base of the arc crust. Alternatively, the high geothermal gradient may be due to localized convection induced by slab dehydration leading to thinning of the sub-arc lithospheric mantle (Arcay *et al.*, 2006). Dehydration-melting of the lower crust resulted in the lithological and chemical differentiation of the island arc crust and in an evolution of the middle crust towards an andesitic composition like that of the continental crust (e.g. Kuno, 1968). In addition, mixing between primitive mafic magmas and crustal melts with garnet-bearing residues could form high Mg-number andesite with compositions similar to the continental crust (Kelemen *et al.*, 2003*a*). The intracrustal differentiation model pictured here for island arcs is similar to that advocated by some workers for intracrustal differentiation and formation of the lower continental crust (e.g. Taylor & McLennan, 1985; Wedepohl, 1991; Johannes & Holtz, 1996).

As suggested by previous workers (e.g. Arndt & Goldstein, 1989; Kay & Kay, 1991, 1993) and quantified by Jull & Kelemen (2001), dense garnet-bearing island

arc roots may delaminate within timescales relevant for arc magmatism. This could occur when oceanic arcs reach a critical thickness of around 25–35 km (equivalent to *c.* 0·8–1·0 GPa) coinciding with the hornblende-out–garnet-in boundary of dehydration-melting of amphibole (Figs 20 and 21c). Delamination of dense mafic to ultramafic crustal roots may yield an andesitic bulk composition for the remaining island arc crust. In addition, it may induce further diapirism of hot mantle into the base of the island arc crust, promoting further melting. Because immature arcs are easily subducted whereas thick, mature arcs are scraped off and accreted to the overriding plate (e.g. Boutelier *et al.*, 2003), preferential accretion of mature arcs with andesitic composition may have contributed to a greater extent than immature basaltic arcs to the growth of the continental crust.

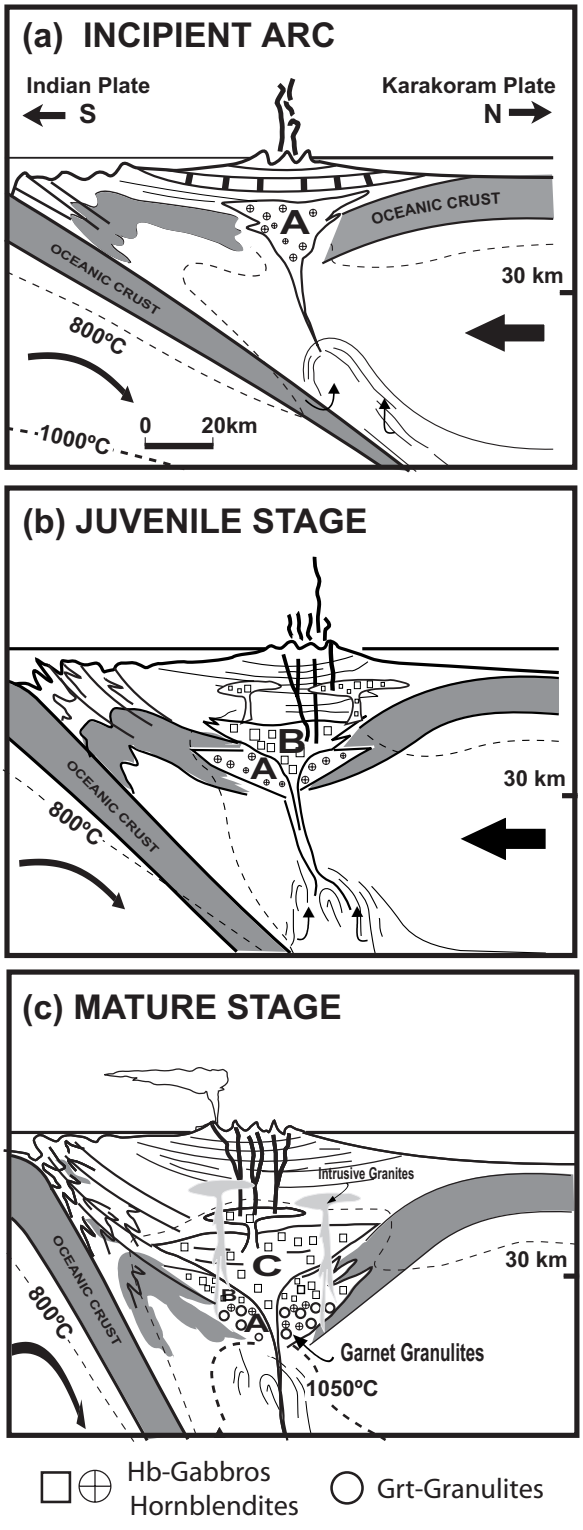

CONCLUSIONS

The lower crust of the Kohistan paleo-island arc exposed along the Indus River comprises two series of metagabbroic rocks, the Jijal and Sarangar sections. Together they represent a unique exposure of the roots of a mature island arc. The gabbroic rocks formed via arc magmatism and are not remnants of oceanic crust generated in a mid-ocean ridge setting. Their garnet-free gabbroic assemblages formed by *in situ* crystallization, with variable trapped melt, of moderately evolved, hydrous island arc basalts. REE abundances in the Jijal garnet granulite cannot be reproduced by crystallization of high Mg-number or derivative andesite, but can be explained by the formation of plagioclase–garnet assemblages with variable trapped melt crystallization from primitive island arc basalts, or through dehydration-melting of Jijal hornblende gabbronorite. In either case the amount of segregated or restitic igneous garnet was low (<5 wt %). Field, petrographic and geochemical data indicate that the primary anhydrous mineralogy of the Jijal garnet granulite was probably formed by dehydration-melting of sources comparable with Jijal hornblende gabbronorite. These granulites contain greater amounts of garnet than predicted by melting models and probably formed by subsolidus reactions concomitant with dehydration-melting. A similar dehydration-melting scenario is proposed for the Jijal garnet-bearing hornblendites. Dehydration-melting generated two types of granites, which now occur as sills and laccoliths in the overlying Patan–Dasu metaplutonic

Fig. 21. Schematic illustration of a possible scenario for the growth of the Mesozoic Kohistan island arc in the (a) incipient, (b) juvenile and (c) mature stages of this island arc, and the formation of the Jijal garnet granulite and the Patan–Dasu metaplutonic complex. The 1050°C geotherm in (c) is a hypothetical thermal front causing a hot geothermal gradient at the base of the island arc crust. This may be caused by localized convection in the mantle wedge as a result of slab dehydration leading to heating and thinning of the island arc lithosphere (Arcay *et al.*, 2006) or upwelling of sub-arc mantle diapirs. (See text for further details.)

complex, leaving the Jijal garnet amphibolite and garnet granulites as restites.

This process occurred at the mature stage of island arc growth when shallower hornblendite-bearing plutonic rocks were buried and heated to depths exceeding 25–30 km and sub-arc temperatures of about 900°C. This thermal evolution is plausible in island arcs if, concomitantly with igneous intrusion in the middle crust, the sub-arc Moho was heated by intrusion of mantle diapirs, lateral flow of hot asthenospheric mantle or thermal erosion of the sub-arc lithosphere as a result of convection instabilities. Dehydration-melting hence resulted in physical and chemical intracrustal differentiation of the island arc crust. It generated dense garnet granulite roots that may have delaminated, triggering further melting of lower hornblende-bearing basaltic lower crust, and driving the composition of the island arc to that of andesite, thus affording a plausible solution to the so-called 'arc paradox' for the formation of continental crust in island arcs.

ACKNOWLEDGEMENTS

We are indebted to Jean-Pierre Bard for providing us with samples and precious field notes of his 1970s and 1980s expeditions to the Himalayas. We also thank Andrew Greene for kindly sharing data for the Talkeetna island arc and Simone Pourtales for assistance during ICP-MS analyses at ISTEEM. Nicholas Arndt is acknowledged for careful editorial work and useful comments, and Steve Foley and Susan DeBari for providing detailed and constructive reviews that helped to improve the manuscript. This work has been supported by the Spanish 'Ministerio de Educación y Ciencia' through a 'Ramón y Cajal' fellowship to C.J.G., 'Accción Integrada Hispano-Francesa HF02-0093', and research grants BTE2001-3308, BTE2004-1489, and the 'Consejería de Innovación y Ciencia' of the 'Junta de Andalucía' research groups RNM-0131 and RNM-0145. This research is supported by the European Funds for Regional Development. Additional financial support came from grants of the Swiss Science Foundation and the French CNRS.

REFERENCES

Alonso-Perez, R., Ulmer, P., Müntener, O. & Thompson, A. B. (2004). Role of garnet fractionation in H_2O undersaturated andesite liquids at high pressure (abstract). *Lithos* **73**, S1–S2.

Anczkiewicz, R. & Vance, D. (2000). Isotopic constraints on the evolution of metamorphic conditions in the Jijal–Patan Complex and Kamila Belt of the Kohistan Arc, Pakistan Himalaya. In: Khan, M. A., Treloar, P. J., Searle, M. P. & Jan, M. Q. (eds) *Tectonics of the Nanga Parbat Syntaxis and the Western Himalaya, Geological Society, London, Special Publications* **170**, 321–331.

Anczkiewicz, R., Thirlwall, M. & Platt, J. (2002). Influence of inclusions and leaching techniques on Sm–Nd and Lu–Hf garnet chronology (abstract). *Geochimica et Cosmochimica Acta* **66**, A19–A19.

Anders, E. & Grevesse, N. (1989). Abundances of the elements—meteoritic and solar. *Geochimica et Cosmochimica Acta* **53**, 197–214.

Arbaret, L. & Burg, J. P. (2003). Complex flow in lowest crustal, anastomosing mylonites: Strain gradients in a Kohistan gabbro, northern Pakistan. *Journal of Geophysical Research-Solid Earth* **108**, article number 2467.

Arcay, D., Doin, M.-P., Tric, E., Bousquet, R. & de Capitani, C. (2006). Overriding plate thinning in suduction zones: localized convection induced by slab dehydration. *Geochemistry, Geophysics, Geosystems* **7(1)**, doi: 10.1029/2005GC001061.

Arculus, R. J. & Johnson, R. W. (1981). Island-arc magma sources: a geochemical assessment of the roles of slab-derived components and crustal contamination. *Geochemical Journal* **15**, 109–133.

Arculus, R. J. & Wills, K. J. A. (1980). The petrology of plutonic blocks and inclusions from the Lesser Antilles Island Arc. *Journal of Petrology* **21**, 743–799.

Arndt, N. T. & Goldstein, S. L. (1989). An open boundary between lower continental crust and mantle—its role in crust formation and crustal recycling. *Tectonophysics* **161**, 201–212.

Ayers, J. (1998). Trace element modeling of aqueous fluid—peridotite interaction in the mantle wedge of subduction zones. *Contributions to Mineralogy and Petrology* **132**, 390–404.

Baker, D. R. & Eggler, D. H. (1983). Fractionation paths of Atka (Aleutians) high-alumina basalts: constraints from phase relations. *Journal of Volcanology and Geothermal Research* **18**, 387–404.

Bard, J.-P. (1983*a*). Metamorphic evolution of an obducted island arc: example of the Kohistan sequence (Pakistan) in the Himalayan collided range. *Geological Bulletin of the University of Peshawar* **16**, 105–184.

Bard, J.-P. (1983*b*). Metamorphism of an obducted island arc: example of the Kohistan sequence (Pakistan) in the Himalayan collided range. *Earth and Planetary Science Letters* **65**, 133–144.

Barker, F. (1979). Trondhjemites: definition, environment and hypothesis of origin. In: Barker, F. (ed.), *Trondhjemites, Dacites and Related Rocks*. Amsterdam: Elsevier, pp. 1–12.

Beard, J. S. (1986). Characteristic mineralogy of arc-related cumulate gabbros—implications for the tectonic setting of gabbroic plutons and for andesite genesis. *Geology* **14**, 848–851.

Beard, J. S. (1995). Experimental, geological, and geochemical constraints on the origins of low-K silicic magmas in oceanic arcs. *Journal of Geophysical Research—Solid Earth* **100**, 15593–15600.

Beard, J. S. & Day, H. W. (1986). Origin of gabbro pegmatite in the Smartville intrusive complex, northern Sierra Nevada, California. *American Mineralogist* **71**, 1085–1099.

Beard, J. S. & Lofgren, G. E. (1991). Dehydration melting and water-saturated melting of basaltic and andesitic greenstones and amphibolites at 1, 3, and 6·9 kbar. *Journal of Petrology* **32**, 365–401.

Blattner, P. (1976). Replacement of hornblende by garnet in granulite facies assemblages near Milford Sound, New Zealand. *Contributions to Mineralogy and Petrology* **55**, 181–190.

Bodinier, J. L. & Godard, M. (2003). Orogenic, ophiolitic, and abyssal peridotites. In: Carlson, R. W. (ed.), *Treatise on Geochemistry. 2. Geochemistry of the Mantle and Core*. Amsterdam: Elsevier, pp. 103–170.

Boutelier, D., Chemenda, A. & Burg, J.-P. (2003). Subduction versus accretion of intra-oceanic volcanic arcs: insight from thermo-mechanical analogue experiments. *Earth and Planetary Science Letters* **212**, 31–45.

Brenan, J. M., Shaw, H. F., Ryerson, R. J. & Phinney, D. L. (1995). Mineral–aqueous fluid partitioning of trace elements at 900°C and 2·0 GPa: constraints on trace element chemistry of mantle and deep crustal fluids. *Geochimica et Cosmochimica Acta* **59**, 3331–3350.

Burg, J. P., Bodinier, J. L., Chaudhry, S., Hussain, S. & Dawood, H. (1998). Infra-arc mantle–crust transition and intra-arc mantle diapirs

in the Kohistan Complex (Pakistani Himalaya); petro-structural evidence. *Terra Nova* **10**, 74–80.

Burnham, C. W. (1997). Magmas and hydrothermal fluids. In: Barnes, H. L. (ed.), *Geochemistry of Hydrothermal Ore Deposits*. New York: John Wiley, pp. 63–123.

Cannat, M. (1993). Emplacement of mantle rocks in the sea-floor at midocean ridges. *Journal of Geophysical Research—Solid Earth* **98**, 4163–4172.

Cannat, M., Karson, J. A. & Miller, D. J. (1995). & Shipboard Scientific Party (eds) (1995), *Ocean Drilling Program, Initial Reports, 153*. College Station, TX: Ocean Drilling Program.

Cannat, M., Lagabrielle, Y., Bougault, H., Casey, J., deCoutures, N., Dmitriev, L. & Fouquet, Y. (1997). Ultramafic and gabbroic exposures at the Mid-Atlantic Ridge: geological mapping in the 15°N region. *Tectonophysics* **279**, 193–213.

Carmichael, I. S. E. (2002). The andesite aqueduct: perspectives on the evolution of intermediate magmatism in west–central (105–99°W) Mexico. *Contributions to Mineralogy and Petrology* **143**, 641–663.

Cawthorn, R. G. & O'Hara, M. J. (1976). Amphibole fractionation in calc-alkaline magma genesis. *American Journal of Science* **276**, 309–329.

Clarke, G. L., Klepeis, K. A. & Daczko, N. R. (2000). Cretaceous high-P granulites at Milford Sound, New Zealand: metamorphic history and emplacement in a convergent margin setting. *Journal of Metamorphic Geology* **18**, 359–374.

Clemens, J. D. (1990). The granulite–granite connection. In: Vielzeuf, D. & Vidal, P. (eds) *Granulites and Crustal Evolution*. Dordrecht: Kluwer Academic, pp. 25–36.

Clemens, J. D. & Vielzeuf, D. (1987). Constraints on melting and magma production in the crust. *Earth and Planetary Science Letters* **86**, 287–306.

Clemens, J. D. & Watkins, J. M. (2001). The fluid regime of high-temperature metamorphism during granitoid magma genesis. *Contributions to Mineralogy and Petrology* **140**, 600–606.

Condie, K. C. (1997). *Plate Tectonics and Continental Evolution*. Oxford: Butterworth–Heinemann.

Conrad, W. K., Kay, S. M. & Kay, R. W. (1983). Magma mixing in the Aleutian Arc—evidence from cognate inclusions and composite xenoliths. *Journal of Volcanology and Geothermal Research* **18**, 279–295.

Daczko, N. R., Clarke, G. L. & Klepeis, K. A. (2001). Transformation of two-pyroxene hornblende granulite to garnet granulite involving simultaneous melting and fracturing of the lower crust, Fiordland, New Zealand. *Journal of Metamorphic Geology* **19**, 547–560.

DeBari, S. M. (1994). Petrogenesis of the Fiambalá gabbroic intrusion, northwestern Argentina. A deep-crustal syntectonic pluton in a continental magmatic arc. *Journal of Petrology* **35**, 679–713.

DeBari, S. M. (1997). Evolution of magmas in continental and oceanic arcs: the role of the lower crust. *Canadian Mineralogist* **35**, 501–519.

DeBari, S. M. & Coleman, R. G. (1989). Examination of the deep levels of an island-arc—evidence from the Tonsina ultramafic–mafic assemblage, Tonsina, Alaska. *Journal of Geophysical Research—Solid Earth and Planets* **94**, 4373–4391.

DeBari, S. M. & Sleep, N. H. (1991). High-Mg, low-Al bulk composition of the Talkeetna island-arc, Alaska—implications for primary magmas and the nature of arc crust. *Geological Society of America Bulletin* **103**, 37–47.

Dick, H. J. B., Natland, J. H. & Miller, D. J. (1999). Shipboard Scientific Party (eds) (1999), *Ocean Drilling Program, Summary, 176*. College Station, TX: Ocean Drilling Program.

Dick, H. J. B., Natland, J. H. & Alt, J. C. *et al.* (2000). A long *in situ* section of the lower ocean crust: results of ODP Leg 176 drilling at the Southwest Indian Ridge. *Earth and Planetary Science Letters* **179**, 31–51.

Dimalanta, C., Taira, A., Yumul, G. P., Tokuyama, H. & Mochizuki, K. (2002). New rates of western Pacific island arc magmatism from seismic and gravity data. *Earth and Planetary Science Letters* **202**, 105–115.

Drummond, M. S., Defant, M. J. & Kepezhinskas, P. K. (1996). Petrogenesis of slab-derived trondhjemite–tonalite–dacite/adakite magmas. *Transactions of the Royal Society of Edinburgh—Earth Sciences* **87**, 205–215.

Ducea, M. N. (2001). The California arc: thick granitic batholiths, eclogitic residues, lithospheric-scale thrusting, and magmatic flare-ups. *Geological Society of America Today* **11**, 4–10.

Ducea, M. N. (2002). Constraints on the bulk composition and root foundering rates of continental arcs: a California arc perspective. *Journal of Geophysical Research—Solid Earth* **107**, article number 2304.

Ducea, M. N. & Saleeby, J. B. (1996). Buoyancy sources for a large, unrooted mountain range, the Sierra Nevada, California: evidence from xenolith thermobarometry. *Journal of Geophysical Research—Solid Earth* **101**, 8229–8244.

Ducea, M. N. & Saleeby, J. (1998a). A case for delamination of the deep batholithic crust beneath the Sierra Nevada, California. *International Geology Review* **40**, 78–93.

Ducea, M. N. & Saleeby, J. B. (1998b). The age and origin of a thick mafic–ultramafic keel from beneath the Sierra Nevada batholith. *Contributions to Mineralogy and Petrology* **133**, 169–185.

Elkins Tanton, L. T., Grove, T. L. & Donnelly-Nolan, J. (2001). Hot, shallow mantle melting under the Cascades volcanic arc. *Geology* **29**, 631–634.

Ellam, R. M. & Hawkesworth, C. J. (1988). Elemental and isotopic variations in subduction related basalts—evidence for a three component model. *Contributions to Mineralogy and Petrology* **98**, 72–80.

Fichaut, M., Marcelot, G. & Clocchiatti, R. (1989). Magmatology of Mt. Pelée (Martinique, F.W.I). II: Petrology of gabbroic and dioritic cumulates. *Journal of Volcanology and Geothermal Research* **38**, 171–187.

Foley, S. F., Tiepolo, M. & Vannucci, R. (2002). Growth of early continental crust controlled by melting of amphibolite in subduction zones. *Nature* **417**, 837–840.

Garrido, C. J. & Bodinier, J. L. (1999). Diversity of mafic rocks in the Ronda peridotite: evidence for pervasive melt–rock reaction during heating of subcontinental lithosphere by upwelling asthenosphere. *Journal of Petrology* **40**, 729–754.

Garrido, C. J., Bodinier, J. L. & Alard, O. (2000). Incompatible trace element partitioning and residence in anhydrous spinel peridotites and websterites from the Ronda orogenic peridotite. *Earth and Planetary Science Letters* **181**, 341–358.

Garrido, C. J., Kelemen, P. B. & Hirth, G. (2001). Variation of cooling rate with depth in lower crust formed at an oceanic spreading ridge: plagioclase crystal size distributions in gabbros from the Oman ophiolite. *Geochemistry, Geophysics, Geosystems* **2**, doi: 10.1029/2000GC000136.

Godard, M., Jousselin, D. & Bodinier, J. L. (2000). Relationships between geochemistry and structure beneath a palaeo-spreading centre: a study of the mantle section in the Oman ophiolite. *Earth and Planetary Science Letters* **180**, 133–148.

Greene, A. R., Kelemen, P. B., DeBari, S. M., Clift, P. D. & Blusztajn, J. (2006). Detailed geochemical study of island arc crust: the Talkeetna arc section, south–central Alaska. *Journal of Petrology* **47**, 1051–1093.

Grove, T. L. & Kinzler, R. J. (1986). Petrogenesis of andesites. *Annual Review of Earth and Planetary Sciences* **14**, 417–454.

Grove, T. L., Gerlach, D. C. & Sando, T. W. (1982). Origin of calc-alkaline series lavas at Medicine Lake volcano by fractionation, assimilation and mixing. *Contributions to Mineralogy and Petrology* **80**, 160–182.

Grove, T. L., Parman, S. W., Bowring, S. A., Price, R. C. & Baker, M. B. (2002). The role of an H_2O-rich fluid component in the generation of primitive basaltic andesites and andesites from the Mt. Shasta region, N California. *Contributions to Mineralogy and Petrology* **142**, 375–396.

Hart, S. R., Blusztajn, J., Dick, H. J. B., Meyer, P. S. & Muehlenbachs, K. (1999). The fingerprint of seawater circulation in a 500-meter section of ocean crust gabbros. *Geochimica et Cosmochimica Acta* **63**, 4059–4080.

Hartel, T. H. D. & Pattison, D. R. M. (1996). Genesis of the Kapuskasing (Ontario) migmatitic mafic granulites by dehydration melting of amphibolite: the importance of quartz to reaction progress. *Journal of Metamorphic Geology* **14**, 591–611.

Heier, K. S. (1973). Geochemistry of granulite facies rocks and problems of their origin. *Philosophical Transactions of the Royal Society of London, Series A* **273**, 429–442.

Helz, R. T. (1976). Phase relations of basalts in their melting ranges at $P_{H2O} = 5$ Kb. 2. Melt compositions. *Journal of Petrology* **17**, 139–193.

Hofmann, A. W. (1988). Chemical differentiation of the Earth—the relationship between mantle, continental crust, and oceanic crust. *Earth and Planetary Science Letters* **90**, 297–314.

Holtz, F., Johannes, W., Tamic, N. & Behrens, H. (2001). Maximum and minimum water contents of granitic melts generated in the crust: a reevaluation and implications. *Lithos* **56**, 1–14.

Jan, M. Q. (1979). Petrography of the Jijal Complex, Kohistan. In: Tahirkheli, R. A. K. & Jan, M. Q. (eds) *Geology of Kohistan, Karakoram Himalaya, Northern Pakistan*. Peshawar: University of Peshawar, pp. 31–49.

Jan, M. Q. (1988). Geochemistry of amphibolites from the southern part of the Kohistan Arc, N. Pakistan. *Mineralogical Magazine* **52**, 147–159.

Jan, M. Q. & Howie, R. A. (1981). The mineralogy and geochemistry of the metamorphosed basic and ultrabasic rocks of the Jijal Complex, Kohistan, NW Pakistan. *Journal of Petrology* **22**, 85–126.

Jan, M. Q. & Karim, A. (1995). Coronas and high-P veins in metagabbros of the Kohistan island arc, northern Pakistan; evidence for crustal thickening during cooling. *Journal of Metamorphic Geology* **13**, 357–366.

Jan, M. Q. & Kempe, D. R. C. (1973). The petrology of the basic and intermediate rocks of upper Swat, Pakistan. *Geological Magazine* **110**, 285–300.

Jan, M. Q. & Windley, B. F. (1990). Chromian spinel silicate chemistry in ultramafic rocks of the Jijal Complex, northwest Pakistan. *Journal of Petrology* **31**, 667–715.

Jochum, K. P., Seufert, H. M. & Thirwall, M. F. (1990). Muti-element analysis of 15 international standard rocks by isotope-dilution spark source mass spectrometry (ID-SSMS). *Analytical Chemistry* **331**, 104–110.

Johannes, W. & Holtz, F. (1996). *Petrogenesis and Experimental Petrology of Granitic Rocks*. Berlin: Springer.

Johnson, M. C. & Plank, T. (1999). Dehydration and melting experiments constrain the fate of subducted sediments. *Geochemistry, Geophysics, Geosystems* **1**, 1999GC000014.

Jull, M. & Kelemen, P. B. (2001). On the conditions for lower crustal convective instability. *Journal of Geophysical Research—Solid Earth* **106**, 6423–6446.

Kawate, S. & Arima, M. (1998). Petrogenesis of the Tanzawa plutonic complex, central Japan: exposed felsic middle crust of the Izu–Bonin–Mariana arc. *Island Arc* **7**, 342–358.

Kay, R. W. & Kay, S. M. (1991). Creation and destruction of lower continental crust. *Geologische Rundschau* **80**, 259–278.

Kay, R. W. & Kay, S. M. (1993). Delamination and delamination magmatism. *Tectonophysics* **219**, 177–189.

Kay, S. M. & Kay, R. W. (1985). Role of crystal cumulates and the oceanic crust in the formation of the lower crust of the Aleutian arc. *Geology* **13**, 461–464.

Kelemen, P. B., Hanghøj, K. & Greene, A. R. (2003a). One view of the geochemistry of subduction-related magmatic arcs, with emphasis on primitive andesite and lower crust. *Treatise on Geochemistry* **3**, 593–659. *Geochemistry of the Crust*. Amsterdam: Elsevier.

Kelemen, P. B., Rilling, J. L., Parmentier, E. M., Mehl, L. & Hacker, B. R. (2003b). Thermal structure due to solid-state flow in the mantle wedge beneath arcs. In: Eiler, J. M. (ed.), *Inside the Subduction Factory, Geophysical Monograph, American Geophysical Union* **138**, 293–311.

Kelemen, P. B., Yogodzinski, G. M. & Scholl, D. W. (2003c). Along strike variation in lavas of the Aleutian island arc: implications for the genesis of high Mg# andesite and the continental crust. In: Eiler, J. M. (ed.), *Inside the Subduction Factory, Geophysical Monograph, American Geophysical Union* **138**, 1–54.

Keppler, H. (1996). Constraints from partitioning experiments on the composition of subduction-zone fluids. *Nature* **380**, 237–240.

Keppler, H. & Wyllie, P. J. (1990). Role of fluids in transport and fractionation of uranium and thorium in magmatic processes. *Nature* **348**, 531–533.

Keppler, H. & Wyllie, P. J. (1991). Partitioning of Cu, Sn, Mo, W, U, and Th between melt and aqueous fluid in the systems haplogranite–H_2O HCl and haplogranite–H_2O Hf. *Contributions to Mineralogy and Petrology* **109**, 139–150.

Khan, M. A. & Coward, M. P. (1991). Entrapment of an intra-oceanic island arc in collision tectonics; a review of the structural history of the Kohistan Arc, NW Himalaya. In: Sharma, K. K. (ed.), *Geology and Geodynamic Evolution of the Himalayan Collision Zone; Part 1*. Oxford: Pergamon, pp. 1–18.

Khan, M. A., Jan, M. Q., Windley, B. F., Tarney, J. & Thirlwall, M. F. (1989). The Chilas mafic–ultramafic igneous complex: the root of the Kohistan island arc in the Himalaya of northern Pakistan. In: Malinconico, L. L.,Jr & Lillie, R. J. (eds) *Tectonics of the Western Himalayas. Geological Society of America: Special Papers* **232**, 75–94.

Khan, M. A., Jan, M. Q. & Weaver, B. L. (1993). Evolution of the lower arc crust in Kohistan, N. Pakistan: temporal arc magmatism through early, mature and intra-arc ritf stages. In: Treloar, P. J. & Searle, M. P. (eds) *Himalayan Tectonics, London, Special Publications, Geological Society* **74** 123–138.

Khan, M. A., Treloar, P. J., Khan, T., Qazi, M. S. & Jan, M. Q. (1998). Geology of the Chalt–Babusar transect, Kohistan terrane, N. Pakistan: implications for the constitution and thickening of island-arc crust. *Journal of Asian Earth Sciences* **16**, 253–268.

Khan, T., Khan, M. A., Jan, M. Q. & Naseem, M. (1996). Back-arc basin assemblages in Kohistan, northern Pakistan. *Geodinamica Acta* **9**, 30–40.

Kogiso, T., Tatsumi, Y. & Nakano, S. (1997). Trace element transport during dehydration processes in the subducted oceanic crust. 1. Experiments and implications for the origin of ocean island basalts. *Earth and Planetary Science Letters* **148**, 193–205.

Kriegsman, L. M. (2001). Partial melting, partial melt extraction and partial back reaction in anatectic migmatites. *Lithos* **56**, 75–96.

Kuno, H. (1968). Origin of andesite and its bearing on the island arc structure, *Bull. Volc.* **32**, 141–176.

Langmuir, C. H. (1989). Geochemical consequences of *in situ* crystallization. *Nature* **340**, 199–205.

Loock, G., McDonough, W. F., Goldstein, S. L. & Hofmann, A. W. (1990). Isotopic compositions of volcanic glasses from the Lau Basin. *Marine Mining* **9**, 235–245.

López, S. & Castro, A. (2001). Determination of the fluid-absent solidus and supersolidus phase relationships of MORB-derived amphibolites in the range 4–14 kbar. *American Mineralogist* **86**, 1396–1403.

Macdonald, R., Hawkesworth, C. J. & Heath, E. (2000). The Lesser Antilles volcanic chain: a study in arc magmatism. *Earth-Science Reviews* **49**, 1–76.

Martin, H. (1986). Effect of steeper Archean geothermal gradient on geochemistry of subduction-zone magmas. *Geology* **14**, 753–756.

Martin, H. (1987). Petrogenesis of Archean trondhjemites, tonalites, and granodiorites from Eastern Finland—major and trace-element geochemistry. *Journal of Petrology* **28**, 921–953.

Martin, H. (1999). Adakitic magmas: modern analogues of Archaean granitoids. *Lithos* **46**, 411–429.

McKenzie, D. (1989). Some remarks on the movement of small melt fractions in the Mantle. *Earth and Planetary Science Letters* **95**, 53–72.

Mehl, L., Hacker, B. R., Hirth, G. & Kelemen, P. B. (2003). Arc-parallel flow within the mantle wedge: evidence from the accreted Talkeetna arc, south central Alaska. *Journal of Geophysical Research—Solid Earth* **108**, (B8), article number 2375.

Mikoshiba, M. U., Takahashi, Y., Takahashi, Y., Kausar, A. B., Khan, T., Kubo, K. & Shirahase, T. (1999). Rb–Sr isotopic study of the Chilas igneous complex, Kohistan, northern Pakistan. In: Macfarlane, A., Sorkhabi, R. B. & Quade, J. (eds) *Himalaya and Tibet; Mountain Roots to Mountain Tops. Geological Society of America, Special Papers* **328**, 47–57.

Miller, D. J. & Christensen, N. I. (1994). Seismic signature and geochemistry of an island arc: a multidisciplinary study of the Kohistan accreted terrane, northern Pakistan. *Journal of Geophysical Research* **99**, 11623–11642.

Miller, D. J., Loucks, R. R. & Ashraf, M. (1991). Platinum-group element mineralization in the Jijal layered ultramafic–mafic complex, Pakistani Himalayas. *Economic Geology* **86**, 1093–1102.

Moore, G. & Carmichael, I. S. E. (1998). The hydrous phase equilibria (to 3 kbar) of an andesite and basaltic andesite from western Mexico: constraints on water content and conditions of phenocryst growth. *Contributions to Mineralogy and Petrology* **130**, 304–319.

Muir, R. J., Weaver, S. D., Bradshaw, J. D., Eby, G. N. & Evans, J. A. (1995). The Cretaceous Separation Point batholith, New Zealand—granitoid magmas formed by melting of mafic lithosphere. *Journal of the Geological Society, London* **152**, 689–701.

Müntener, O., Kelemen, P. B. & Grove, T. L. (2001). The role of H_2O during crystallization of primitive arc magmas under uppermost mantle conditions and genesis of igneous pyroxenites: an experimental study. *Contributions to Mineralogy and Petrology* **141**, 643–658.

O'Connor, J. T. (1965). A classification for quartz-rich igneous rocks based on feldspar ratios. *US Geological Survey, Professional Papers* **525-B**, 79–84.

Pattison, D. R. M. (2003). Petrogenetic significance of orthopyroxene-free garnet + clinopyroxene + plagioclase ± quartz-bearing metabasites with respect to the amphibolite and granulite facies. *Journal of Metamorphic Petrology* **21**, 21–34.

Pearcy, L. G., Debari, S. M. & Sleep, N. H. (1990). Mass balance calculations for two sections of island-arc crust and implications for the formation of continents. *Earth and Planetary Science Letters* **96**, 427–442.

Peate, D. W. & Pearce, J. A. (1998). Causes of spatial compositional variations in Mariana arc lavas: trace element evidence. *Island Arc* **7**, 479–495.

Petford, N. & Atherton, M. (1996). Na-rich partial melts from newly underplated basaltic crust: the Cordillera Blanca batholith, Peru. *Journal of Petrology* **37**, 1491–1521.

Petterson, M. G. & Windley, B. F. (1985). Rb–Sr dating of the Kohistan arc-batholith in the trans- Himalaya of North Pakistan, and tectonic implications. *Earth and Planetary Science Letters* **74**, 45–57.

Petterson, M. G. & Windley, B. F. (1991). Changing source regions of magmas and crustal growth in the Trans-Himalayas—evidence from the Chalt volcanics and Kohistan batholith, Kohistan, Northern Pakistan. *Earth and Planetary Science Letters* **102**, 326–341.

Petterson, M. G., Windley, B. F. & Sullivan, M. (1991). A petrological, chronological, structural and geochemical review of Kohistan Batholith and its relationship to regional tectonics. *Physics and Chemistry of the Earth* **17**(Part II), 47–70.

Petterson, M. G., Crawford, M. B. & Windley, B. F. (1993). Petrogenetic implications of neodymium isotope data from the Kohistan Batholith, North Pakistan. *Journal of the Geological Society, London* **150**, 125–129.

Rapp, R. P. (1995). Amphibole-out phase-boundary in partially melted metabasalt, its control over liquid fraction and composition, and source permeability. *Journal of Geophysical Research—Solid Earth* **100**, 15601–15610.

Rapp, R. P. & Watson, E. B. (1995). Dehydration melting of metabasalt at 8–32 kbar: implications for continental growth and crust–mantle recycling. *Journal of Petrology* **36**, 891–931.

Rapp, R. P., Watson, E. B. & Miller, C. F. (1991). Partial melting of amphibolite eclogite and the origin of Archean trondhjemites and tonalites. *Precambrian Research* **51**, 1–25.

Rapp, R. P., Shimizu, N., Norman, M. D. & Applegate, G. S. (1999). Reaction between slab-derived melts and peridotite in the mantle wedge: experimental constraints at 3·8 GPa. *Chemical Geology* **160**, 335–356.

Rapp, R. P., Shimizu, N. & Norman, M. D. (2003). Growth of early continental crust by partial melting of eclogite. *Nature* **425**, 605–609.

Reymer, A. & Schubert, G. (1984). Phanerozoic addition rates to the continental crust and crustal growth. *Tectonics* **3**, 63–77.

Rolland, Y. (2002). From intra-oceanic convergence to post-collisional evolution: example of the India–Asia convergence in NW Himalaya, from Cretaceous to present. *Journal of the Virtual Explorer* **8**, 185–208.

Rolland, Y., Picard, C., Pecher, A., Lapierre, H., Bosch, D. & Keller, F. (2002). The Cretaceous Ladakh arc of NW Himalaya—slab melting and melt–mantle interaction during fast northward drift of Indian Plate. *Chemical Geology* **182**, 139–178.

Rollinson, H. R. & Windley, B. F. (1980). Selective elemental depletion during metamorphism of Archean granulites, Scourie, NW Scotland. *Contributions to Mineralogy and Petrology* **72**, 257–263.

Romick, J. D., Perfit, M. R., Swanson, S. E. & Shuster, R. D. (1990). Magmatism in the Eastern Aleutian Arc—temporal characteristic of igneous activity on Akutan Island. *Contributions to Mineralogy and Petrology* **104**, 700–721.

Romick, J. D., Kay, S. M. & Kay, R. W. (1992). The influence of amphibole fractionation on the evolution of calc-alkaline andesite and dacite tephra from the Central Aleutians, Alaska. *Contributions to Mineralogy and Petrology* **112**, 101–118.

Rose, E. F., Shimizu, N., Layne, G. D. & Grove, T. L. (2001). Melt production beneath Mt. Shasta from boron data in primitive melt inclusions. *Science* **293**, 281–283.

Rudnick, R. & Presper, T. (1990). Geochemistry of intermediate to high-pressure granulites. In: Vielzeuf, D. & Vidal, P. (eds) *Granulites and Crustal Evolution*. Dordrecht: Kluwer Academic, pp. 523–550.

Rudnick, R. L. (1992). Restites, Eu anomalies, and the lower continental crust. *Geochimica et Cosmochimica Acta* **56**, 963–970.

Rudnick, R. L. (1995). Making continental crust. *Nature* **378**, 571–578.

Rudnick, R. L. & Gao, S. (2003). Composition of the continental crust. In: Rudnick, R. L. (ed.), *Treatise on Geochemistry. Vol. 2. Geochemistry of the Crust*. Amsterdam: Elsevier, pp. 1–64.

Rushmer, T. (1993). Experimental high-pressure granulites—some applications to natural mafic xenolith suites and Archean granulite terranes. *Geology* **21**, 411–414.

Schaltegger, U., Zeilinger, G., Frank, M. & Burg, J. P. (2002). Multiple mantle sources during island arc magmatism: U–Pb and Hf isotopic evidence from the Kohistan arc complex, Pakistan. *Terra Nova* **14**, 461–468.

Schubert, G. & Sandwell, D. (1989). Crustal volumes of the continents and of oceanic and continental submarine plateaus. *Earth and Planetary Science Letters* **92**, 234–246.

Searle, M. P., Windley, B. F., Coward, M. P., Cooper, D. J. W., Rex, A. J., Rex, D., Li, T. D., Xiao, X. C., Jan, M. Q., Thakur, V. C. & Kumar, S. (1987). The closing of Tethys and the tectonics of the Himalaya. *Geological Society of America Bulletin* **98**, 678–701.

Sen, C. & Dunn, T. (1994). Dehydration melting of a basaltic composition amphibolite at 1·5 and 2·0 GPa: implications for the origin of adakites. *Contributions to Mineralogy and Petrology* **119**, 422–432.

Shah, M. T. & Shervais, J. W. (1999). The Dir-Utror metavolcanic sequence, Kohistan arc terrane, northern Pakistan. *Journal of Asian Earth Sciences* **17**, 459–475.

Sisson, T. W. & Grove, T. L. (1993a). Experimental investigations of the role of H_2O in calc-alkaline differentiation and subduction zone magmatism. *Contributions to Mineralogy and Petrology* **113**, 143–166.

Sisson, T. W. & Grove, T. L. (1993b). Temperatures and H_2O contents of low-MgO high-alumina basalts. *Contributions to Mineralogy and Petrology* **113**, 167–184.

Smith, D. R. & Leeman, W. P. (1987). Petrogenesis of Mount St. Helens dacitic magmas. *Journal of Geophysical Research—Solid Earth and Planets* **92**, 10313–10334.

Smithies, R. H. (2000). The Archaean tonalite–trondhjemite–granodiorite (TTG) series is not an analogue of Cenozoic adakite. *Earth and Planetary Science Letters* **182**, 115–125.

Springer, W. & Seck, H. A. (1997). Partial fusion of basic granulites at 5 to 15 kbar: implications for the origin of TTG magmas. *Contributions to Mineralogy and Petrology* **127**, 30–45.

Stalder, R., Foley, S. F., Brey, G. P. & Horn, I. (1998). Mineral aqueous fluid partitioning of trace elements at 900–1200°C and 3·0–5·7 GPa: new experimental data for garnet, clinopyroxene, and rutile, and implications for mantle metasomatism. *Geochimica et Cosmochimica Acta* **62**, 1781–1801.

Tahirkheli, R. A. K., Mattauer, M., Proust, F. & Tapponier, P. (1979). The Indian–Eurasia suture in northern Pakistan. Synthesis and interpretation of data on plate scale. In: Farah, A. & Dejong, K. (eds) *Geodynamics of Pakistan*. Quetta: Geological Survey of Pakistan, pp. 125–130.

Tamura, Y. & Tatsumi, Y. (2002). Remelting of an andesitic crust as a possible origin for rhyolitic magma in oceanic arcs: an example from the Izu–Bonin Arc. *Journal of Petrology* **43**, 1029–1047.

Taylor, S. R. & McLennan, S. M. (1985). *The Continental Crust: its Composition and Evolution*. Oxford: Blackwell.

Taylor, S. R., Rudnick, R. L., McLennan, S. M. & Eriksson, K. A. (1986). Rare-earth element patterns in Archean high-grade metasediments and their tectonic significance. *Geochimica et Cosmochimica Acta* **50**, 2267–2279.

Thompson, A. B. (1999). Some time–space relationships for crustal melting and granitic intrusion at various depths. In: Castro, A., Fernandez, C. & Vigneresse, J.-L. (eds) *Understanding Granites: Integrating Modern and Classical Techniques, Geological Society, London, Special Publications,* **158** 7–25.

Thompson, A. B. & Connolly, J. A. D. (1988). Generation and migration of deep crustal fluids during regional metamorphism. *Chemical Geology* **70**, 165–165.

Treloar, P. J., Petterson, M. G., Jan, M. Q. & Sullivan, M. A. (1996). A re-evaluation of the stratigraphy and evolution of the Kohistan arc sequence, Pakistan Himalaya: implications for magmatic and tectonic arc-building processes. *Journal of the Geological Society, London* **153**, 681–693.

Vielzeuf, D. & Schmidt, M. W. (2001). Melting relations in hydrous systems revisited: application to metapelites, metagreywackes and metabasalts. *Contributions to Mineralogy and Petrology* **141**, 251–267.

Vielzeuf, D., Clemens, J. D., Pin, C. & Moinet, E. (1990). Granites, granulites, and crustal differentiation. In: Vielzeuf, D. & Vidal, P. (eds) *Granulites and Crustal Evolution*. Dordrecht: Kluwer Academic, pp. 59–86.

Wedepohl, K. H. (1991). Chemical composition and fractionation of the continental crust. *Geologische Rundschau* **80**, 207–223.

Whalen, J. B. (1985). Geochemistry of an island-arc plutonic suite—the Uasilau–Yau-Yau intrusive complex, New Britain, Papua New Guinea. *Journal of Petrology* **26**, 603–632.

Wilson, M. (1989). *Igneous Petrogenesis*. London: Unwin Hyman.

Wolf, M. B. & Wyllie, P. J. (1991). Dehydration-melting of solid amphibolite at 10 kbar—textural development, liquid interconnectivity and applications to the segregation of magmas. *Mineralogy and Petrology* **44**, 151–179.

Wolf, M. B. & Wyllie, P. J. (1993). Garnet growth during amphibolite anatexis—implications of a garnetiferous restite. *Journal of Geology* **101**, 357–373.

Wolf, M. B. & Wyllie, P. J. (1994). Dehydration-melting of amphibolite at 10 kbar—the effects of temperature and time. *Contributions to Mineralogy and Petrology* **115**, 369–383.

Wyllie, P. J. & Wolf, M. B. (1993). Amphibolite dehydration-melting: sorting out the solidus. In: Prichard, H. M., Alabaster, T., Harris, N. B. W. & Neary, C. R. (eds) *Magmatic Processes and Plate Tectonics. A Volume in Commemoration of the Work of Ian Gass, Geological Society, London, Special Publications* **76**, 405–416.

Yamamoto, H. (1993). Contrasting metamorphic *P–T*–time paths of the Kohistan granulites and tectonics of the western Himalayas. *Journal of the Geological Society,* **150**, 843–856.

Yamamoto, H. & Nakamura, E. (1996). Sm–Nd dating of garnet granulites from the Kohistan Complex, northern Pakistan. *Journal of the Geological Society,* **153**, 965–969.

Yamamoto, H. & Nakamura, E. (2000). Timing of magmatic and metamorphic events in the Jijal Complex of the Kohistan Arc deduced from Sm–Nd dating of mafic granulites. In: Khan, M. A., Treloar, P. J., Searle, M. P. & Jan, M. Q. (eds) *Tectonics of the Nanga Parbat Syntaxis and the Western Himalaya. Geological Society, London, Special Publications* **170**, 321–331.

Yamamoto, H. & Yoshino, T. (1998). Superposition of replacements in the mafic granulites of the Jijal complex of the Kohistan arc, northern Pakistan: dehydration and rehydration within deep arc crust. *Lithos* **43**, 219–234.

Yoshino, T. & Okudaira, T. (2004). Crustal growth by magmatic accretion constrained by metamorphic *P–T* paths and thermal models of the Kohistan Arc, NW Himalayas. *Journal of Petrology* **45**, 2287–2302.

Yoshino, T., Yamamoto, H., Okudaira, T. & Toriumi, M. (1998). Crustal thickening of the lower crust of the Kohistan arc (N. Pakistan) deduced from Al zoning in clinopyroxene and plagioclase. *Journal of Metamorphic Geology* **16**, 729–748.

Zeilinger, G. (2002). Structural and geochronological study of the Lowest Kohistan Complex, Indus Kohistan Region in Pakistan, NW Himalaya. Ph.D. thesis, ETH, Zürich.

Zellmer, G. F., Hawkesworth, C. J., Sparks, R. S. J., Thomas, L. E., Harford, C. L., Brewer, T. S. & Loughlin, S. C. (2003). Geochemical evolution of the Soufrière Hills Volcano, Montserrat, Lesser Antilles volcanic arc. *Journal of Petrology* **44**, 1349–1374.